Master's thesis

NTNU
Norwegian University of Science and Technology
Faculty of Engineering
Department of Marine Technology

Karin Assev Øyen

Assessment of Operational Risks in Polar Areas

Risk Assessment using the Polar Operational Limits Assessment Risk Indexing System (POLARIS) and Predictive Simulations

Master's thesis in Marine Technology

Supervisor: Ekaterina Kim

June 2020

NTNU
Norwegian University of Science and Technology

The Norwegian University of Science and Technology
Faculty of Engineering
Department of Marine Technology

MSc-ASSIGNMENT for

Stud. Karin Assev Øyen

Spring 2020

Assessment of Operational Risks in Polar Areas – Risk Assessment using the Polar Operational Limits Assessment Risk Indexing System (POLARIS) and Predictive Simulations

Background

To maintain safe ship operations and protect the polar environment, risks present in the polar waters must be addressed. Polar Operational Limit Assessment Risk Indexing System (POLARIS) was developed as a collective effort based on the administrative and operating experience from several countries and is currently considered as an acceptable methodology for assessment of operational limitations in ice infested waters by the International Maritime Organization (IMO).

Overall Objective and Scope

The objective of this work is to analyse operational risks and speeds during research voyages in the ice infested waters using the IMO's POLARIS. The assessment should be prepared based on the following points:

1) Give a review of research on the development and use of POLARIS.

2) Collect, analyse, and evaluate essential data from ASSIST Data Network that are necessary for the risk assessment.

3) Implement risk evaluation procedure (POLARIS) as a MATLAB code following the IMO recommendations.

4) Analyse risks and speeds associated with the voyages from Pt.2.

5) For selected critical cases establish a link between the operational risk index and global ice load using predictive simulation software, e.g., Simulator for Arctic Marine Structures.

The work scope may prove to be larger than initially anticipated. Subject to approval from the supervisor, topics may be deleted from the list above or reduced in extent.

Ownership

NTNU has, according to the present rules, the ownership of the thesis. Any use of the thesis must be approved by NTNU (or external partner when this applies). The department has the right to use the thesis as if an NTNU employee carried out the work if nothing else has been agreed in advance.

At NTNU, Associate Professor Ekaterina Kim will be the responsible advisor. The work shall follow the guidelines given by NTNU for the MSc Thesis work. The workload shall be in accordance with 30 ECTS, corresponding to 100% of one semester courses.

NTNU

Norwegian University of
Science and Technology

MASTER THESIS

ASSESSMENT OF OPERATIONAL RISKS IN POLAR AREAS

RISK ASSESSMENT USING THE POLAR OPERATIONAL LIMITS ASSESSMENT RISK INDEXING SYSTEM (POLARIS) AND PREDICTIVE SIMULATIONS

Author:
ØYEN, Karin Assev

Supervisor:
KIM, Ekaterina

Submission date:
JUNE 2020

NORWEGIAN UNIVERSITY OF SCIENCE AND TECHNOLOGY
FACULTY OF ENGINEERING
DEPARTMENT OF MARINE TECHNOLOGY

Preface

This master thesis is written at the Department of Marine Technology at the Norwegian University of Science and Technology (NTNU) in Trondheim during the spring of 2020. The thesis is the final part of graduating with the degree *Master of Science* with specialization within Marine System Design.

The master thesis has been interesting, though challenging, to work with. It has its foundation in predictive simulations of operations in polar areas. I found the work fulfilling because it investigates real issues and can be used to improve today's methods and software. A significant amount of time was spent on the set-up of the predictive simulations, and obstacles such as software updates and bugs, have been overcome to obtain the results. My project thesis from the autumn of 2019, has partly served as preparatory work for the master thesis. It has been a different semester then expected due to COVID-19, but the best has been made out of the situation.

I would like to thank my supervisor, Associate Professor Ekaterina Kim, for valuable guidance and useful discussion throughout the semester. I would also like to thank postdoc Marnix van den Berg for helpful contributions and support with the software SAMS. Last but not least, I want to thank the ladies at office C1.072 for support and loads of fun during the five years at NTNU.

Trondheim, June 10, 2020

Karin Assev Øyen

Summary

Maritime accidents in polar areas have increased over the last decade and the ship activity in ice infested waters is expected to increase in the future. It is of interest to maintain safe ship operations and keep all ships within their operational limitations. International agreement on a risk evaluation methodology is an important step to prevent future maritime accidents.

This master thesis presents a methodology for assessing operational risk and global ice loads based on sea ice observations. The thesis investigates whether ships remain within their operational limitations according to Polar Operational Limit Assessment Risk Indexing System (POLARIS). The International Maritime Organization accepts POLARIS as a methodology for the assessment of operational limitations in ice infested waters. As of today, the risk level defined by POLARIS sets the framework for when ships are allowed to enter different ice regimes. For operations to remain safe, it is necessary with a sufficiently strong hull to withstand the ice loads. The risk level must reflect the global ice loads in order for the operation to be performed in a safe environment.

Sea ice observations from research voyages are available from the open-source Arctic Shipborne Sea Ice Standardization Tool Data Network. The accuracy and reliability of the data must be analyzed to ensure high quality for the data basis of the risk evaluation. The result of the analysis is discussed in terms of variations in input data and errors. The main findings from evaluation of risk according to POLARIS is that for those vessels exposed to a high level of risk, measures are taken to reduce risk. Some ships are systematically exposed to a high level of risk, and the reason may be due to poor voyage planning or incorrectly reporting of ice conditions. The risk is not directly dependent on the speed. Nevertheless, a correlation between the speed and the risk is identified from the data.

A simulation model framework has been created to establish a link between the operational risk index and global ice loads. The main findings from a case study conducted with this model and sea ice data indicates no clear correlation between the two parameters. However, the case study is performed for a small selection of low-risk cases for one ship. Thus, for a more extensive selection of vessel types and risk, a dependency could be identified. The study highlights the impact on global ice loads from the choice of speed and human factors. This indicates that the risk level is dependent on several other aspects than only the ones considered in POLARIS. The main achievement from the current work is the established methodology process of evaluating POLARIS and if its operational risk index reflects the actual risk level due to the ice loads. The development of a methodology establishes the basis for more comprehensive predictive simulations.

Sammendrag

Sjøulykker i polare områder har økt det siste tiåret, og skipets aktivitet i farvann med havis forventes å øke i fremtiden. Det er av interesse å opprettholde sikker skipsdrift og holde alle skip innenfor sine operasjonelle begrensninger. En internasjonal avtale om metodikk for risikovurdering er et viktig skritt for å forhindre fremtidige sjøulykker.

Denne masteravhandlinger presenterer en metodikk for å vurdere operasjonell risiko og globale isbelastninger basert på observasjoner av havis. Oppgaven undersøker om skip forblir innenfor sine operasjonelle begrensninger i henhold til Polar Operational Limit Assessment Risk Indexing System (POLARIS). Den internasjonale sjøfartsorganisasjonen godtar POLARIS som en metodikk for vurdering av operasjonelle begrensninger i farvann med havis. Per i dag setter risikonivået definert av POLARIS rammen for når skip får lov til å gå inn i forskjellige isregimer. For at operasjoner skal forbli trygge, er det nødvendig med et tilstrekkelig sterkt skrog for å motstå isbelastningen. Risikonivået må gjenspeiles i de globale isbelastningene for at operasjonen skal kunne utføres i trygge omgivelser.

Observasjoner av havis fra forskningsturer er tilgjengelige fra den åpne kilden Arctic Shipborne Sea Ice Standardization Tool Data Network. Dataens nøyaktighet og pålitelighet må analyseres for å sikre høy kvalitet for datagrunnlaget for risikovurderingen. Resultatet av analysen blir diskutert med tanke på variasjoner i inputdata og feil. De viktigste funnene fra evaluering av risiko i henhold til POLARIS er at det blir iverksatt tiltak hvis et skip er utsatt for et høyt risikonivå. Noen skip er systematisk utsatt for et høyt risikonivå, og årsaken kan skyldes dårlig planlegging av seilas eller feilrapportering av isforhold. Risikoen er ikke direkte avhengig av hastigheten. Likevel identifiseres en sammenheng mellom hastigheten og risikoen fra dataene.

Det er laget et rammeverk for en simuleringsmodell med hensikt å etablere en kobling mellom den operasjonelle risikoindeksen og de globale isbelastningene. De viktigste funnene fra en studie utført med denne modellen og data om havis, indikerer ingen klar sammenheng mellom de to parameterne. Imidlertid utføres studien for et lite utvalg av lavrisiko saker for ett skip. For et mer omfattende utvalg av skipstyper og risiko kan en avhengighet identifiseres. Studien belyser virkningen på globale isbelastninger fra valg av hastighet og menneskelige faktorer. Dette indikerer at risikonivået er avhengig av flere andre aspekter enn bare de som er vurdert i POLARIS. Hovedprestasjonen fra det nåværende arbeidet er den etablerte metodeprosessen for å evaluere POLARIS, og om dens operasjonelle risikoindeks reflekterer det faktiske risikonivået på grunn av isbelastningen. Utviklingen av en metodikk etablerer grunnlaget for mer omfattende prediktive simuleringer.

Contents

Preface i

Summary iii

Sammendrag v

Table of Contents vii

List of Tables x

List of Figures xii

Abbreviations xv

1 Introduction 1
- 1.1 Background and Motivation . . . 1
- 1.2 Objective . . . 2
- 1.3 Limitations . . . 2
- 1.4 Outline of the Thesis . . . 2

2 Polar Operational Limit Assessment Risk Indexing System 5
- 2.1 Development of POLARIS . . . 6
  - 2.1.1 Level Ice Thickness Limitations . . . 6
  - 2.1.2 Align with WMO Egg Codes . . . 7
  - 2.1.3 Partial Concentrations . . . 8
  - 2.1.4 Decayed Ice . . . 8
  - 2.1.5 Escorted Operations . . . 8
- 2.2 Methodology of POLARIS . . . 8
  - 2.2.1 Risk Evaluation . . . 9
  - 2.2.2 Operational Limitations & Evaluation of Risk . . . 9
  - 2.2.3 Ice Decay, Icebreaker Escort & Glacial Ice . . . 11
- 2.3 Use of POLARIS . . . 12
- 2.4 Egg Code . . . 13

3 Observational Data 15
- 3.1 Data from ASSIST Data Network . . . 15
  - 3.1.1 General . . . 16
  - 3.1.2 Ice . . . 16
  - 3.1.3 Meteorology . . . 19
  - 3.1.4 Photos & Comments . . . 19
- 3.2 Risk Evaluation Procedure in Matlab . . . 19

4 Simulator for Arctic Marine Structures **21**
4.1 Bodies . . . 22
4.2 Collision Detection and Contact Processing . . . 23
4.3 Contact Force Solver . . . 25
4.4 Fluid Forces . . . 25
4.5 Ice Fracture . . . 26
4.5.1 Splitting Failure . . . 27
4.5.2 Bending Failure . . . 28
4.6 Validation . . . 29

5 Assessment of Data and Risk **31**
5.1 Evaluation of Available Observational Data . . . 31
5.2 Polar Class Vessels . . . 33
5.3 Evaluation of Areas . . . 34
5.4 Ice Conditions and Risk . . . 38
5.5 Voyage . . . 42
5.6 The Impact of Speed . . . 44
5.7 Speed Evaluation . . . 46
5.7.1 North of Alaska . . . 48
5.7.2 Fram Strait . . . 48
5.7.3 North of Svalbard . . . 49
5.7.4 Georg Land . . . 50
5.8 Comparison . . . 50

6 Predictive Simulation **53**
6.1 Critical Cases . . . 53
6.2 Ice Field Generation . . . 54
6.3 Input Parameters SAMS . . . 55
6.4 Route Choice . . . 58
6.5 Running the Analysis . . . 59
6.6 Different Segments of the Route . . . 60
6.7 Frequency . . . 60
6.8 Confinements . . . 61

7 Results from Predictive Simulation **63**
7.1 Comparison of all Results . . . 63
7.1.1 Outliers . . . 68
7.2 Individual Study . . . 69
7.3 Concluding Remarks . . . 73
7.4 Executive Methodology . . . 74

8 Discussion **75**

9 Conclusion and Further work **79**
9.1 Conclusion . . . 79
9.2 Further Work . . . 79

Bibliography **81**

Appendix A ASSIST **I**

Appendix B Data Evaluation and Associated Matlab Codes **V**

Appendix C Route Information **XIX**

Appendix D Individual Study of RIO for Individual Areas **XXV**
D.1 Alaska XXV
D.2 Fram Strait XXVII
D.3 Svalbard XXVIII
D.4 Georg Land XXX

Appendix E Ice Charts Comparison **XXXIII**

Appendix F Simulation in SAMS **XXXVII**
F.1 Configuration File XXXVII
F.2 Structure File XXXVIII
F.3 Track File XXXVIII

Appendix G Global Load Comparison **XLI**

List of Tables

2.1 Polar Class Notations (IACS, 2016) . . . 7
2.2 Ice Type & Ice Type Symbol (IMO, 2016) . . . 9
2.4 Risk Index Outcome Criteria (IMO, 2016) . . . 9
2.3 POLARIS Risk Index Value (IMO, 2016) . . . 10
2.5 Recommended speed limits for elevated risk operations (IMO, 2016) . . . 11
2.6 Egg Code: Stage of development (WMO, 2014) . . . 14
2.7 Egg Code: Form of Ice (WMO, 2014) . . . 14

3.1 Ship Activity Character (Hutchings et al., 2018) . . . 16
3.2 Open Water Character (Hutchings et al., 2018) . . . 17
3.3 Ice Type (Hutchings et al., 2018) . . . 17
3.4 Flow Size (Hutchings et al., 2018) . . . 18
3.5 Snow Type (Hutchings et al., 2018) . . . 18
3.6 Topography Type (Hutchings et al., 2018) . . . 18
3.7 Visibility (Hutchings et al., 2018) . . . 19
3.8 Ice Type Equivalence ASSIST and POLARIS . . . 20

4.1 Global Splitting Failure Parameters (Berg et al., 2019) (Lubbad, Loset, et al., 2018) . . . 28
4.2 Local Bending Failure Parameters (Berg et al., 2019) (Lubbad, Loset, et al., 2018) . . . 29

5.1 Observational Data . . . 32
5.2 Excerpt of data from Oden 2012 . . . 33
5.3 Vessel Ice Class Notation . . . 34
5.4 North of Alaska IceWatch, 2019 . . . 35
5.5 Fram Strait . . . 35
5.6 North of Svalbard . . . 35
5.7 North of Georg Land . . . 36
5.8 Voyage Time and Length . . . 37
5.9 Ship Speed Data Sets, North of Alaska . . . 46
5.10 Ship Speed Data Sets, Fram Strait . . . 47
5.11 Ship Speed Data Sets, North of Svalbard . . . 47
5.12 Ship Speed Data Sets, Georg Land . . . 47

6.1 Egg Codes . . . 54
6.2 Egg Code Information (IceWatch, 2019) . . . 54
6.3 SAMS Simulation setting . . . 55
6.4 SAMS Advanced User Input . . . 56
6.5 SAMS Ice field properties (Raza et al., 2019) . . . 56
6.6 SAMS Structure Properties . . . 57
6.7 SAMS Ice 3D Export Settings . . . 57
6.8 SAMS Environmental Properties . . . 58

C.1 Route Information, North of Alaska (IceWatch, 2019) XX
C.2 Route Information, Fram Strait (IceWatch, 2019) XXI
C.3 Route Information, North of Svalbard (IceWatch, 2019) XXII
C.4 Route Information, Georg Land (IceWatch, 2019) XXIII

D.1 RIO North of Alaska, max & min values XXVI
D.2 RIO Fram Strait, max & min values XXVIII
D.3 RIO North of Svalbard, max & min values XXIX
D.4 RIO Georg Land, max & min values XXXI

E.1 Recordings 22 September 2015 Alaska (IceWatch, 2019) XXXIII
E.2 Egg Codes 22 September 2015 Alaska (IceWatch, 2019) XXXIV

List of Figures

2.1 Process for developing POLARIS (IMO, 2014) . . . 6
2.2 Limitations for level ice – MSC93 draft with operational experience from Canada, Finland/Sweden and Russia (IMO, 2014) . . . 7
2.3 Egg Code (WMO, 2014) . . . 13
2.4 Egg Code Additions (WMO, 2014) . . . 14
a Stage of Development . . . 14
b Form of Ice . . . 14

3.1 Ice Cover for various fractions (Government of Canada, 2005) (Hutchings et al., 2018) 17

4.1 Simulation Loop SAMS . . . 22
4.2 Contact type flow chart (Berg, M. van den, 2019) . . . 23
4.3 Compliant Contacts in SAMS (Berg, M. van den, 2019) . . . 24
a Ice-Ice Contact . . . 24
b Ice-Structure Contact . . . 24
4.4 Loading-unloading curve for ice-ice or ice-structure contact . . . 25
4.5 Overall logic of the fracture algorithm within SAMS at each time instant (Berg, M. van den, 2019) . . . 27

5.1 All routes and defined areas . . . 33
5.2 All routes North of Alaska . . . 35
5.3 All routes Fram Strait . . . 35
5.4 All routes Svalbard . . . 35
5.5 All routes Georg Land . . . 36
5.6 TC distribution for the different areas . . . 38
5.7 Ice type distribution for the different areas . . . 38
5.8 Polar Class distribution for the different areas . . . 39
5.9 Probability density distribution of RIO for the different areas . . . 40
a North of Alaska . . . 40
b Fram Strait . . . 40
c North of Svalbard . . . 40
d Georg Land . . . 40
5.10 Distribution of ships and areas . . . 40
5.11 Distribution of RIO for all ships . . . 41
5.12 Boxplot of RIO for each PC . . . 42
5.13 RIO during voyage of CCGS St. Laurent in 2013 . . . 43
5.14 RIO during voyage of RV Lance in 2015 . . . 43
5.15 pdf of all speed records . . . 44
5.16 Distribution of Ship Activity and Ship Speed . . . 45
5.17 Distribution of Ship Activity and Ship Speed . . . 46
5.18 Box plot of RIO and Speed, Alaska . . . 48
5.19 Box plot of RIO and Speed Transit in Ice, Alaska . . . 48

5.20 Box plot of RIO and Speed, Fram Strait . . . 49
5.21 Box plot of RIO and Speed, Svalbard . . . 49
5.22 Box plot of RIO and Speed Transit in Ice, Svalbard . . . 50
5.23 Box plot of RIO and Speed, Georg Land . . . 50
5.24 Speed of the vessel plotted against the RIO along with a best fit curve for the mean speeds for corresponding RIO values (Panci et al., 2020) . . . 51
5.25 Safe speed in ice and weather conditions (ENFOTEC Technical Services Inc et al., 1996) . . . 52

6.1 The chosen routes, indicated as a red line, for the different ice fields . . . 59
a Routes Egg Code 1 . . . 59
b Routes Egg Code 2 . . . 59
c Routes Egg Code 3 . . . 59
d Routes Egg Code 4 . . . 59
e Routes Egg Code 5 . . . 59
f Routes Egg Code 6 . . . 59
6.2 Time-Average Total Ice Force for different frequencies . . . 60
6.3 Interaction between Oden and ice floe for different frequencies . . . 61
a Frequency 10 Hz . . . 61
b Frequency 50 Hz . . . 61
c Frequency 100 Hz . . . 61
d Frequency 150 Hz . . . 61
6.4 Time-Average Total Ice Force with and without confinements . . . 62
a Egg Code 1 Route 1 TC = 10 % . . . 62
b Egg Code 4 Route 1 TC = 80 % . . . 62

7.1 Box Plot of Time-Average Surge Force for all Egg Codes . . . 64
7.2 Time-Averaged Total Ice Force in Surge Direction: Egg Code 4 Route 2 . . . 65
7.3 Time-Averaged Total Ice Force in Surge Direction . . . 66
a Egg Code 3 Route 2 . . . 66
b Egg Code 5 Route 1 . . . 66
7.4 Large ice floe with ice rubble interacting with structure in SAMS, underwater view . . . 67
7.5 Small ice floe with ice rubble interacting with structure in SAMS, underwater view . . . 67
7.6 Box Plot of Time-Average Surge Force for all Egg Codes excluding most extreme routes 68
7.7 Egg Code 3 Route 2: Ice Total Force . . . 69
7.8 Egg Code 3 Route 2, Time 1493 s in SAMS Simulation . . . 69
a Top View of the structure . . . 69
b View from underneath the structure . . . 69
7.9 Boxplot of Time-Average Surge Force for Individual Study. Left: Normal Ice Properties. Right: Weaker Ice Properties . . . 70
7.10 Time-Averaged Total Ice Force in Surge Direction For Egg Code 3 Route 2 for different ship speeds . . . 72
a Normal Ice - Speed 2 knots . . . 72
b Normal Ice - Speed 6 knots . . . 72
c Normal Ice - Speed 10 knots . . . 72
7.11 Structure-Ice interaction in same ice field for different ship speeds . . . 73
a Speed 2 knots . . . 73
b Speed 4 knots . . . 73
c Speed 6 knots . . . 73
d Speed 8 knots . . . 73

e Speed 10 knots 73
7.12 Methodology for Assessment of Operational Risk 74

A.1 ASSIST Header Codes II
A.2 ASSIST Data Fields and Codes III

D.1 pdf of RIO for different ships, North of Alaska XXV
D.2 pdf of RIO and concentrations, North of Alaska XXVI
D.3 pdf of RIO for different PC's, Fram Strait XXVII
D.4 pdf of RIO and concentrations, Fram Strait XXVII
D.5 pdf of RIO for different PC's, North of Svalbard XXVIII
D.6 pdf of RIO and concentrations, North of Svalbard XXIX
D.7 pdf of RIO and Concentrations, Georg Land XXX
D.8 pdf of RIO and Concentrations, Georg Land XXX

E.1 Ice Chart Alaskan Coast 22 September 2015 (Canadian Ice Service, 2020) XXXIV

Abbreviations

Arctic Ice Regime Shipping System	AIRSS
Arctic Shipborne Sea Ice Standardization Tool	ASSIST
Crushing Specific Energy	CSE
Gilbert-Johnsen-Keerthi distance algorithm	GJK
International Association of Classification Societies	IACS
Ice Multiplier	IM
International Maritime Organization	IMO
Ice Numeral	IN
Mixed Linear Complementarity Problem	MLCP
Maritime Safety Committee	MSC
Primary * (Partial Ice Type)	P*
Polar Class	PC
Probability Density Function	pdf
Polar Operational Limit Assessment Risk Indexing System	POLARIS
Polar Water Operational Manual	PWOM
Risk Index Outcome	RIO
Risk Index Value	RIV
Russian Maritime Register of Shipping	RMRS
Secondary * (Partial Ice Type)	S*
Tertiary * (Partial Ice Type)	T*
Total Concentration	TC
World Meteorological Organization	WMO

Chapter 1

Introduction

The following section presents the background and motivation behind the research of this thesis. The main objectives of the thesis will be defined and explained. It will briefly discuss the limitations of the work. Finally, the outline of the thesis will be described.

1.1 Background and Motivation

According to IMO, 2020 the maritime activity in the polar areas is expected to grow in volume and diversity. Operation in such harsh, remote, and vulnerable polar areas is prone to several unique risks. A challenge for the mariners is the lack of adequate communications systems, charts, and other navigational aids, in addition to poor weather conditions. It is costly and challenging to perform rescue or clean-up operations due to the remoteness of the areas. The cold temperatures may reduce the effectiveness of several different components on the ship. Additional loads on the hull, propulsion system, and appendages may be imposed due to interaction with sea ice. To maintain the safety of ships operating under such conditions, the International Maritime Organization (IMO) developed the Polar Codes, an International Code for Ships Operating in Polar Waters. The Polar Code entered into force on 1 January 2017, and it covers design, construction, equipment, operational, training, search and rescue, and environmental protection.

Nevertheless, according to Hindley, 2016 there exists a need for a detailed description of the limiting ice conditions that can be used in practice. For addressing the risk present in the polar waters, an approach for evaluation of risks posed to a vessel must be developed. Polar Operational Limit Assessment Risk Indexing System (POLARIS) is an approach for evaluation of the risks posed to a vessel by ice conditions concerning the assigned ice class of the vessel when operating in polar waters. POLARIS was developed as a collective effort based on the administrative and operating experience from several countries. It is currently considered as an acceptable methodology for the assessment of operational limitations in ice infested waters by IMO.

The ice class rules indicated the limiting ice conditions until POLARIS was established. These rules included only one single ice type descriptor and an assumed or nominal level of thickness. According to Hindley, 2016 for real ice conditions, it is rare with ice coverage of only one ice type. With POLARIS, it is possible to describe more complex ice conditions. For different ice regimes, the structural capabilities and limitations can be evaluated for operating vessels. POLARIS is a decision support system that considers both the ice class of the ship and the encountered ice conditions when determining the risk. (IMO, 2014) (Transports Canada, 2019)

Rules and regulations are continually evolving. From the application of these, one can evaluate its

performance and learn from its use. If it works as intended or whether any other aspects should be taken into consideration. POLARIS only recently entered into force, and it is important to evaluate that it works for its purpose and adequately reflect the level of risk.

1.2 Objective

The main objective of the present master thesis is to develop a methodology for assessing operational risk, using the IMO's POLARIS, and global ice loads based on sea ice observations during research voyages. This includes a detailed study of the observational sea ice data, and its operational risk and speeds. A selection of critical cases is considered in predictive simulations. By considerations of these results, a link between the operational risk index according to POLARIS and the global ice load can be established.

1.3 Limitations

In this thesis, only POLARIS will be considered. It would be beneficial to explore different risk evaluation procedures and to compare their performance. Thus, it could be evaluated which methodology performs best for the task at hand.

The results will be limited by the accuracy and extent of available data. The more data with high quality that is available, the better the basis is for obtaining correct results from the risk evaluation and predictive simulations.

In the software Simulator for Arctic Marine Structures, limitations exist in the theory on which the software is built. In addition, there are some limitations as to what conditions can be simulated.

1.4 Outline of the Thesis

This thesis includes the following chapters:

Chapter 2 review and describe the background, methodology, and use of POLARIS. A broader understanding of the methodology is gained, and an understanding of why the risk differs is obtained. This insight is essential for the evaluation of risk.

Chapter 3 describes the standardization of sea ice observation and how this data can be considered in the risk evaluation procedure POLARIS. A description of the implementation in Matlab is given. Thus, the basis for the performance of risk evaluation is found.

Chapter 4 presents the basis and theory for the software Simulator for Arctic Marine Structures, which performs a predictive simulation of a structure in an ice field. An understanding of the software is essential for the evaluation of the output results.

Chapter 5 describes the evaluation of the accuracy and reliability of the available observational data. The relevant data sets are defined and considered for further evaluation. The evolvement of risk during the voyage is investigated to identify any risk patterns. The data sets with a considerable amount of speed data are identified. Further, these data sets are considered to find a correlation between speed and risk.

Chapter 6 present the selection of different cases to be investigated in the predictive simulation software Simulator for Arctic Marine Structures. The different input data and parameters necessary for the simulations and the implementation of the model is presented.

Chapter 7 describes the results of the predictive simulations from the software Simulator for Arctic Marine Structures. From the performed simulations, a link between the operational risk index and the global ice load is established.

Chapter 8 present a general discussion and evaluation of the performance of the open-source data, the risk analysis, and the simulation work. Also, it discusses the limitations of the work.

Chapter 9 covers the concluding remarks of the thesis, together with a recommendation of challenges that should be addressed in further work.

Chapter 2

Polar Operational Limit Assessment Risk Indexing System

By studying the development of POLARIS, one can gain a broader understanding of the methodology. In the development process of POLARIS, the best practices and experience from regional and national systems are considered. Systems that have been considered for an extended period of time. Thus, even though POLARIS first recently was in place, there exists much experience linked to the methodology. It exists an understanding of which factors influence the risk and what considerations to take in particular situations. When evaluating risk, it is crucial to understand why the risk differs. This chapter reviews the development, methodology, and use of POLARIS.

A proposal to coordinate an informal discussion regarding issues related to the technical aspects associated with the ice class rules was made by the International Association of Classification Societies (IACS) (IMO, 2014). Following this offer, other delegations with experience of setting operational limitations in ice that approached IACS and offered to contribute technical information for validating. IACS and these delegations formed a technical working group to ensure efficiency in this work. The purpose of the technical group was to work with technical aspects of validating and refining the limitations. The working group consisted of delegations from Finland, Canada, and Russia in addition to IACS. At the beginning of the development process of POLARIS, the technical group set the following purpose of the work.

The purpose of the technical work for the small technical content group is to develop guidance, based on the existing content in Part B, which can be used by the Administration and Masters to identify limitations and to ensure the guidance suitably aligns with the content of the Polar Ship Certificate. IMO, 2014

The technical group set a set of key elements needed to identify limitations. Earlier, the limitations for a single level ice thickness was used. In the new key elements, the focus was an accurate representation of the ice conditions. The key elements were identified as partial concentrations, summer/winter conditions and icebreaker escort (IMO, 2014). When developing POLARIS, the best practices and experience from the Arctic Ice Regime Shipping System (AIRSS) of Canada and the Russian Ice Certificate was incorporated. In addition to the pilot ice assistance, as prescribed in the Rules of Navigation on the water area of the Northern Sea Route, and other methodologies supplemented these practices (IMO, 2016). In the following, it is necessary to define ice regimes. According to IMO, 2016 an ice regime is a description of an area with a relatively consistent distribution of any mix of ice types, including open water.

2.1 Development of POLARIS

The development process of POLARIS consists of five main categories. In the following, these five categories are stated and explained in detail. This section is in accordance with IMO, 2014, unless other is stated. Figure 2.1 illustrate the development process of POLARIS. It indicates which experiences and practices were considered for which part of the process. From Figure 2.1, one can gain a better understanding of the different aspects of the process. The main categories are:

1. Initial validation of the level ice thickness limitations in Part I-B of the Code.
2. Align the limitations for level ice with the WMO Egg Code descriptions as far as possible.
3. Adjust the limitations for level ice for partial concentrations.
4. Adjust limitations for Summer (decayed ice).
5. Escorted operations.

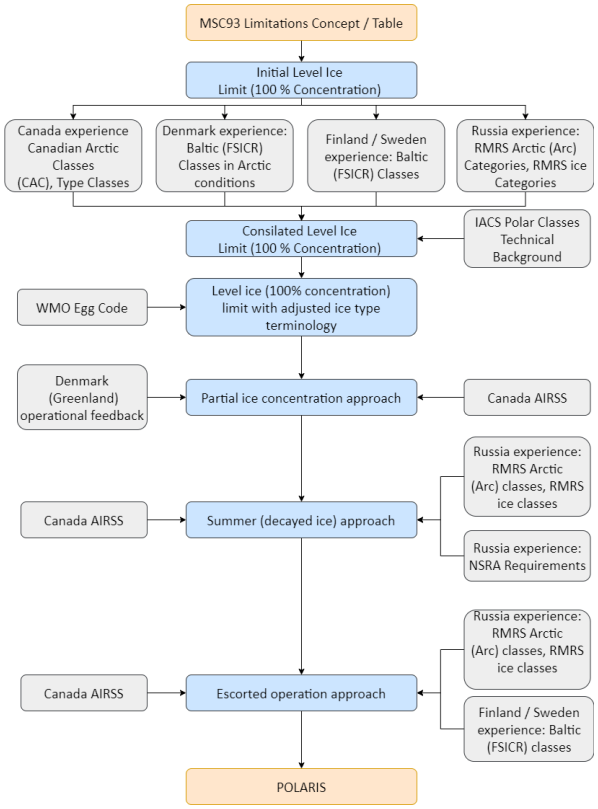

Figure 2.1: Process for developing POLARIS (IMO, 2014)

2.1.1 Level Ice Thickness Limitations

The initial validation of the level ice thickness with a concentration of a 100 % was based on the experience from the operation of open water and ships of ice classes from the Russian Arctic, the Canadian Arctic, Gulf of St. Lawrence, off the Greenland coast, in the Baltic, and the design and background to the IACS Polar Class Rules. The code requirements are divided into different Polar Classes (PC) with different notations and description following IACS, 2016. To select an appropriate PC based on the intended voyage or service is the responsibility of the owner. The different PC

describes the operational capability and strength of the vessel. The PC descriptions can be found in Table 2.1.

Table 2.1: Polar Class Notations (IACS, 2016)

Polar Class	Ice Descriptions (based on WMO Sea Ice Nomenclature)
PC1	Year-round operation in all polar waters.
PC2	Year-round operation in moderate multi-year ice conditions.
PC3	Year-round operation in second-year ice which may include multi-year ice inclusions.
PC4	Year-round operation in thick first-year ice which may include old ice inclusions.
PC5	Year-round operation in medium first-year ice which may include old ice inclusions.
PC6	Summer/autumn operation in medium first year ice which may include old ice inclusion.
PC7	Summer/autumn operation in thin first-year ice which may include old ice inclusions.

It is necessary to find the equivalent PC to each of the classification society's ice classes to compare their limitations. Figure 2.2 plot the level of ice limits from the different experiences to compare the different levels. Also, it illustrates how different traffic systems treated different ice types. The boundary for each ice type is plotted against the ice class. Figure 2.2 indicate that the suggested limitations are in the same area. The plot indicates a broad agreement regarding the limits between the different systems and experiences.

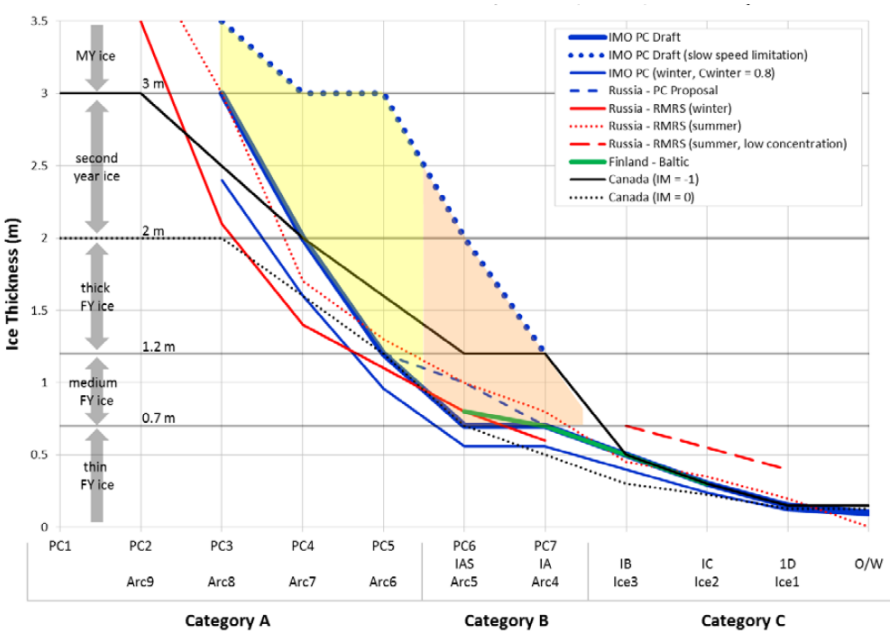

Figure 2.2: Limitations for level ice – MSC93 draft with operational experience from Canada, Finland/Sweden and Russia (IMO, 2014)

2.1.2 Align with WMO Egg Codes

The ice charts for the Arctic and Antarctic consider a standardized terminology following WMO, 2014. For the limitation system to work in practice, the limitations must be consistent with those from WMO

as far as possible. The Egg Codes system is described in detail in Section 2.4.

2.1.3 Partial Concentrations

To systematically evaluate the risk within one ice regime for the separate partial ice types are of interest. A relative level of risk is set when the level of ice limitations have been validated. Following this, a systematic approach for evaluation of partial ice concentrations was developed following experience from the methodology of AIRSS. Experience regarding the operation in partial ice concentration from Russia, Denmark, and Finland was also considered.

AIRSS is according to the Government of Canada, 2017 a four-step process. In the first step, the user characterizes the ice regime. The characterization includes consideration of factors such as the ice concentration, thickness, age, stage of decay, and roughness. In the second step, weighting factors called Ice Multipliers (IM) are obtained based on the vessel class. IM considers the different levels of risk for different ice types. According to the capabilities of the vessel in ice-covered waters, it is assigned to a vessel class. This differentiation is important as different ships have different capabilities in such conditions. To determine the Ice Numeral(IN) is the third step. The determination is based on combining information regarding the ice regime and the IM. The danger present in different ice regimes is related to the strength of the hull. The fourth and last step consider the IN and decide whether the ship can proceed through the ice regime or if it is necessary to find an alternative route. Positive or zero values indicate not likely to be hazardous, while negative values consider the ice regime as hazardous. It must be emphasized that, in the end, it is the master who is responsible for the safety of the ship.

2.1.4 Decayed Ice

The ice is weaker in decayed ice or during summer. Thus, it is possible to adjust the level of risk for these conditions. The decay of ice is considered explicit in AIRSS, while it is considered implicit in the Russian regulations. AIRSS addresses the influence of decayed ice and allows adjustment of the Ice Multipliers. Reduced strength for first-year ice is considered, while for multi-year ice, there exists a little reduction in strength. AIRSS allows an adjustment, but it is not provided an interpretation of how it should be performed. The Russian Maritime Register of Shipping (RMRS) defines two seasons, where the limit for level thickness is adjusted for summer navigation. An adjustment on the limit of level ice with a coefficient of 0.8 was proposed. As a result, an impact on the risk level is introduced for different seasons.

2.1.5 Escorted Operations

It was agreed to decrease the risk of escorted operations compared to individual operations. Two options were considered here, either the track of the ice breaker should be considered as a part of the evaluated ice regime or that further adjustments to the level ice curve were made. The approach following AIRSS is to consider the icebreaker track as a separate ice regime and then evaluate the risk according to the procedure described in Section 2.1.3. The approach proposed by Finland was adjusting the RIO by a specific value to take into account the reduced risks when operating with assistance from icebreakers. To add a correction factor of + 10 to the RIO was initially suggested.

2.2 Methodology of POLARIS

The methodology of the final rules and regulations of POLARIS is explained following IMO, 2014 and IMO, 2016.

2.2.1 Risk Evaluation

POLARIS utilizes Risk Index Outcome (RIO) to assess the limitations for operation in ice. An RIO can be determined for each ice regime the ship encounters. The index determines whether the operation is within the risk limits and if it can be performed. The RIO is determined by Equation 2.1 (IMO, 2016). It is a summation of the Risk Index Value (RIV) for the present ice types multiplied by the ice concentration. The RIV is an evaluation of the relative risk for the ice class notation and the given ice regime. The ice type symbols are defined in Table 2.2 and the RIV is given according to Table 2.3. In Equation 2.1, the C represents the concentrations (in tenths) of ice types within the ice regime. The summation of all values of C is always equal to 10. Thus the total concentration is 100 %. The RIO depends on the surrounding ice regime. An ice regime can change throughout the operation, and the RIO should be defined when the ice regime changes to evaluate the changing risk. Some exceptions to the calculation of RIO exist, and they are commented on in Section 2.2.3.

$$RIO = (C_1 \cdot RIV_1) + (C_2 \cdot RIV_2) + (C_3 \cdot RIV_3) + ... + (C_n \cdot RIV_n) \tag{2.1}$$

Table 2.2: Ice Type & Ice Type Symbol (IMO, 2016)

Ice Type	Ice type Symbol
Ice free / Open water	IF / OW
New	N
Grey	G
Grey White	GW
Thin FY, 1^{st} stage	TNFY1
Thin FY, 2^{nd} stage	TNFY2
Medium FY($<$1 M)	MFY-1
Medium FY	MFY
Thick FY ice	TKFY
Second year ice	SY
Light multi year ($<$2.5 M)	LMY-2.5
Heavy multi year	HMY

2.2.2 Operational Limitations & Evaluation of Risk

Three levels of operation are defined in POLARIS to evaluate the RIO independently. The three levels are normal operation, elevated operational risk, and operation subjected to special considerations. The levels are defined in Table 2.4, according to RIO and PC.

Table 2.4: Risk Index Outcome Criteria (IMO, 2016)

RIO_{SHIP}	PC1 - PC7	Ice class below PC7 and ships not assigned an ice class
RIO $\geq$ 0	Normal Operation	Normal operation
-10 $\leq$ RIO $<$ 0	Elevated operational risk	Operation subjected to special consideration
RIO $<$ -10	Operation subjected to special consideration	Operation subjected to special consideration

For normal operation, no special considerations must be made, and the operation can continue as intended.

Table 2.3: POLARIS Risk Index Value (IMO, 2016)

Ice type Symbol	IF / OW	N	G	GW	TNFY1	TNFY2	MFY-1	MFY	TKFY	SY	LMY-2.5	HMY
Egg code / Vessel Category	**1 or 2**		**4**	**3 or 5**	**8**	**7 or 9**		**1·**	**6 or 4·**	**8·**		
PC1	3	3	3	3	2	2	2	2	2	2	1	1
PC2	3	3	3	3	2	2	2	2	2	1	1	0
PC3	3	3	3	3	2	2	2	2	2	1	0	-1
PC4	3	3	3	3	2	2	2	2	1	0	-1	-2
PC5	3	3	3	3	2	2	1	1	0	-1	-2	-2
PC6	3	2	2	2	2	1	1	0	-1	-2	-3	-3
PC7	3	2	2	2	1	1	0	-1	-2	-3	-3	-3
IA Super (Type A)	3	2	2	2	2	1	0	-1	-2	-3	-4	-4
IA (Type B)	3	2	2	2	1	0	-1	-2	-3	-4	-5	-5
IB (Type C)	3	2	2	1	0	-1	-2	-3	-4	-5	-6	-6
IC (Type D)	3	2	1	0	-1	-2	-3	-4	-5	-6	-7	-8
Not ice strengthened (Type E)	3	1	0	-1	-2	-3	-4	-5	-6	-7	-8	-8

For ships operating with elevated risk, the speed should be limited according to Table 2.5. Other operational measures, such as additional watchkeeping or use of icebreaker support, may be included. If the speed reduction affects the maneuverability of the ship, the operation should be avoided. The recommended speed limits should be included in the Polar Water Operational Manual (PWOM). For route planning, areas with potentially elevated risk should be avoided in general. If elevated risk operations are identified and included in the voyage plan, contingency plans must be in place and be documented in the PWOM.

When navigating in the ice where operations are subjected to special considerations, extreme caution should be exercised by the Master and the officers in charge of the navigational watch. If a vessel has encountered such an ice regime, then suitable procedures contained in the PWOM should be followed. These procedures contain guidance to the operator on reducing the increased risks present to the ship and should include course alteration or re-routing, further reduction in speed, and other special measures. When planning a voyage, ice regimes identified as operations subjected to special considerations should be avoided.

Table 2.5: Recommended speed limits for elevated risk operations (IMO, 2016)

Ice Class	Recommended Speed Limit
PC1	11 knots
PC2	8 knots
PC3 - PC7	5 knots
Below PC5	3 knots

2.2.3 Ice Decay, Icebreaker Escort & Glacial Ice

In general, the RIV values from Table 2.3 are to be considered unless the occurrence of ice decay. To consider other RIV values, it is necessary with definitive local data or reporting on decayed conditions. For such a case, the RIV values are adjusted by adding a value of one to Medium and Thick First Year Ice for PC5 and lower PC's.

For vessels under icebreaker escort, the ice regime is defined as the ice immediately ahead of the vessel. The ice regime must include the track from the icebreaker. If the beam of the escorted vessel is wider than the icebreaker, any unmodified ice to the extent of the beam of the escorted vessel must be considered as part of the ice regime. The icebreaker must evaluate its own risk and calculate an RIO along its intended route. The escorted operations should, in general, be reconsidered if the escorted vessel or the icebreaker is subjected to special considerations. For voyage planning with icebreaker escort, a value of ten can be added to an RIO calculated from non-escorted historical ice data. However, it must be emphasized that this is an average value that varies significantly. During operations, the RIO should be calculated according to the descriptions above and not be modified by adding a value of ten.

Operations in ice regimes containing glacial ice should be approached with caution. The presence of such ice represents additional risks to the ship. It is necessary to provide appropriate training for those in charge of the navigational watch when navigating in such areas. Training on identification and avoidance of glacial ice and the consequences of a collision. Measures to avoid glacial ice must be documented in the PWOM. When encountering glacial ice, a safe stand-off distance should be considered in addition to the RIO. The stand-off distance should be recorded in the PWOM.

2.3 Use of POLARIS

The Polar Code is as of 1 January 2017 mandatory for all new and existing vessels operating on domestic or international voyages within the IMO-defined boundaries of Arctic waters and the Antarctic area. The Polar Code requires an approved methodology to determine the operational limitations of a ship, and POLARIS is accepted as such methodology. POLARIS is therefore highly relevant for all vessels sailing within the relevant areas. (American Bureau of Shipping, 2016)

According to IMO, 2016 the purpose of POLARIS is to give a methodology for the assessment of ship-specific capabilities and limitations in different ice regimes and operational modes. Also, multiple advantages follow the methodology, and it can be considered for several purposes. According to IMO, 2016 and Hindley, 2016, POLARIS is a risk assessment tool to be used aboard a vessel in real-time, for voyage planning aboard or ashore. Also, it can be considered at the design stage when selecting the ice class of the vessel. To obtain an acceptable level of risk while exposed to different ice regimes and types of operation in ice is necessary. When planning a voyage or an operation, the structural capabilities of the ship, the ship characteristics, type of operation and current and expected ice conditions must be considered.

In real-time aboard a vessel, POLARIS is to be considered as a guide to help the Master relate the structural safety level of the ship with the visible ice. It is emphasized in the rules that POLARIS is not intended to replace the judgment of the Master. When planning a voyage, POLARIS can be consulted to verify that for the voyage, the risk level is within reasonable limits. Both aboard and ashore the structural limitations, and ice charts can be utilized when deciding the route plan. Following IMO, 2017 when planning a voyage, if there exists limited available information or uncertainty of the quality, this should be considered as a risk for the voyage planning. When designing a ship, the anticipated area of operation can be known. If the area is known, then historical data can be considered, and the limiting ice conditions in the area can be identified. Then an ice class with a low level of risk in the operational area can be selected based on the established limiting ice conditions. This way, an appropriate ice class can be selected for the designed ship.

How POLARIS can be used to perform a maritime risk assessment is investigate in Stoddard et al., 2016. By use of open-access sea-ice information, one can perform an assessment and subsequently, a risk visualization. For an observer of the maritime activity, such as the Canadian Coast Guard, areas with higher risk due to unexpected kinematic behavior can be identified. This valuable information can support several functions. It can monitor vessels to ensure that they remain safely within their operational limitations in ice. The information can be an aid in route planning and evaluation using historical data. It can also identify vessels exhibiting unexpected kinematic behavior. Such use of POLARIS can consider a large area of interest or a particular route, and be the basis for scenario risk maps for a specific ice class. Such simplified risk visualization is user-friendly and allows an understanding of the ice influence on the behavior of a vessel.

When evaluating historical maritime accidents, POLARIS can be utilized. Over the last decade in the Arctic, there exists a significant increase in maritime accidents, with eight in 2006 (ALLIANZ, 2016) and 71 in 2017 (ALLIANZ, 2018). This increase highlights that safe navigation in the Arctic is a pressing issue of concern. The study by Fedi et al., 2020, maps and performs an analysis of maritime accidents in the Russian Arctic in the period 2007-2017 through the lens of the Polar Code and POLARIS system. The study considers multiple cases and concludes that the role of ice is the determining factor in marine casualties in the period 2004-2017. It also concludes that the Polar Code, combined with POLARIS, is a valuable decision support tool and an appropriate mitigation response to ice risk. The significant importance of the officers' skills and experience to assess critical

situations accurately is emphasized.

2.4 Egg Code

The international system for sea ice symbols following WMO, 2014, is illustrated in Figure 2.3. The symbol is called an Egg Code and lists basic data concerning concentration, stage of development, and form of ice. According to Transports Canada, 2019 the Egg Codes are a standard way of reporting ice conditions and describe the observed ice conditions in a specific area. They are intended for use on ice charts. For planning and operational purposes, it is of interest to obtain accurate and timely ice and weather information. This can be obtained from the ice charts. For voyage planning or in real-time from the bridge, either historical or current ice charts may be used.

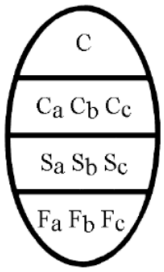

Figure 2.3: Egg Code (WMO, 2014)

One ice regime can consist of different ice types, including open water. For the various ice types within one ice regime, information regarding the partial ice type can be listed in the Egg Code. A maximum of three types of ice is described in the Egg Code. Below, the different symbols in the Egg Code are explained.

- *C:* Total concentration of ice in the area, reported in tenths.
- C_a, C_b, C_c*:* Partial concentration of thickest (C_a), second thickest (C_b) and third thickest (C_c) ice, reported in tenths. If concentration is less than 1/10 then the ice type is not reported.
- S_a, S_b, S_c Partial stage of development of ice respectively corresponding to the partial thickness. Reported following Table 2.6.
- F_a, F_b, F_c Partial form of ice (floe size) respectively corresponding to the partial thickness. Reported following Table 2.7.

The presented Egg Code is the international system for sea-ice symbols. Nevertheless, regional or national systems can have additional symbols. Adjustments can be provided as long as they do not overlap or contradict with the international system (WMO, 2014).

There exist a few minor variants of the Egg Code. These are illustrated in Figure 2.4. In general, the stage of development is restricted to a maximum of three significant classes, but in exceptional cases, some additions can be made. In Figure 2.4a S_0 is given for an ice type thicker than S_a, but with less concentration than 1/10. If any remaining classes are reported, then their stage of development is described by S_d. No concentrations are reported for these additional classes. The form of ice can be reported either as in Figure 2.3 or Figure 2.4b. For Figure 2.4b, the predominant (F_p) and the secondary (F_s) floe size are reported without any reference to stage of development and are therefore independent of S_a, S_b and S_c. If the layout of Figure 2.3 is considered and there are only two partial ice type, then a dash (-) must be reported in the place of F_c, to separate between the two variants.

Table 2.6: Egg Code: Stage of development (WMO, 2014)

Stage of Development (Ice Type)	Thickness	Symbol
New Ice		1
Nilas; ice rind	$<$ 10cm	2
Young Ice	10-30cm	3
Grey Ice	10-15cm	4
Grey-White Ice	15-30cm	5
First-Year Ice	30-200cm	6
Thin First-Year Ice	30-70cm	7
Thin FY, 1^{st} stage	30-50cm	8
Thin FY, 2^{nd} stage	50-70cm	9
Medium First-Year Ice	70-120cm	1 ·
Thick First-Year Ice	$>$120 cm	4 ·
Old Ice		7 ·
Second Year Ice		8 ·
Multi Year Ice		9 ·
Ice of land origin		▲ ·
Undetermined or unknown		x

Table 2.7: Egg Code: Form of Ice (WMO, 2014)

Element	Symbol
Pancake Ice	0
Small ice cake; brash ice	1
Ice Cake	2
Small Floe	3
Medium Floe	4
Big Floe	5
Vast Floe	6
Giant Floe	7
Fast Ice, growlers or floebergs	8
Icebergs	9
Undetermined or unknown	x

(a) Stage of Development **(b)** Form of Ice

Figure 2.4: Egg Code Additions (WMO, 2014)

Chapter 3

Observational Data

The performance of a risk evaluation procedure is necessary to maintain safe ship operations and protect the polar areas. For an evaluation to reflect the real world, data from sea ice observations should be considered. To report visual observations of sea ice has proven to be a challenge, but following Worby et al., 1999 efforts to standardize sea ice observations are made. In the software Arctic Shipborne Sea Ice Standardization Tool (ASSIST), sea ice observations are archived in the same format. Obtaining an understanding of the available data and its standardization is necessary to utilize the data for risk evaluation. In this chapter, the system for the available observational data is considered in detail. The risk evaluation procedure can be executed in the software Matlab. Implementation of POLARIS in Matlab is performed according to the standardization of data according to ASSIST. Following this, the basis for the performance of risk evaluation is found.

3.1 Data from ASSIST Data Network

To support the collection and archiving of sea ice data, the software ASSIST has been developed at the Geographic Information Network of Alaska (GINA). A possibility to record sea ice conditions for observers is established through the ASSIST software. The open-source software can record and share all observations from the Northern Hemisphere. Through the Ice Watch Program, all archived sea ice conditions throughout the Arctic Ocean are available in the same format at IceWatch, 2019. An ice watch must be conducted correctly. According to Hutchings et al., 2018 the sea ice should be recorded every hour throughout the day and night when the ship is in motion. If the ship is not in motion, then the same ice conditions can be reported several times, it is therefore recommended that the ship moves at least three nautical miles in between recordings. It is essential that the ship moves due to its propulsion power and is not drifting with the ice. If the ship drifts with the ice, then even though the ship has a new position, it is still surrounded by the same ice pack. When conducting observations, the archived ice conditions must represent the whole surrounding ice field. Therefore it is essential to view ice within one nautical mile from the vessel, have a 360 °view, and that the observation period lasts for ten minutes.

ASSIST categorizes the observational data in the four categories general, ice, meteorology, and photos. Some data is compulsory to report, but most of the input fields are optional. As a result, the extent of the data sets can vary, but the minimum of logged data must be the same. Comments from the observer can be made at any point. The following descriptions of each category are according to Hutchings et al., 2018. Insight to which form data is reported on is necessary knowledge to gain when the data is evaluated. All ASSIST header codes and data fields and codes can be found in Appendices A.1 and A.2.

3.1.1 General

Reporting data regarding the primary observer, observation date and time, latitude, and longitude are compulsory. The date and time are automatically filled out and converted to UTC from the time set on the computer. Special care must be taken when entering data regarding latitude and longitude, as the format is of importance. The position of the ship can be given either in decimal degrees, as degrees and decimal minutes or as degrees minutes and seconds (DDD.DDD, DD MM.MMM, or DDD MM SS). All formats are converted to decimal degrees, and for the conversion to be correct, the position must be logged on one of the given formats.

One can specify information about an additional observer, the ship, surrounding fauna, and notes. The ship information that can be recorded is the heading in degrees, the speed in the nearest knot, the power as fourths of full power, and the ship activity as defined in Table 3.1. The ship activity is useful information to understand the movements of the ship. Fauna can be described by entering the number of species together with the quantity of each.

Table 3.1: Ship Activity Character (Hutchings et al., 2018)

		Ship Activity (ShA)
		Not specified
10	::	Traveling in leads
20	::	Traveling in ice
30	::	Backing and ramming
40	::	On station
50	::	Traveling along ice edge

3.1.2 Ice

It is compulsory to state the total ice concentration, which is given in tenths. The different ice concentrations are defined and illustrated in Figure 3.1. The associated ice thickness is defined in centimeters but is optional to specify.

Within one region, one might encounter multiple types of ice, and all categories should be recorded. Three ice type categories can be classified, and they are referred to by decreasing thickness. The categories are defined as the primary (P), secondary (S), and tertiary (T) partial ice Type. For each category, the information described in this section can be recorded for each of the partial ice types.

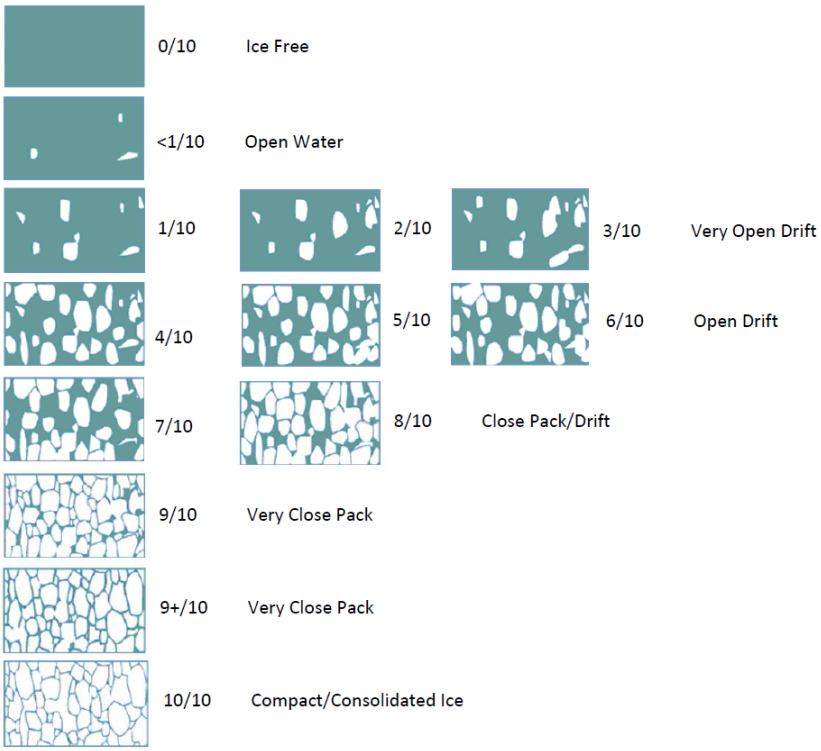

Figure 3.1: Ice Cover for various fractions (Government of Canada, 2005) (Hutchings et al., 2018)

Form description of open water described together with the ice concentration gives a detailed description of observed sea ice. The open water description refers to the form of the water openings within the ice pack. It is defined according to Table 3.2. The ice types are identified following descriptions from WMO, 2014. The different ice types can be identified from considerations of form, thickness, and whether the ice morphology indicates aging. They are defined according to Table 3.3.

Table 3.2: Open Water Character (Hutchings et al., 2018)

		Open Water (OW)
0	::	No openings
1	::	Small cracks
2	::	Very narrow breaks, $<$ 50m
3	::	Narrow breaks, 50 - 200m
4	::	Wide breaks, 200 - 500m
5	::	Very wide breaks, $>$ 500m
6	::	Leads
7	::	Polynya
8	::	Water broken only by scattered floes
9	::	Open sea
10	::	Strips and patches

Table 3.3: Ice Type (Hutchings et al., 2018)

		Ice Type (*T)
10	::	Frazil
11	::	Shuga
12	::	Grease
13	::	Slush
20	::	Nilas
30	::	Pancakes
40	::	Young Grey Ice, 10-15cm
50	::	Young Grey Ice, 15-30cm
60	::	First Year, $<$ 70cm
70	::	First Year, 70-120cm
80	::	First Year, $>$ 120cm
75	::	Second Year
85	::	Multiyear
90	::	Brash
95	::	Fast Ice

Description of the ice floe extent is defined according to the categories in Table 3.4. These floe sizes follow standard language from WMO, 2014. It is important to note that certain floe sizes are only for specific ice types. A layer of snow can be found at the ice surface. The snow type should be recorded according to Table 3.5. The mean snow depth can be reported in centimeters.

Table 3.4: Flow Size (Hutchings et al., 2018)

		Flow Size (*F)
100	::	Pancakes
200	::	New Sheet Ice
300	::	Brash/Broken Ice
400	::	Cake Ice, $<$ 20m
500	::	Small Floes, 20-100m
600	::	Medium Floes, 100-500m
700	::	Large Floes, 500-2000m
800	::	Vast Floes, $>$ 2000m
900	::	Bergy Floes

Table 3.5: Snow Type (Hutchings et al., 2018)

		Snow Type (*SY)
00	::	No snow observation
01	::	No snow, ice or brash
02	::	Cold new snow, $<$ 1 day old
03	::	Cold old snow
04	::	Cold wind-packed snow
05	::	New melting snow (wet new)
06	::	Old melting snow
07	::	Glaze
08	::	Melt slush
09	::	Melt puddles
10	::	Saturated snow
11	::	Sastrugi

The topography type of the ice is identified following Table 3.6. Also, the concentration in tenths of the fractional ice area of the specified topography type can be given. If there exist any ridges, then measurements of their heights must be performed and rounded to the nearest half meter. Also, the three following questions can be confirmed or denied. Is the topography feature old? Is the topography feature consolidated? Is the topography feature snow-covered?

Table 3.6: Topography Type (Hutchings et al., 2018)

		Topography Type (*Top)
100	::	Level ice
200	::	Rafted pancakes
300	::	Cemented Pancakes
400	::	Rafting
500	::	Ridges

If there exists surface melting, then the melt ponds (puddles) can be reported. The area covered by melt ponds for each ice type can be estimated in tenths. Further on, more detailed information regarding the melt ponds can be given. The melt pond depth, the melt pond pattern, the melt pond surface type, the melt pond freeboard, the melt pond bottom, the melt dried ice, and the rotten melt ice. How these different categories are reported can be seen in more detail in Appendix A.

The algae growth can affect the ice, and if present, the ice will have coloring. In ASSIST algae growth can be recorded in the category *Other* in the ice records. The algae density decides if the coloring of the ice is not visible, trace, light, medium, or strong. The algae concentration is recorded as the fractional coverage of algae on the specific ice type. It can be located either top, middle, or bottom of the floes. Also, the ice type can be covered in sediment. Such sediment laden ice can come as a result of ice forming on shelf seas where turbulence entrained sediments from the seafloor. The sediment concentration can be recorded as the percentage fraction of the ice type covered in the sediment.

3.1.3 Meteorology

Considerations regarding visibility are made to gain an understanding of what area of ice is represented in the observations. To report visibility is mandatory, and it is defined following Table 3.7.

Table 3.7: Visibility (Hutchings et al., 2018)

		Visibility (V)
90	::	$<$ 50m
91	::	50-200m
92	::	200-500m
93	::	500-1000m
94	::	1-2km
95	::	2-4km
96	::	4-10km
97	::	$>$ 10km

Cloud information can be reported, and the clouds are divided into the three groups high cloud, medium cloud, and low cloud. The cloud heights are reported in km, and the height interval for each of the cloud's height varies. The high cloud height is from 3 - 8 km, the medium cloud height from 2 - 4km, and the low cloud height from the water surface to 2km. Based on this, different cloud types are defined for each cloud group, and the type of clouds varies from two to five different types. The cloud cover can also be recorded where the cover for total cloud, high cloud, medium cloud, and low cloud can be recorded in eights of oktas.

More of the surrounding meteorology can be recorded. The wind speed in nearest knot, the wind direction in nearest degree, the water temperature in nearest degree, the relative humidity in nearest % and the air pressure in nearest mBar. In addition, a more detailed description of the weather can be made by eleven different categories. All categories with several more detailed descriptions. All the options can be found in Appendix A.

3.1.4 Photos & Comments

Any number of photos taken during the observation can be attached in ASSIST. The photo perspective can be defined as either not specified, port, forward, or other. Thus, the understanding of the photos' perspective is expanded. It is highly recommended that the photographs are given filenames that identify with the associated observation. Any number of comments can be attached to the observations.

3.2 Risk Evaluation Procedure in Matlab

Risk evaluation of operational limitations in ice can be performed if sea ice data is available. The methodology of POLARIS, as described in Chapter 2, is implemented in Matlab to perform such analysis. The complete Matlab code is found in Appendix B. From the open-source at IceWatch, 2019, data sets containing sea ice data are found. The data files are given as .CSV-files, but it is more user-friendly to handle them as .mat-files. The file format is therefore changed. The data format follows the descriptions in Section 3.1. For evaluation of the risk level, the RIO for each data point must be found. The RIO is calculated according to Equation 2.1. To find the RIO, the different partial ice present in the ice regime, their partial concentration, and the RIV values must be available.

The RIV is dependent on the ice type and the polar class of the vessel. In Table 3.8 the equivalent POLARIS ice type are found for the ice types as defined in ASSIST. When both the concentration and the respective RIV value is established, the RIO for the ice regime can be found. Equation 2.1 is modified for the Matlab-script and the RIO will be calculated based on Equation 3.1. Since the data from IceWatch, 2019 have a maximum of three different ice types, Equation 3.1 considers open water and three partial ice types. An evaluation of the risk can be performed when the RIO is known for each data point.

$$RIO = (10 - TC) \cdot RIV_{OW} + PPC \cdot RIV_{PT} + SPC \cdot RIV_{ST} + TPC \cdot RIV_{TT} \tag{3.1}$$

According to IMO, 2014 the ice types in POLARIS generally conform with those from WMO, 2014. The definitions in WMO, 2014 and Table 2.2 are compared with the ice types defined in ASSIST. An equivalence for the ice types are identified and is given in Table 3.8. The ice of 10, 11, 12, 13, 20, 30, 40, 50, 80, and 75 were directly transferable categories. For the rest of the ice types, certain consideration in regards to the thickness was necessary. In POLARIS, there exist two categories for thin first-year ice, medium first-year ice, and multi-year ice. ASSIST defines fewer categories for these thicknesses. The most conservative category from POLARIS is chosen for these three cases to include the most severe ice conditions. The two ice types, 90 and 95, respectively brash and fast ice, are not easy to define. Brash ice is not defined either in WMO, 2014 or Hutchings et al., 2018. According to Ashley Roach, 2018 a discussion on the treatment of brash ice is something that to include in a future review of POLARIS. Since the ice type is not included as of today, the logged data, including brash ice, is not to be considered further. For fast ice, WMO, 2014 states *Fast ice may be more than one year old and may then be prefixed with the appropriate age category (old, second-year, or multi year)*. A conservative choice is made and the heavy multi-year category is chosen.

Table 3.8: Ice Type Equivalence ASSIST and POLARIS

ASSIST	**ASSIST**	**POLARIS**
*T = 10, 11, 12, 13, 20, 30	Frazil, Shuga, Grease, Slush, Nilas, Pancakes	New Ice (N)
*T = 40	Young Grey Ice, 10 - 15cm	Grey (G)
*T = 50	Young Grey Ice, 15 - 30cm	Grey White (GW)
*T = 60	First Year, $<$ 70cm	Thin FY 2nd Stage (TNFY2)
*T = 70	First Year, 70 - 120cm	Medium FY (MFY)
*T = 80	First Year, $>$ 120cm	Thick FY Ice (TKFY)
*T = 75	Second Year	Second Year Ice (SY)
*T = 85	Multiyear	Heavy Multi Year (HMY)
*T = 90	Brash	Not defined
*T = 95	Fast Ice	Heavy Multi Year (HMY)

The data quality must be checked before the sets are considered in an analysis. The data sets can include errors or incomplete data. Since POLARIS is not defined for brash ice, no data sets, including this ice type, are considered. From Section 3.1, in ASSIST it is not mandatory to log the partial concentrations, only the total concentration. Thus, only data points with one or more partial concentrations should be considered. The total concentration must be equal to the given partial concentrations. If not, it indicates an error in the input data or missing information regarding the partial ice types. RIO can maximum have a value of 30. Since the maximum RIV value is three, and the sum of all concentrations are 10. When calculating RIO, the sum of the concentrations in Equation 3.1 must be equal to ten. If this is not the case, then it indicates incomplete data or an input error. As a direct consequence of the mentioned cases, the RIO for some data points will not be included in the risk evaluation.

Chapter 4

Simulator for Arctic Marine Structures

The software Simulator for Arctic Marine Structures (SAMS) is used to perform predictive simulations of a structure advancing in an ice field. In this chapter, the basis and theory for SAMS are described in detail. Validation of the software is described. An understanding of the software and its simplifications and limitations is essential for the evaluation of results. The information in the chapter follows Berg, M. van den, 2019, if nothing else is stated.

The recent increase of activity in the Arctic has led to an increased need for more cost-effective analysis based on numerical solutions. There exists little experience from relevant operations due to the high expenses from full-scale tests. Therefore a simulation tool of sufficient quality will have significant benefits. As described in Raza et al., 2019 and Lubbad, Løset, et al., 2018, a spin-off company from the Norwegian University of Science and Technology (NTNU) called Arctic Integrated Solutions AS (ArcISo) released a numerical model for the analysis of offshore and coastal structure in Arctic conditions in 2017. The software package was based on research performed during the Centre for Research-based Innovation – Sustainable Arctic Marine and Coastal Technology (SAMCoT), and it was called Simulator for Arctic Marine Structures (SAMS). SAM-CoT laid the foundation for a versatile and highly accurate high-fidelity numerical simulator for offshore structure in various ice conditions such as level ice, broken ice, and ice ridges.

SAMS is a 3-dimensional multi-body time-domain simulator specifically designed for the simulation of ice-structure interaction. According to Lubbad, Løset, et al., 2018, SAMS consists of the following three building blocks: The non-smooth discrete element modeling (NDEM) or multi-body dynamics module, the fracture module, and the hydrodynamic module. These blocks agree with the more complementary key aspects of SAMS, according to Berg et al., 2019, which are listed below.

- Accurate contact force prediction based on multi-body dynamics, ice material properties, and exact contact geometry.
- Ice failure based on the occurring contact forces, using analytical solutions.
- Ship and ice floe hydrodynamics, including drag, added mass, and hydrostatic buoyancy.

The time-domain simulation in SAMS generally follows eight steps in one loop. The steps are illustrated in Figure 4.1.

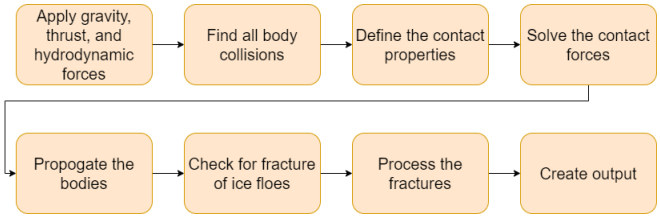

Figure 4.1: Simulation Loop SAMS

The created output contains loads from the ice on the structure. These loads are a result of the interaction between dynamic bodies. The hydrodynamic forces are first applied. For the ice floes, this includes hydrostatic forces from the submerged geometry and drag forces. For the structure, there are user-specified drag forces and added mass. In every time step, it is performed collision detection, and the contact forces are solved. There exist two types of contact forces, compliant and rigid, where the compliant contact force can result in ice failure. Two types of ice failure exist, splitting and bending failure, and it is based on the occurring contact forces and their magnitude whether ice failure occurs or not.

4.1 Bodies

Each dynamic body consists of geometry information and has six degrees-of-freedom (DOF's), three transitional and three rotational. Elastic deformation within the bodies is not taken into account. SAMS defines the following three different body types: the structure bodies, the ice bodies, and the confinement bodies.

It is of interest to assess the ice loads under certain ice conditions on a specific object. A rigid structure body represents this object. Thus there is no deformation or failure of the structure. The motion of the structure is fully dynamic. The structure bodies can interact with the simulation world with two different mechanisms, either rigid or flexible. Through these mechanisms, the structure is connected to a virtual point in the simulation, which can either be static or move with constant velocity. If rigidly connected, then the structure will follow the virtual point with no deviations. Thus, it will not dynamically react forces, and non-contact loads are not calculated. For the flexible interaction mechanism, the structure is flexibly connected to the virtual point. Then it can react dynamically, and the non-contact forces are taken into account. These non-contact forces are gravity, buoyancy, hydrodynamics, and thrust.

There are two types of ice bodies, the finite level and level ice bodies. The finite level ice bodies represent ice floes of finite size with level, uniform thickness. These bodies are fully dynamic, may fail in splitting and bending, contain inertial properties, and velocity information, which is necessary for dynamic simulation. Also, the finite level ice bodies contain ice material properties needed for calculation of contact force. The infinite ice bodies represent level ice with a size equal to the field domain. They will not dynamically react to forces due to the infinite assumption giving infinite mass. Infinite ice bodies will not split in failure as the infinite level ice is not bounded in the horizontal direction.

The domain can have two types of confinements of static bodies, vertical walls and a horizontal bottom. The vertical walls do not interact with the structure bodies but can interact with the ice floes and prevent them from leaving the domain.

4.2 Collision Detection and Contact Processing

For the detection of collisions, the collision algorithms from the Buller Physics Engine are used. For each time step, first, broad collision detection is performed to find potential collisions. For this, the dynamic axis-aligned bounding box is used. In the algorithm, the body is approximated by a bounding box, before checking if any of the boxes overlap. Such overlapping indicates possible contact and potential collisions. For the cases with possible contact, a mid-phase collision detection algorithm is considered, the Gilbert-Johnsen-Keerthi (GJK) distance algorithm. The GJK algorithm is efficient and determines first if there is a collision or not, and secondly, it identifies one or more contact points and their normal directions.

When contact has been detected, contact information must be obtained for the contact force to be calculated in the solver step. There are four types of contact in SAMS, and which contact is applicable depends on what body types are in contact, the location of contact relative to the location of the structure, and the size of ice bodies in contact. The accuracy of the applied processing algorithm depends on the importance of the contact and the prediction of contact forces. The four types of contacts are rigid contacts, rigid contacts with an upper limit, compliant ice - non-structure contacts, and compliant ice - structure contact. The body type, structure region, and floe sized determines the type of contact. Figure 4.2 illustrates how to distinguish between the different contacts. The structure region is determined to decide which contacts are in the vicinity of the structure. This is important since the contacts close to the structure may impact failure events. The size of the floes will impact the processing of the ice-structure contact and whether the contact is considered rigid or compliant.

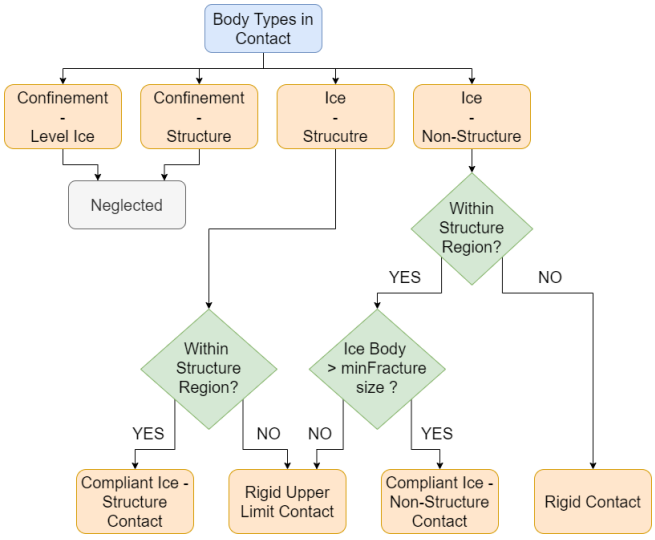

Figure 4.2: Contact type flow chart (Berg, M. van den, 2019)

Rigid contacts are considered the contacts are far from the structure. These contacts are considered to be fully plastic. The contact points and normal directions found in the GJK algorithm are used in the solver.

Rigid contacts with an upper limit have a contact force with a defined upper limit. This limit is dependent on the crushing specific energy (CSE) and a user-defined upper limit area (A_l). From Equation 4.1 the force upper limit can be found. It is necessary with an upper limit, because if not the assumption of rigid contact will give time-dependent forces that may grow very large when small time steps are considered. The limited size of the ice floes justifies the upper limit. These rigid forces should be time-averaged when considering the resistance since the peaks are not meaningful.

The time-average resistance is considered accurate enough. The rigid forces are named *Rubble Forces* in the output of SAMS. The rubble forces should be time-averaged by seconds, and before the evaluation of the results can start. The forces will be time-averaged by every third second.

$$F_{max} = CSE \cdot A_l \tag{4.1}$$

For some contacts, an accurate prediction of the contact force is important, for such cases compliant contacts area considered. For all compliant contacts, ice failure may occur. Figure 4.2 illustrates the contact determination process. To define the contact compliance parameters the exact contact geometry must be determined. These parameters can then be considered in the solver when performing computations on contact forces. The body geometry is considered to determine the overlap of geometry points and planes, such that the contact geometry can be found. It is assumed that local contact crushing will occur so that the contact compliance parameters can be found. A constant energy dissipation per unit crushed volume of ice, the CSE, is assumed in SAMS. Following this, the crushing pressure will be constant. The CSE and the projected contact area (A_{proj}), will define the contact force where crushing starts (F_{cr}) as determined by Equation 4.2. While the increase in the contact force (F) with penetration (δ) is determined by Equation 4.3. The force-penetration gradient ($\frac{\Delta F}{\Delta \delta}$) represents that the energy from the contact area increase with penetration. A_{proj}^{prop} defines the contact projected area when the contacting bodies are propagated with their current velocity.

$$F_{cr} = A_{proj} \cdot CSE \tag{4.2}$$

$$\frac{\Delta F}{\Delta \delta} = \left(\frac{(A_{proj}^{prop} - A_{proj})CSE}{\Delta \delta} \right) \tag{4.3}$$

For ice-ice and ice-structure, the contact coefficients will be determined differently since the structure geometry does not deform. The difference is illustrated in Figure 4.3. A and **n** are respectively the contact project area and the contact normal.

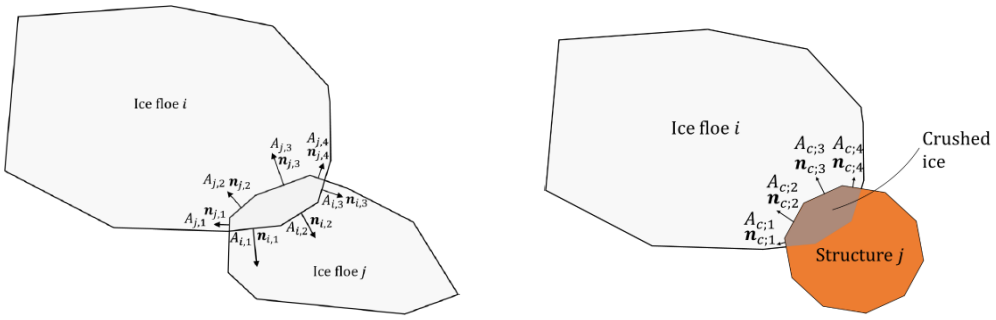

(a) Ice-Ice Contact **(b)** Ice-Structure Contact

Figure 4.3: Compliant Contacts in SAMS (Berg, M. van den, 2019)

The compliant contact behavior can be viewed as hysteric damping, where the crushing of ice dissipates all available kinetic energy. SAMS distinguishes by the following three types of compliant behavior; the crushing contact, the resting contact, and the separating contact. The crushing contact is when the ice crushes and the penetration of ice increases as crushing force are exceeded so that further penetrations are not prevented. The resting contact is when the relative contact velocity is zero between the interacting bodies. Then the penetration remains the same, and the crushing force is not exceeded, but the resting contact remains. The separating contact is when the relative contact velocity is negative, and the contact penetration decreases. This results in the contact force dropping to zero.

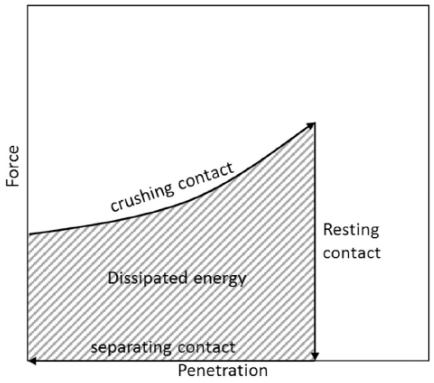

Figure 4.4: Loading-unloading curve for ice-ice or ice-structure contact

4.3 Contact Force Solver

To solve the contact forces and body dynamics, SAMS uses an implicit method where both rigid and compliant contacts can be handled. A mixed linear complementarity problem (MLCP) is solved in each time step for all contact forces within a network. In SAMS the MLCP in Equation 4.4 is described on compact format. The solver is based on the Gauss-Seidel method and is solved by consideration of a proprietary iterative solver. More detailed descriptions of these methods can be found in Berg et al., 2019.

$$\begin{bmatrix} \mathbf{M} & -\mathbf{J_h} & -\mathbf{J_c} \\ \mathbf{J_h^T} & \sum_{\mathbf{h}} & \mathbf{0} \\ \mathbf{J_h^T} & \mathbf{0} & \sum_{\mathbf{c}} \end{bmatrix} \begin{bmatrix} \Delta\dot{\mathbf{u}} \\ \lambda_{\mathbf{h}} \\ \lambda_{\mathbf{c}} \end{bmatrix} + \begin{bmatrix} \mathbf{0} \\ \mathbf{Y_h} \\ \mathbf{Y_c} \end{bmatrix} = \begin{bmatrix} \mathbf{0} \\ \mathbf{0} \\ \alpha \end{bmatrix}, \quad 0 \leq \lambda_{\mathbf{c}}^{\mathbf{T}} \perp \alpha^{\mathbf{T}} \geq 0 \tag{4.4}$$

The parameters in Equation 4.4 is explained in the following. **M** is the diagonal mass matrix containing the inertial properties for all bodies within the simulation. $\mathbf{J}_h$ and $\mathbf{J}_c$ are matrices containing constraints Jacobians, which express the influence of contact impulses on body velocities. $\Delta\dot{u}$ is a vector containing the velocity change (both linear and rotational) of each body in the simulation domain. λ_h and λc are vertices containing the constraint impulses, which express the time-integrated contact forces within one time step. $\sum_h$ and $\sum_c$ are matrices containing the impulse dependent compliance factors. $\mathbf{Y}_h$ and $\mathbf{Y}_c$ contain the compliance factors which are independent from the contact impulses. α is a vector of residuals with no physical meaning. The subscripts are; h - holonomic constraints, i.e., no upper or lower limits to the impulses. c - non-holonomic constraints, i.e., the constraints for which upper and lower limits bound impulses.

The contact compliance parameters $\sum$ and **Y**, are derived by consideration of the equation of motion and considering constant average acceleration in each time step. The derivation can be study in detail in Berg, M. van den, 2019.

4.4 Fluid Forces

The effects of hydrodynamics are present since the interaction between the structure and ice occurs in the fluid domain. The current version of SAMS include possible drift simulations due to wind and current, hydrostatic forces due to buoyancy, hydrodynamic forces drag forces and added mass and the propeller flow.

Wind- and current can be applied in SAMS, and their forces on the structure and ice floes can be calculated. The hydrostatic force on submerge bodies is calculated based on the volume and centroid of the submerged body. If the top of an ice floe is partly submerged, then ventilation will occur. Ventilation is the delay in the backfill of water on the ice floes.

The hydrodynamic drag force on a rigid body is typically considered as the combination of the so-called pressure drag and skin-friction drag. The pressure drag arises because of the shape of the body and follows the quadratic drag equation. It is higher for bodies with a larger presented cross-section and increases with the flow velocity. The skin friction is caused by the viscous forces in the boundary layer at the body/fluid interface. It is directly related to the wetted surface of the body and rises with the square of the velocity component parallel to the wetted surface. The total hydrodynamic drag force on the structure is calculated as the sum of the quadratic drag due to pressure, arbitrary linear drag, skin friction in the boundary layer, and a custom force defined by the user.

The structure effects of added mass can be modeled, and a constant added-mass matrix can be considered. From the propeller flow, a wash effect on the ice floes can be found. In the current version of SAMS, only the axial component of the propeller flow is considered as it is assumed to be dominant. Due to the propeller thrust, there will be an acceleration of the velocity of the fluid behind the vessel. The wake of the thruster will impact the dynamics of the ice and make additions to the drag forces.

4.5 Ice Fracture

Ice fracture due to ice-structure interactions has a vital effect on the ice loads on the structure. The process can be considered as a load releasing mechanism as ice forces exerted on the structure can not be larger than the strength of the ice feature. The ice loads may differ depending on the failure pattern. The failure pattern may vary depending on the interaction with the structure, the contact properties, the interaction speed, the ice material properties, and the surrounding ice conditions. Analytical solutions are considered in order to analyze which failure mode is the most probable one and the one leading to the lowest ice loads during the ice-structure interaction. Specific failure modes are assumed in advance, thus excluding some potential failure modes. Also, these analytical methods are often valid only for idealized ice geometries.

For compliant contacts, the three most common failure modes are included in SAMS. These are contact crushing, bending, and splitting. SAMS assumes that local contact crushing will occur, and overlapping bodies represent this. For a detected compliant contact, the overall logic of the fracture algorithm for each time step is illustrated in Figure 4.5. The fracture algorithm can lead to either a local or a global failure. The splitting failure mode is a global, in-plane failure. While bending is an out-of-plane local failure. For a failure mode to happen, the available contact force must be less than the force criterion for each of the possible fractures.

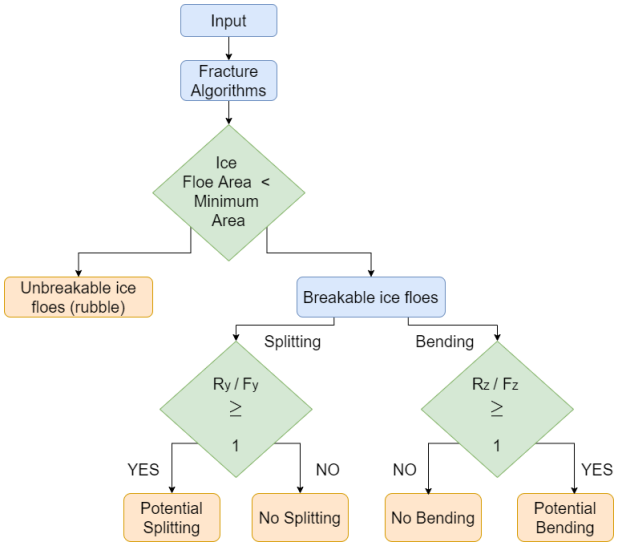

Figure 4.5: Overall logic of the fracture algorithm within SAMS at each time instant (Berg, M. van den, 2019)

R_Y is the available contact force in the splitting direction, as found from Equation 4.5 by solving Equation 4.6. The bending force R_Z is the available contact force in the vertical direction, which may lead to the bending failure, found from Equation 4.7. The contact forces are functions of time and usually increases from zero and to the force criterion.

$$\mathbf{R}_Y = CSE \times (\sum A_{c,i}^{right} \mathbf{n}_{c,i}^{right}) \cdot \mathbf{n}_y \tag{4.5}$$

$$0 = CSE \times (\sum A_{c,i} \mathbf{n}_{c,i}) \cdot \mathbf{n}_y \tag{4.6}$$

$$\mathbf{R}_Z = CSE \times (\sum A_{c,i} \mathbf{n}_{c,i}) \cdot \mathbf{e}_3 \tag{4.7}$$

Equation 4.8 states the global splitting force criterion and Equation 4.9 states the local bending force criterion. If either one of these criteria is fulfilled, then the respective failure will occur. In some cases, both force criteria are exceeded, and then it must be decided which failure mode to consider. The force which exceeds its criteria with the most is considered as the final failure mode.

$$R_Y / F_Y \geq 1 \tag{4.8}$$

$$R_Z / F_Z \geq 1 \tag{4.9}$$

4.5.1 Splitting Failure

The global splitting failure has two types of contact, the centric and off-center contact. Following Lubbad, Loset, et al., 2018 the centric force component is found according to Equation 4.10. The off-centre force component is found according to Equation 4.11. The parameters are described in Table 4.1.

$$F_Y = \frac{t\sqrt{L}}{H(a,0)} K_{IC} \tag{4.10}$$

$$
\begin{aligned}
F_Y &= \frac{f(A_0/W_1)}{tK_{IC}\sqrt{W_1}} \\
f(A_0/W_1) &= \sqrt{\frac{\pi}{\pi^2-4}}\left(\frac{A_0}{W_1}\right)^{-\frac{1}{2}} + \sqrt{6}\left[1+\frac{0.3532}{(A_0/W_1)^{\frac{1}{2}}}+\frac{0.0116}{(A_0/W_1)^1}\right]\left(\frac{A_0}{W_1}\right)
\end{aligned}
\tag{4.11}
$$

The splitting crack often kinks into the direction of the closest border. This is after a crack kink algorithm is introduced and considered for all scenarios. Following these implementations, a smaller ice piece will be produced. Thus, more effort must be made in the forthcoming simulation loop to break more ice. The splitting failure can easily travel in order of magnitude larger than the structural size. Most of the situations for splitting failures are in between the two simplified extreme situations of centric or off-center. Therefore SAMS calculates both and considers the minimum of the force components further.

Table 4.1: Global Splitting Failure Parameters (Berg et al., 2019) (Lubbad, Loset, et al., 2018)

h	Sea ice thickness [m]
K_{IC}	Fracture toughness of sea ice [kPa$\sqrt{m}$]
L	Length of defined bounding box [m]
W	Width of defined bounding box [m]
H(a,0)	Weight function of rectangular ice floe with a centered edge crack (Dempsey and Mu, 2014)
A	Crack length [m]
a	non-dimensional crack length given by a = A/L
A_0	Length of initial crack [m]
W_1	Distance from contact point to the closest edge [m]

4.5.2 Bending Failure

Local failure is defined as the failures which occur within two times the characteristic length of a plate on an elastic foundation. In SAMS, the local failure considered is the out-of-plane bending. Equation 4.12 is employed when calculating the contact force component F_Z.

$$
F_Z = \begin{cases} \frac{\sigma_f t^2}{3} tan(\frac{\alpha}{2}) \left[1.05 + 2\frac{\delta}{l} + 0.5(\frac{\delta}{l})^2\right] & (\alpha \leq 90) \\ \frac{m\sigma_f t^2}{3} tan(\frac{\alpha}{2m}) \left[1.05 + 2\frac{\delta}{l} + 0.5(\frac{\delta}{l})^2\right] & (90 \leq \alpha \leq 180) \end{cases}
\tag{4.12}
$$

Bending failure is a type of flexural failure mode. The ice fail in a "radial cracking" feature, and the current version of SAMS has implemented bending failure formations of circumferential cracks. The consequence of this is that for smaller ice floes, the radial cracking criteria are higher. Besides, there exists an effect of the speed as the increase in speed will decrease the bending radius. This will have an impact on the size of the rubble ice.

Table 4.2: Local Bending Failure Parameters (Berg et al., 2019) (Lubbad, Loset, et al., 2018)

σ_f	Flexural strength of sea ice [kPa]
h	Sea ice thickness [m]
α	Wedge angle of where the local bending occurs [deg]
δ	Maximum penetration depth [m]
m	Number of wedges that are bent off from the original ice sheet
l	Characteristic length of sea ice [m]

4.6 Validation

SAMS has been validated in several validation studies, where the result from SAMS has been compared with real data measurements from icebreakers. The studies Lubbad, Loset, et al., 2018 and Raza et al., 2019 are validations studies with measurements from respectively level ice conditions and broken ice conditions. From these two studies, it is confirmed that the numerical modeling results from SAMS are valid.

In the study Raza et al., 2019, numerous simulations of Oden transiting in level ice with constant heading and speed in SAMS are performed. The results from the simulations are used together with the full-scale net-thrust curve of Oden to derive the relationship between the ice thickness and the maximum velocity of Oden, the h-v curve. The h-v curve from the simulations is compared with full-scale h-v curves. The comparison shows that the results are favorable and that the measurements from the numerical modeling results and the full-scale measurements are in good agreement.

In the study Lubbad, Loset, et al., 2018, a comparison between average values and standard deviations of simulations results and full-scale data is performed. During the Oden Arctic Technology Research Cruise 2015 (OATRC2015), data regarding performance from the icebreakers Oden and Frej were collected. From the performance data, the scenario could be recreated in SAMS, and the average value and standard deviation for the ice load in surge direction and the velocity in surge direction could be found for both the full-scale data and the simulation. When comparing the difference between the simulation results and the full-scale data results, it is found that for the average values of ice loads and velocity, the simulation deviates with less than 5 %. The standard deviation for the ice loads has a difference of around 1 %, which is a remarkable small difference. Though it must be expressed that this should be treated with caution since the standard deviation is calculated from filtered simulations. The standard deviation for the velocity in surge direction is 3.8 times higher for the simulation than in reality. This is most likely because of the difference between the ice fields in the simulation and the full-scale fields.

Chapter 5

Assessment of Data and Risk

Data from the ASSIST Data Network is available at the open-source IceWatch, 2019. All presented data in this chapter is from IceWatch, 2019. In this chapter, an evaluation of the accuracy and relevance of the sea ice data is performed. Based on data from different vessels, some representative areas are defined. Relevant data sets within these areas are considered for further evaluation. Then differences in ice conditions and risk levels between the fields are identified. Further, for two individual cases, the evolvement of risk during the voyage is investigated to identify any risk patterns. The level of risk is directly dependent on the ice conditions, and the speed is, in general, chosen based on the surrounding ice conditions. Thus, the level of risk and the speed are not directly connected, but in this chapter, the influence of speed on the risk will be evaluated. First, it must be considered if the data sets from IceWatch, 2019 include enough speed data. The data sets that meet this requirement are considered to find a correlation between the speed and the risk level.

5.1 Evaluation of Available Observational Data

As described in Chapter 3, there exist multiple parameters to describe an ice regime in ASSIST. When evaluating the risk involved in operations in ice areas, this information can be of great use. It is of interest to evaluate the available data and investigate how it can be used in an analysis. Information regarding all available data is listed in Table 5.1. The data points represent how many times ice conditions were reported during one voyage, and photos and speed list if data is available and from which year.

At the open-source IceWatch, 2019, data from 53 voyages are available. Taking a closer look at the content of each data set in Table 5.1, large variations is observed in the individual data sets. Variations in the number of data points, speed and photos can be identified. The data must be representative for the actual ice conditions to utilize the information. It is necessary to have access to enough, correctly logged data to obtain a certain quality of the data. With more extensive data sets, there is a greater chance that the data is representative of a larger surrounding area. Following this, it is easier to discover deviations indicating incorrect logging. It is difficult to determine the necessary number of data points to obtain the correct quality of the data. To substantiate an evaluation of the data quality one can consider the number of data points, the extent of the time period and the movements of the ship, this can substantiate an evaluation of the data quality. Despite changing ice conditions from different years, identifying similarities and trends from one area should be possible and can substantiate a quality check.

Table 5.1: Observational Data

Vessel	Year	Data points	Photos	Speed
RV Akademik Fedorov	2013	0	No	No
CCGS Amundsen	2018	10	No	No
IB Araon	2012	0	No	No
RV Arctic Sunrise	2012	0	No	No
MS Expedition	2016	8	No	Partly
USCGC Healy	2011, 2015, 2018	66, 25, 64	No	Partly 2018
RV Kronprins Haakon	2018(2)	34, 98	No	2018(2)
RV Lance	2012, 2013, 2014(2), 2015(3), 2016, 2017	115, 36, 112, 34, 152, 113, 90, 104, 61	2017	2014(2), 2015(3), 2016, partly 2017,
RV Oden	2012, 2013, 2018	64, 74, 97	No	2018
IB 50 let Pobedy	2015, 2016, 2017, 2018(3), 2019(3)	41, 32, 41, 18, 15, 17, 23, 20, 10	2019(3)	2015, 2016, 2017, 2018(3), 2019(3)
RV Polarstern	2012, 2014, 2015, 2017, 2018	260, 285, 192, 24, 329	2018	2015, 2018
RV Sikuliaq	2015, 2019	407, 299	No	2019
CCGS St. Laurent	2006 - 2018	320, 362, 88, 195, 77, 195, 40, 327, 191, 502, 65, 79, 161	No	2015, partly 2016, 2017, partly 2018
KV Svalbard	2015	24	No	No

In Table 5.1 three vessels, RV Akademik Fedorov, IB Araon and RV Arctic Sunrise, are listed despite no existence of data. This result in a misinterpretation of the extent of the available data. The vessels CCGS Amundsen and MS Expedition have logged respectively 10 and 8 data points. As mentioned, it is difficult to verify the quality with small data sets. In further analysis, these data sets will not be under consideration. IB 50 let Pobedy have data sets with only 10, 15 and 17 data points, but the sets are from the same year, same season and have comments from the observer which substantiates the data logging. Thus, the three data sets from each year validate each other.

The route of each voyage is given in latitude and longitude coordinates. It is of interest to evaluate areas with a higher concentration of available data sets because it will provide a more detailed result, and deviations and errors will be more visible. Figure 5.1 illustrate all routes and four different areas are defined. The voyages located outside the specified areas or which consist of unsatisfying data sets, are not considered anymore. Out of 53 data sets, only 41 is still under review. From Figure 5.1 deviations from the overall pattern are identified and can indicate potential errors in the input from the observer. In the Fram Strait, the voyage of Oden in 2012 is identified with significant differences. In Table 5.2 the time and position of the three last data points are listed. Such movement in less than 24 hours is highly unlikely and implies an error in the input. Such errors are essential to be aware of as they will give the wrong information regarding the ice conditions at the specified location. The data set will be considered in the analysis, with the assumption of a wrongly logged position.

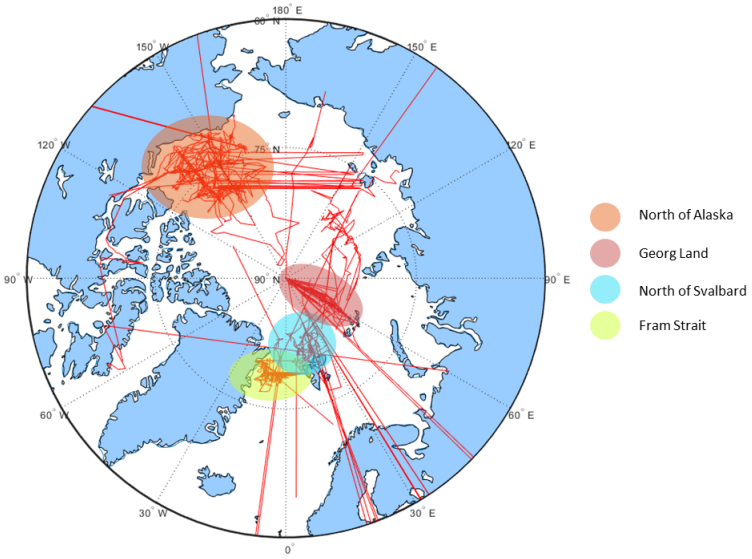

Figure 5.1: All routes and defined areas

Knowing that input errors from the user exist, it is important to verify the data. With the existence of two open-sources, verification is possible. Ice conditions could be verified with photos of the conditions. From Table 5.1 it is established that photos are rare. To be sure the data is credible, only data from areas with multiple large data sets will be considered. Thus, any remarkable deviations could be identified. Sometimes written comments are attached to describe the conditions and they can verify the logged data. Unfortunately, written comments are not common practice.

Table 5.2: Excerpt of data from Oden 2012

Date	LAT	LON
2012-09-12 06:04:00 UTC	81.7865	-3.9876
2012-09-13 05:05:00 UTC	45.5850	-8.5008
2012-09-13 18:04:00 UTC	81.0001	-3.0987

5.2 Polar Class Vessels

For the RIO the polar class of the vessel is of relevance, but the relevant vessels have ice classes defined by different classification societies. Since all rule systems regarding ice class are unique, it is not easy to establish an exact equivalence to the IACS Polar Class. To find the equivalent polar class for all vessels Daley, 2014 is considered. In Table 5.3 the ice class notation for all relevant ships are listed with the IACS Polar Class Equivalent. It is commented on the most uncertain equivalent polar classes.

Table 5.3: Vessel Ice Class Notation

Vessel	Ice Class	Ice Class Reference	IACS Polar Class Equivalent
USCGC Healy	Medium Icebreaker	Wikipedia, 2020	PC2 *
RV Kronprins Haakon	Polar Class 3	ARICE, 2020d	PC3
RV Lance	DNV ICE-1A	Norwegian Polar Institute, 2017	PC7
RV Oden	GL100 ABS A5 AC3	ARICE, 2020a	PC1 **
IB 50 let Pobedy	Russian LL1 Class	Ship Technology, 2020	PC1 ***
RV Polarstern	GL 100 A5 ARC3	ARICE, 2020b	PC2
RV Sikuliaq	Polar Class 5	ARICE, 2020c	PC5
CCGS Louis St. Laurent	Arctic Class 4	Government of Canada, 2020	PC3
KV Svalbard	DNV GL Icebreaker Polar 10	Wikipedia, 2019	PC4

* Since it is an icebreaker, it is most likely either PC1 or PC2. To not overestimate its structural properties, consider it to be PC2.

** Due to American Bureau of Shipping notation ABS A5, consider it to be PC1.

*** Is a Russian nuclear icebreaker, therefore consider it to be PC1.

5.3 Evaluation of Areas

In this Section, each area is evaluated separately according to extension and accuracy, before the characteristics of the areas are analyzed. From Figure 5.1 it is identified which voyages are relevant for each area. The software Matlab is utilized to handle a large amount of data. In Appendix B the Matlab codes for evaluation of risk can be found. The code for one area is given as an example and the format is representative for all.

Table 5.4 lists the 15 relevant routes north of Alaska. Figure 5.2 illustrate the routes and highlights deviations in the data. For USCGC Healy in 2018, it is discovered that as a consequence of the alternating longitude sign, the voyage includes the East Siberian Sea. From IceWatch, 2019 it is known that the USCGC Healy voyage of 2018 was part of the SODA project, located in the Beaufort Sea. Therefore it is concluded that the voyage took place at only western longitudes. For CCGS St. Laurent in 2017, the voyage is located in the East Siberian Sea. According to Williams and Zimmermann, 2017 the objective of the voyage was to contribute to the Joint Ice-Ocean Study and Beaufort Gyre Exploration Program. Since the study is of the Beaufort Gyre, it is assumed that the longitudinal coordinates should be given as western. A few single lines are outside the defined area. These are identified as user errors according to the reasoning in Section 5.1. All voyages in Table 5.4 are evaluated further.

Ship	Year
USCGC Healy	2018
RV Sikuliaq	2015 & 2019
CCGS St. Laurent	2006, 2007, 2008, 2009, 2010, 2012, 2013, 2014, 2015, 2016, 2017 & 2018

Table 5.4: North of Alaska IceWatch, 2019

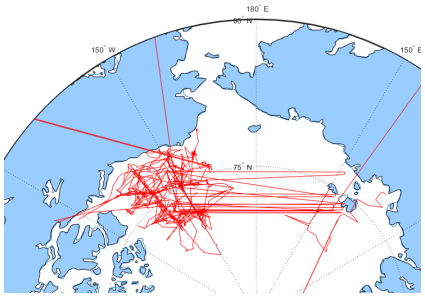

Figure 5.2: All routes North of Alaska

Table 5.5 lists the ten routes in the Fram Strait, these are illustrated in Figure 5.3. Deviations which originates from RV Oden in 2012 and RV Polarstern in 2014 are identified. Following closer consideration of the data and similar reasoning as in Section 5.1, it is established that the deviations are due to logging errors by the user. Thus, all data from the voyages listed in Table 5.5 is to be considered.

Ship	Year
RV Oden	2012 & 2013
RV Lance	2012, 2013, 2014, 2015, 2016 & 2017
RV Polarstern	2014
RV Kronprins Haakon	2018

Table 5.5: Fram Strait

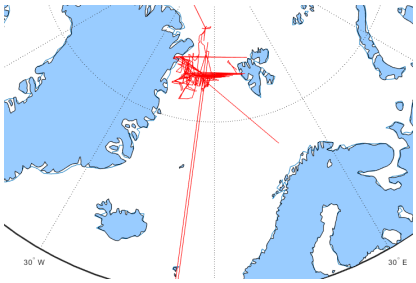

Figure 5.3: All routes Fram Strait

Table 5.6 lists the eighth routes north of Svalbard and Figure 5.4 illustrate these. Multiple positions of the vessel deviate from the defined area. These deviations are identified from the voyages of KV Svalbard of 2015, RV Polarstern of 2017 and RV Oden of 2018. Following closer consideration of the data and similar reasoning as in Section 5.1, it is established that the deviations are due to logging errors by the user. Thus, all data from the voyages listed in Table 5.5 is to be considered.

Ship	Year
RV Lance	2014 & 2015(2)
KV Svalbard	2015
RV Polarstern	2015 & 2017
RV Oden	2018
RV Kronprins Haakon	2018

Table 5.6: North of Svalbard

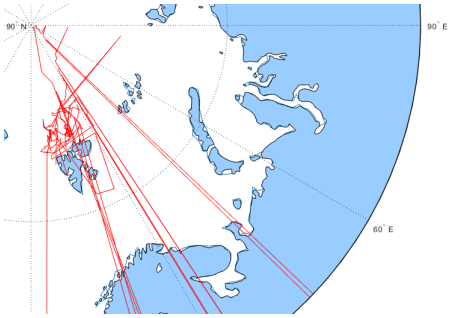

Figure 5.4: All routes Svalbard

Table 5.7 lists the eighth routes from Georg Land and Figure 5.5 illustrate these. Non clear deviations from the routes can be identified in the illustration.

Ship	Year
IB 50 let Pobedy	2015, 2016, 2017, 2018(3) & 2019(3)

Table 5.7: North of Georg Land

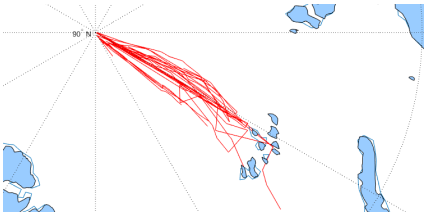

Figure 5.5: All routes Georg Land

According to Section 3.1 numerous information can be reported in each data set. A certain consistency is of importance when the data is compared. To report the time and total concentration is compulsory, though in general, the open water characteristics and one or more partial ice types are reported. The more information included in the data set, the larger the understanding one can obtain about the ice conditions. Reporting of multiple partial ice types are in general, not made for all data points. In most cases, the number of primary ice types is somewhat less than the number of data points. For secondary ice types, the number is decreasing, and tertiary ice types are only included for a small share of the total number of data points. With the exception of Georg Land, where both the primary and secondary ice types are given for almost all data points. More detailed information regarding each voyage can be found in Appendix C. On main advantage with POLARIS is that it describes more complex ice conditions, but from the reported data it can be seen that it is most common to only describe one partial ice type. Thus, POLARIS can not be exploited to its fullest.

The total number of data points for each voyage varies greatly. The voyages vary in length, and it is of interest to study the time step between each logging to compare the consistency. The number of reported data points per sailing day in ice is found, due to no distinct pattern in the time steps. For each of the areas, the average each ice day varies with a wide range. The average between all voyages is around ten for Alaska, eight for the Fram Strait, four for Svalbard, and five for Georg Land. From this information, it is observed little consistency between the logging procedure of the data sets. Therefore it is considered that the data sets are extensive and accurate enough to be evaluated further.

Ice conditions vary through the year and the season must be taken into account. The date and time of each data point are available through IceWatch, 2019. A summarize of the main trends are found in Table 5.8. For Alaska, most of the data sets are from August, September and October, in addition to some contributions from July and November. In general, the period of the samplings is between 20 and 30 days, though both higher and lower exceptions exist. For the voyages in the Fram Strait, most of the data is collected in August and September. Except for the RV Polarstern in July of 2014 and RV Lance in May of 2017. The period is shorter than for the Alaskan waters, varying around 15 days. North of Svalbard, there is a large variety of the time of year when the voyages were completed. KV Svalbard of 2015 was in January, the voyages with RV Lance varies from February to June, the voyages for RV Polarstern is from the end of May until mid-June, while the voyages for Rv Oden and RV Kronprins Haakon in 2018 took place in August and September. Overall the dates vary from January until September. Thus, there must be considered significant seasonal changes in the data. Also, the length of the voyages differs significantly from one week until many months. For Georg Land the data sets are from the end of June, July and until mid-August. The length of the voyages varies from a few days to a couple of weeks. For the data sets of the shortest period, there are other data sets from the same year and close in time. There exist some differences as to which period the data was collected. However, most data sets are from the summer and early autumn, except for those from Svalbard, where they variate from January to June. When considering the ice conditions, this must be taken into account, as the conditions from Svalbard are likely to be more severe in winter than during the summer.

Table 5.8: Voyage Time and Length

Area	Voyage Month	Length of Voyage
Alaska	August - October	20 days - 30 days
Fram Strait	August - September	15 days
Svalbard	January - September	one week - months
Georg Land	June - Mid-August	a few days - couple of weeks

Data is not always reported every day and no reason is given for this inconsistency. One reason could be that many of the vessels are doing research and in periods might not move considerable distances. As defined in Section 3.1, the ships must move a certain distance before data is logged. Another reason could be that the vessel is not moving in ice every day. The number of ice days is found, as the days the total concentration is zero. Finding the number of days for the voyage, the number of days with data reporting and the number of ice days. When comparing these, for many of the voyages, the data logging's are consistent with the number of ice days. Though without any stated reason, it is difficult to know the real reason. Most of the data sets have logged data for 70 % of the duration of the voyage. For some, the ratio is much lower. At Svalbard for RV Polarstern of 2017 and RV Oden of 2018 this ratio is around 30 % and there are extended periods with no data logging's. It seems as the data is collected in two time periods, but documented in the same data set. This gives a misleading interpretation of the length of the voyage and a solution could be to report two separate data sets instead as it would be a better representation of the data set. Similar to some of IB 50 let Pobedy voyages.

In the evaluation process of observed sea ice data there is much to considered. The data sets from ASSIST are extensive and the setup opens up for significant differences between the data sets. The extent of the data sets vary according to number of data points, what data is reported, the period of reporting and the time step between each reporting. In order to evaluate the data it is necessary to evaluate each data according to extent and accuracy. For the evaluation in this thesis only 41 of the given 53 routes are considered in the evaluation of the risk. There are several different observers, both in one and between the different data sets. This is reflected in the logging differences in the data sets, due to the flexibility in choice of parameters that can be reported. In these data sets multiple deviations and errors are found. It is of interest to have two open-sources to verify that the reported data are correct. From IceWatch, 2019 this is not possible at the moment since few photos or comments are attached. Therefore it must be considered that not all data is valid.

ASSIST is user-friendly which is positive, but it opens up for errors. It must be emphasized that multiple errors are discovered in the data. There are mismatches between the ice type and ice thickness. For example have reported thicknesses off 20cm for nilas, which are defined only up to 10cm by WMO, 2014. For some cases where partial ice concentrations are reported, the sum of these are not equal the total concentration. Either the wrong concentration are reported or a partial concentration is missing even though the rest of the data exists for this exact partial ice type. The findings of multiple errors raises questions to how much one can trust these results. These errors are found due to checking data against each other. Though there is much information that can not be compared. Therefore it must be considered that this can indicate even more severe errors.

5.4 Ice Conditions and Risk

A risk assessment based on the data from IceWatch, 2019 for the different areas is performed. The risk level is dependent on three factors: the ice concentration, the ice type and the polar class of the vessel. In Figure 5.6 the probability density distribution(pdf) for the total ice concentration for the areas Alaska, Fram Strait, Svalbard and Georg Land are illustrated. The areas Alaska, Svalbard and Georg Land have a similar distribution, with a high probability for high total concentration. While, the Fram Strait have a more even distribution of total concentration, with low probability for total concentration of ten.

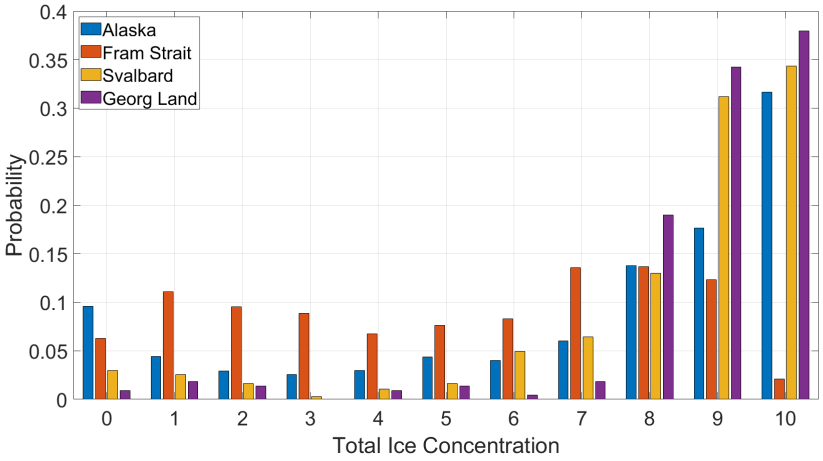

Figure 5.6: TC distribution for the different areas

In Figure 5.7 the probability density distribution of the ice types for the areas are illustrated. The ice type is in general varying from first year ice to multi year ice. In Alaska there also recordings of younger ice.

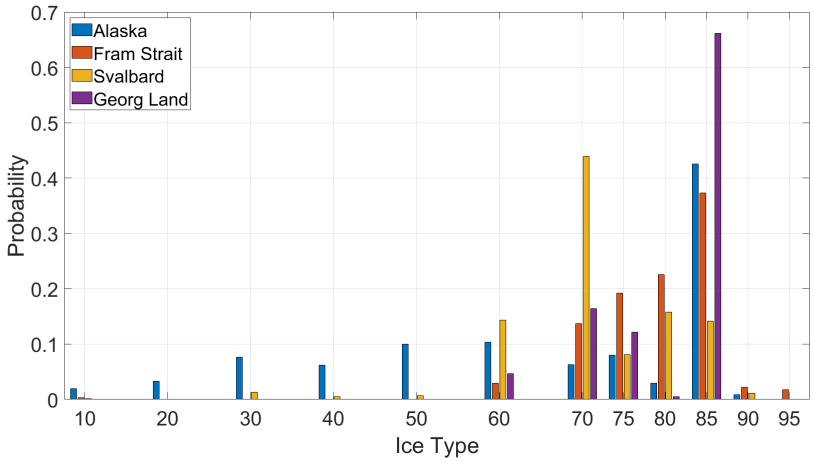

Figure 5.7: Ice type distribution for the different areas

In Figure 5.8 the probability density distribution for the Polar Classes of each area is illustrated. There is a clear distinction of PC's for the different areas.

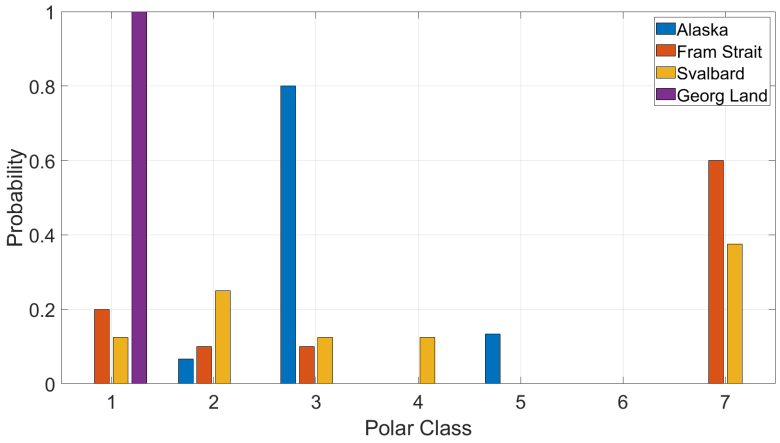

Figure 5.8: Polar Class distribution for the different areas

In Figure 5.9 the probability density distribution of RIO for all areas are illustrated. Large differences in the distribution is identified. Georg Land is the only area with just normal operations. While for north of Alaska there exist a small probability for elevated risk. Finally, both the Fram Strait and north of Svalbard are exposed to a high level of risk. The ice conditions north of Georg Land consist of mainly multiyear ice and have high total concentrations which can indicate high RIO values. IB Pobedy is the only vessel sailing in this area and due to it being a PC1 vessel, the RIO is a variety of medium low risk indexes. The Alaskan ice conditions consist most likely of high total concentrations of either multiyear, pancake or young grey ice. These ice conditions indicate that depending on the compositions of concentrations, ice type and PC the RIO can vary. In from Figure 5.9c it is found that it is by far highest probability for an RIO of 30, the most significant contribution to this is recognized to be from RV Sikuliaq. RV Sikuliaq have PC5, which is a lower PC than the other vessels in the area. It can therefore be considered that with such distribution of low risk the vessel must have been exposed to less severe ice conditions than the rest of the voyages in the Alaskan area. If the voyages of RV Sikuliaq are omitted, then the probability for a RIO of 30 would be significant lower.

Svalbard differs from the other areas by considering winter conditions and by having its highest probability of ice type for first year ice. Due to seasonal changes, the concentration and distribution of ice types would probably be different for summer conditions due to melting of first year ice. The three voyages with RV Lance are the only which contribute to the negative RIO values. The share of negative RIO values are significant. It must be pointed out that RV Lance is in ice conditions to severe for its structural capabilities. Due to the seasonal changes it might be that RV Lance can sail in these waters during the summer season, but in the winter the risk level is too high according to POLARIS. For the Fram Strait the total concentrations are lower, but the most probable ice conditions is multiyear ice, followed by first-year and second year ice. RV Kronprins Haakon have a small possibility of RIO -10, but the rest of its risk level is at an acceptable level. It is assumed that the vessel came across more severe ice conditions than expected, but that this is a rare exception. RV Lance is on the other hand exposed to a significant risk for large parts of the reported voyages. From Figure 5.9 and the evaluation of the different areas. It is found that in general the vessels are exposed to low risk and according to POLARIS can operated normal. Nevertheless, it is found that some vessels are sailing in areas with too severe ice conditions for their structural capabilities. Specially RV Lance, which in both the Fram Strait and north of Svalbard is exposed to significant risk. Detailed evaluation of each individual area can be studied closer in Appendix D.

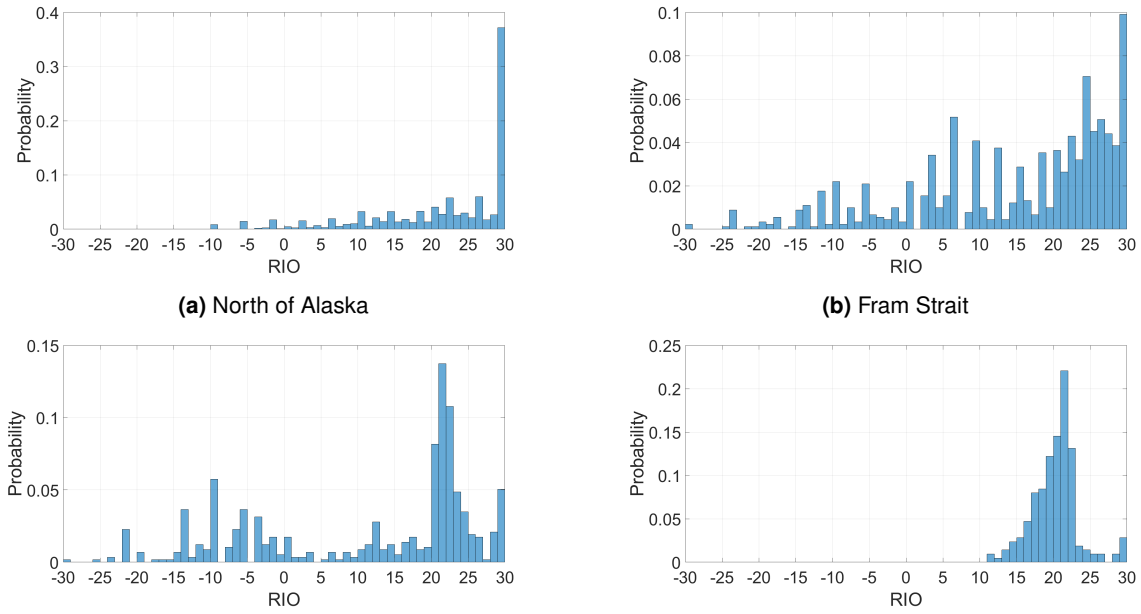

(a) North of Alaska

(b) Fram Strait

(c) North of Svalbard

(d) Georg Land

Figure 5.9: Probability density distribution of RIO for the different areas

In Figure 5.10 the distribution of the areas for the different voyages are illustrated. The plot type in Figure 5.11 is based on a function published by Carmeli, 2020.

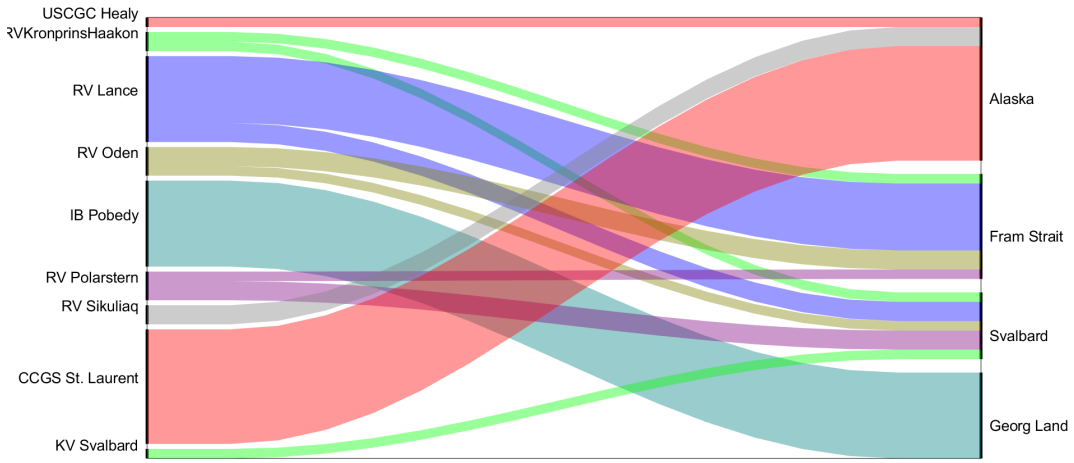

Figure 5.10: Distribution of ships and areas

In Figure 5.11 the RIO distribution for all vessels are illustrated. It indicates what risk each vessel is exposed to. A significant share of the data points have RIO higher than zero, indicating no restrictions of the normal operations. Most of these data points have RIO above 20 and thus low risk. From Table 2.4, it is known that RIO from zero and to -10 indicate elevated risk, while RIO's below -10 indicate high risk and operation subjected to special consideration. Four vessels have RIO values below zero: RV Lance, CCGS St. Laurent, RV Kronprins Haakon and RV Sikuliaq. RV Kronprins Haakon and RV Sikuliaq are exposed to elevated risk few times during their voyages and these occasions are considered coincidental. RV Lance is exposed to high risk a significant number of times. While CCGS St. Laurent is less frequently exposed to high risk, but still more than what is recommended. It is

of interest to investigate why these vessels are exposed to such risks. This is considered closer in Section 5.5.

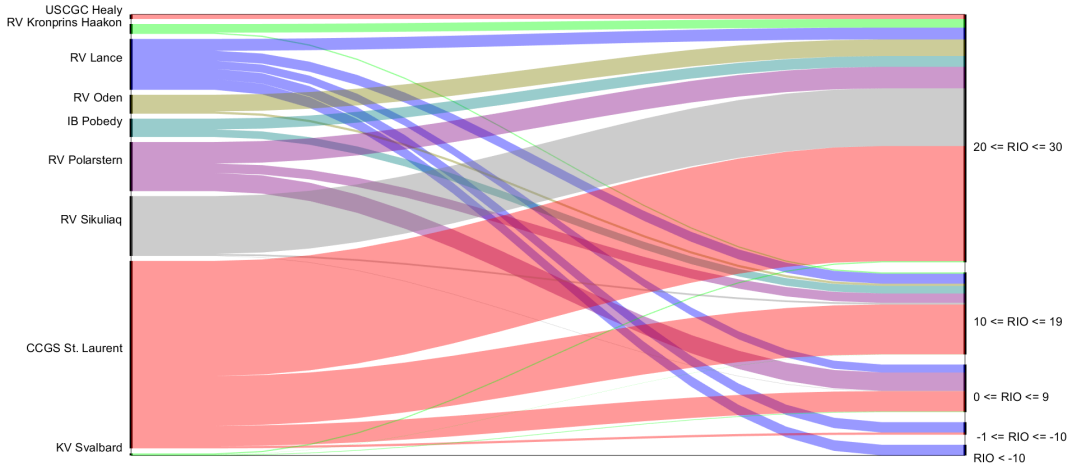

Figure 5.11: Distribution of RIO for all ships

Figure 5.12 illustrates the box plot of RIO for the different Polar Classes. The median and its trend line are plotted to illustrate the general trends. To gain an overall understanding of the development of the mean, the trend line is plotted as a linear line. A clear tendency of decreasing RIO values as the polar class decreases is indicated in Figure 5.12. In other words, vessels designed for less severe ice conditions are exposed to higher risk in the polar areas. It seems as the PC decrease the vessels are operating in ice conditions to severe for its own structural capabilities. This is substantiate by the data from IceWatch, 2019 and Figure 5.11 when considering the polar classes of CCGS St. Laurent and RV Lance. From Table 5.3 it is known that CCGS St. Laurent is of PC3 and RV Lance is of PC7. From Figure 5.12 it can be seen that for PC3, which are RV Kronprins Haakon and CCGS St. Laurent, the lower quartile is above a RIO of ten. While the minimum of RIO is minus ten. This can indicate that the vessels in general sail in ice conditions according to their structural capabilities, but that the vessel has come across more severe ice conditions than usual. From Figure 5.12 it can be seen that for PC7 and RV Lance the situation is different. The mean is close to zero and that the distribution of RIO include negative RIO values, though it is not very common with RIO values below minus 10. When the vessel to such extent is exposed to high risk, it is possible that the vessel have been sailing in ice conditions to severe for its structural capabilities. It is difficult to know the reason for this, but it can be a result of poor voyage planning or that the ice conditions were more severe than expected.

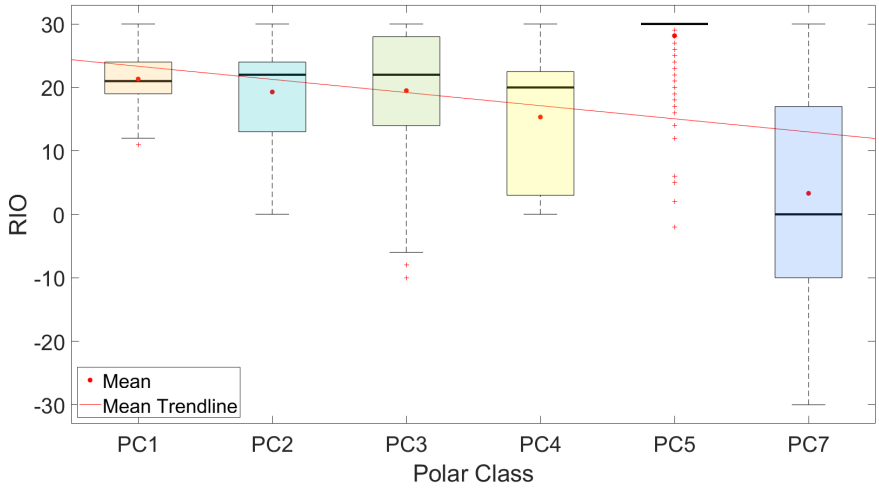

Figure 5.12: Boxplot of RIO for each PC

5.5 Voyage

It is established that multiple reports have risk values in the elevated area according to POLARIS. From Figure 5.11 only a small share have RIO below zero. Nonetheless it is of interest to consider the evolvement of the risk level during a voyage. CCGS St. Laurent in 2013 and RV Lance in 2015 is considered closer, as it is established that these two vessels too often are in ice conditions resulting in high risk. The extreme values and probability density distribution for each vessel can be studied closer in Appendix D. In Figure 5.13 and Figure 5.14 the variation in risk level for the duration of the voyage are illustrated. The plots are not continuous since the the data points considered as incomplete according to Section 3.2 are removed.

Figure 5.13 consider the voyage of CCGS St. Laurent of 2013. From Figure 5.13 it can be seen that when the RIO value is negative it most often is only a negative peak and that the following values have a higher value. It seems that as the vessel is in elevated risk, the vessel heads for an area with less risk. Though sometimes the RIO can be seen to alternate quite frequently between a positive and negative value. Specially in the beginning and the last part of Figure 5.13. It can clearly be seen that the vessel does not stay in the elevated risk area, but shifts from having a negative RIO value and a positive one, from this is it gives the impression that the vessel is taking measures and actively trying to decrease the risk it is exposed to.

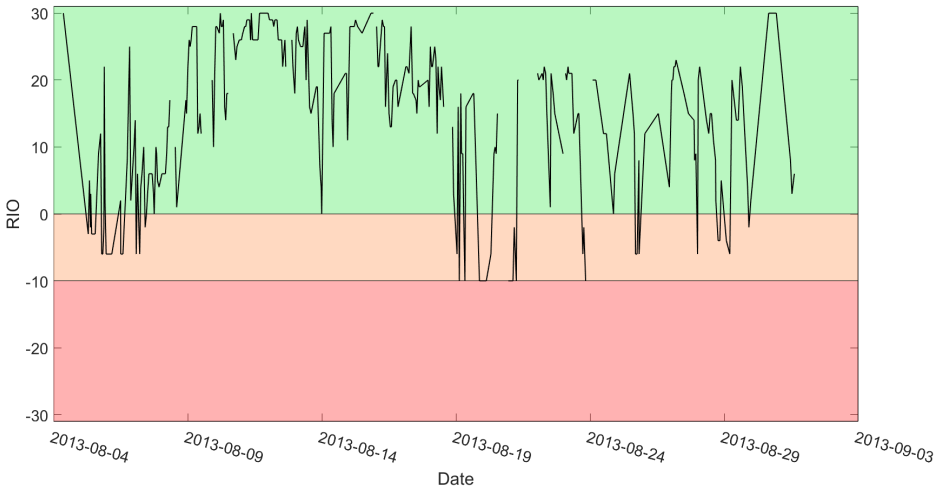

Figure 5.13: RIO during voyage of CCGS St. Laurent in 2013

In Figure 5.14 the voyage of RV Lance in 2015 is illustrated. Since RV Lance had such high risk levels it is interesting to look closer at the voyage. This voyage is representative for all the voyages of RV Lance as the pattern in this illustration can be recognized in some of the other years. What is interesting to see from Figure 5.14 is the alternating risk level. It can be seen that when a low RIO value is logged then the ship heads for lower risk. Though it is interesting that throughout the voyage it alternates between high and low risk and it does not seem to stay at one risk level. This does indicate that the severity of the ice conditions are changing along the route.

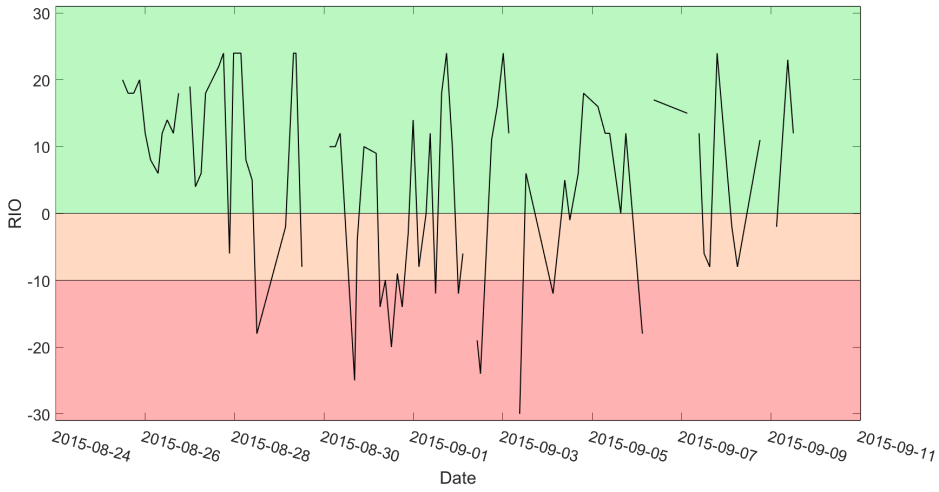

Figure 5.14: RIO during voyage of RV Lance in 2015

It is found that the vessel do not stay in the areas with high risk, but it seems as measures are taken with the purpose of reducing the risk. Nevertheless, Figure 5.14 indicate that the voyage include areas with to severe ice conditions for the given vessel. The reason for this is difficult to establish, but it can be a result of poor voyage planning or incorrectly reporting of ice conditions. This can be a result of wrong ice conditions in the ice charts. To perform an comparison between an ice chart from Canadian Ice Service, 2020 and reported ice conditions from IceWatch, 2019 would be interesting. As it can uncover if the ice conditions considered when planning a voyage and the actual ice conditions reported from the ice fields matches.

In Appendix an example of how the quality of ice charts can be evaluated is performed. Ice charts are of importance for voyage planning, and it is therefore important that its quality is high. From the comparison, it can be concluded that the ice charts estimate ice conditions that are equal or more severe than the ones the ships actually are experiencing and recording. Only one ice chart and three points from the same day are compared. Therefore it is not easy to know if this is representative in general. The three recordings were chosen randomly, and they are not necessarily representative of the entire surrounding ice regime. When choosing recordings to compare with the ice chart, more care should be taken in order to choose representative ice conditions. More extensive comparisons should be performed in order to check multiple ice charts against more evaluated recordings. Nevertheless, the comparison can be considered as a procedure to analyses the similarities between the ice chart and recordings from a ship.

5.6 The Impact of Speed

From IceWatch, 2019 30 of the data sets include speed information, but how extensive this information varies greatly. Thus, individual evaluations must be performed. A general trend is that in the recent years more speed data is available. A few errors are discovered in the input data. For CCGS St. Laurent in 2015 the maximum speed is 190 knots, and for Polarstern in 2018 the lowest speed is -6 knots. To disregard unlikely values, only speeds between zero and 20 knots are considered. Figure 5.15 illustrate the probability density distribution for all recorded speed.

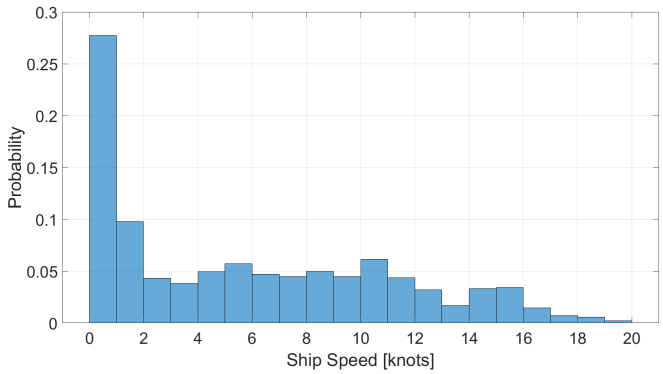

Figure 5.15: pdf of all speed records

The speed is divided into categories to compare data. The range of the categories is based on the maneuverability of vessels and the probability density distribution. Below 5 knots, the ship it is difficult to maneuver and at 10 knots, a shift in the distribution in Figure 5.15 is identified. The categories are as follows.

- Zero speed
- Slow Speed: 1 - 4 knots
- Medium Speed: 5 - 10 knots
- High Speed: Above 10 knots

It is important to emphasize that in Figure 5.15 all data sets are included to see the general distribution. Further, only the data sets with extensive logging of speed is to be evaluated. If speed is not reported, then the field should be left empty. From Figure 5.15, zero knots is the most probable speed. An

individual evaluation must be performed to investigate if the observer has logged zero, indicating zero speed or no available information. Before this is known, it must be taken into account that the speed distribution in Figure 5.15 might not reflect the data correctly.

The ship activity, as defined in Table 3.1, gives an indication to if the speed is correct. Data points with a distinct error or no logging are defined as not specified. Figure 5.16 illustrate the distribution for each ship activity and their associated speed. A greater understanding of the ship movements for each activity can be obtained. To not specify the activity or the speed is the most common according to Figure 5.16. Thus, for the data points with speed the ship activity is known in most cases. The activity *On Station* has a significant share of data points. For these vessels, it is difficult to learn how the ship performs in ice due to the vessel not moving through icy waters. The speed is then dependent on the specific activity and not the ice conditions. When analyzing the influence of the speed on the risk level, it is of interest to considered closer those activities where the ship is performing operations approximately as usual. The activity *Traveling in ice* is the most relevant.

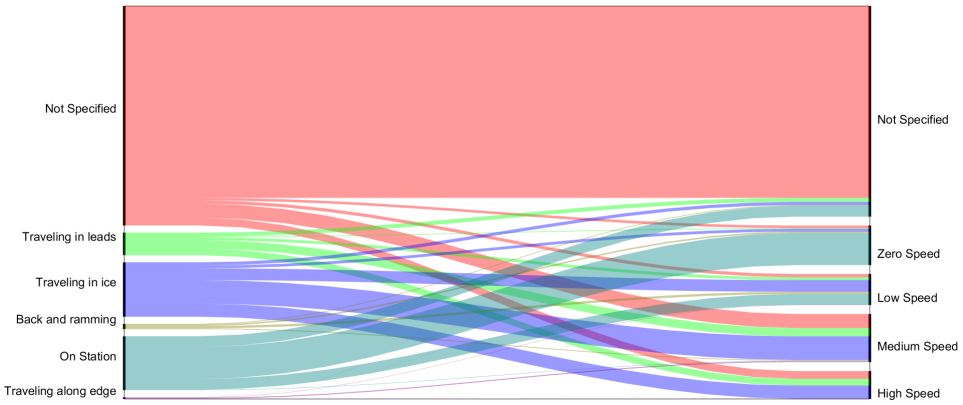

Figure 5.16: Distribution of Ship Activity and Ship Speed

Figure 5.17 illustrate the distribution of the ship activities and the risk level. All ship activities are exposed to several levels of risk. The majority of the shares from each activity have a low risk level. The higher risk levels have contributions mainly from *Not specified, traveling in ice* and *on station*. Due to the somewhat limited extent of data for cases with high risk, it may be considered to include data from all activities when evaluating the influence of speed on the risk. If relevant, it would be of interest to investigate which impact the different ship activities have on the level of risk in regards to the speed.

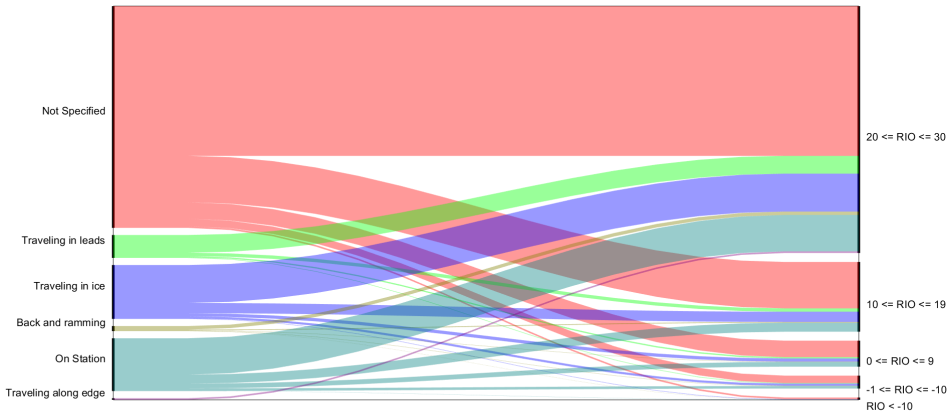

Figure 5.17: Distribution of Ship Activity and Ship Speed

5.7 Speed Evaluation

An evaluation of the data sets from the individual areas will be performed. Those sets marked with a * imply that there exists enough data for the sets to be considered. Also, reporting of zero speeds seems plausible due to realistic change in movement and time compared to the surrounding data points. From Section 5.3, the number of voyages for each area is known. In Table 5.9, Table 5.10, Table 5.11 and Table 5.12 the data sets are listed for their respectively areas. The reasoning regarding which data sets is considered is stated. The data sets from 2018 and 2019 in Table 5.12 are included despite their few data points due to the existence of multiple data sets for one year logged close in time.

Table 5.9: Ship Speed Data Sets, North of Alaska

Ship	Evaluation
USCGC Healy 2018	Considered *
RV Sikuliaq 2015	No speed logged. Data set will not be considered.
RV Sikuliaq 2019	Considered *
CCGS St. Laurent 2014	Very few data points. Data set will not be considered.
CCGS St. Laurent 2015	Considered *
CCGS St. Laurent 2016	Very few data points. Data set will not be considered.
CCGS St. Laurent 2017	Considered *
CCGS St. Laurent 2018	Considered *

Table 5.10: Ship Speed Data Sets, Fram Strait

Ship	Evaluation
RV Kronprins Haakon 2018	Considered *
RV Lance 2012	No speed logged. Data set will not be considered.
RV Lance 2013	No speed logged. Data set will not be considered.
RV Lance 2014	Considered *
RV Lance 2015	Considered *
RV Lance 2016	Considered *
RV Lance 2017	Considered *
RV Oden 2012	No speed logged. Data set will not be considered.
RV Oden 2013	No speed logged. Data set will not be considered.
RV Polarstern 2014	Very few data points. Data set will not be considered.

Table 5.11: Ship Speed Data Sets, North of Svalbard

Ship	Evaluation
RV Lance 2014	No speed logged. Data set will not be considered.
RV Lance 2015	Considered *
RV Lance 2015	Considered *
KV Svalbard 2015	Few data points. Data set will not be considered.
RV Polarstern 2015	Considered *
RV Polarstern 2017	One data point. Data set will not be considered.
RV Oden 2018	Consider the logging to be correctly. Data set will be considered.
RV Kronprins Haakon 2018	Considered *

Table 5.12: Ship Speed Data Sets, Georg Land

Ship	Evaluation
IB Pobedy 2015	Considered
IB Pobedy 2016	Considered *
IB Pobedy 2017	Very few data points. Data set will not be considered.
IB Pobedy 2018 (1)	Considered
IB Pobedy 2018 (2)	Very few data points. Data set will not be considered.
IB Pobedy 2018 (3)	Considered
IB Pobedy 2019 (1)	Considered
IB Pobedy 2019 (2)	Considered
IB Pobedy 2019 (3)	Considered

To investigate if there is any correlation between the ship speed and the RIO, it is of interest to see how the speed varies with an increasing RIO. Intuitively one would assume that low speed results in a low level of risk. The speed and risk are plotted with speed as the dependent value for each of the individual areas. The mean is marked and its trend line of first order is plotted to identify the general trend the mean value. It must be pointed out that after the evaluation of speed recordings, the data is somewhat limited. As a result of this, it might be challenging to evaluate if the data is general enough to reflect actual trends.

5.7.1 North of Alaska

From Figure 5.18 a distinct relation is difficult to identify. A small increase in the mean with increasing RIO is identified. From Table 5.9 and Figure 5.10, CCGS St. Laurent is identified as the main contributor to data in this area. It is known from IceWatch, 2019 that the purpose of CCGS St. Laurent is performing research as a part of JOIS. When performing research, the ship probably does not operate as normal. To investigate if there is any stronger correlation between speed and risk, only the cases with the ship activity *transiting in ice* are considered in Figure 5.19. Comparing Figure 5.18 and 5.19 a stronger dependence is indicate in Figure 5.19. The main difference is identified as the exclusion of the lowest speeds and as the RIO increases, so do the lower quartile in Figure 5.19. For increased RIO, the distribution of speed shifts to higher values indicating higher speeds in low risk areas.

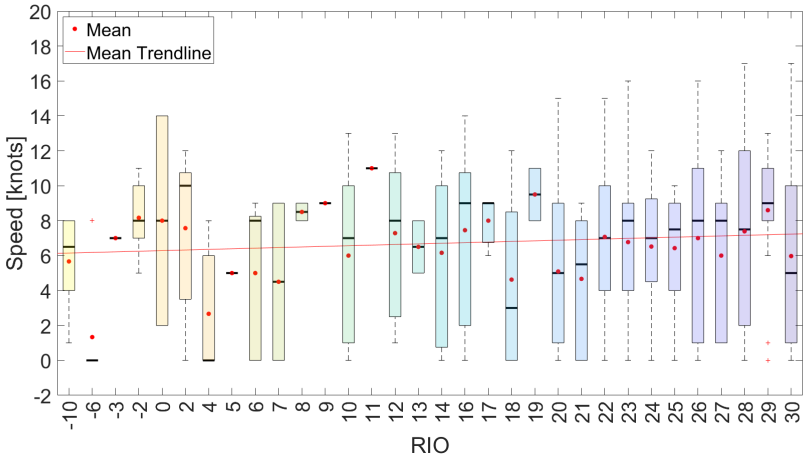

Figure 5.18: Box plot of RIO and Speed, Alaska

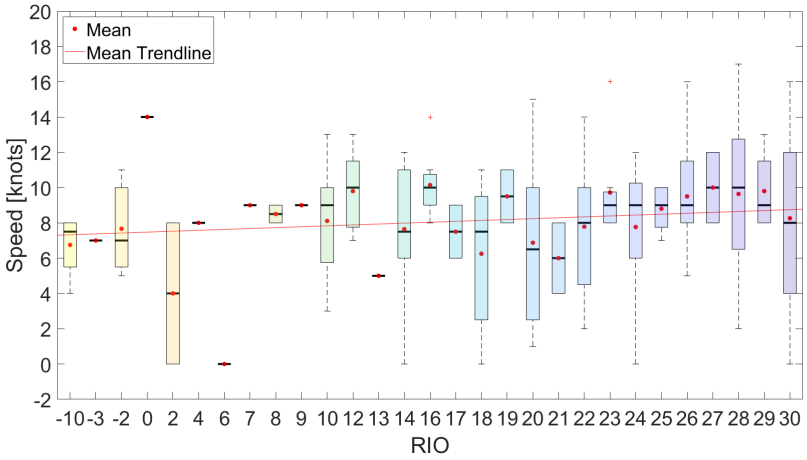

Figure 5.19: Box plot of RIO and Speed Transit in Ice, Alaska

5.7.2 Fram Strait

From Figure 5.20 the higher RIO values have a wider distribution of speeds. This indicates that for lower risk, the vessel more often has a higher speed. It is common with lower speeds for voyages

with research as its purpose. As the RIO increase, so do the value of the upper quartile. In Figure 5.20 all ship activities are considered, and even with such variation in activity a correlation is distinct.

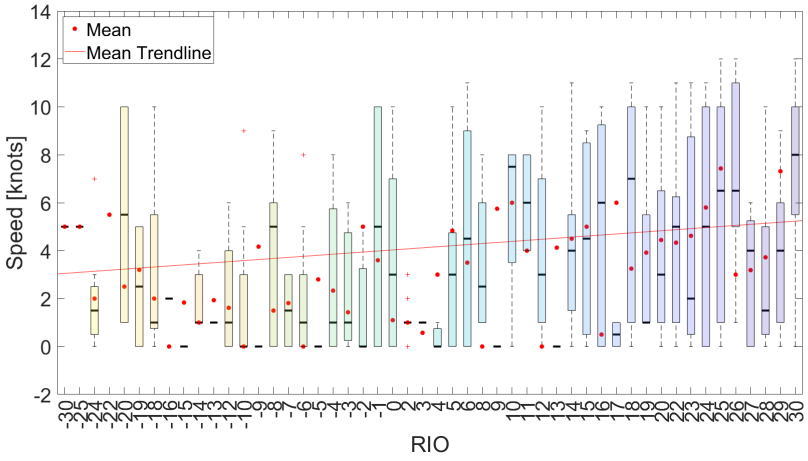

Figure 5.20: Box plot of RIO and Speed, Fram Strait

5.7.3 North of Svalbard

Figure 5.21 include all ship activities, while Figure 5.22 only consider transit in ice. A clear difference in the relevant RIO values are identified, as Figure 5.21 include both lower and higher values. In Figure 5.22 it is noticed that for an increase in RIO, the lower quartile also increases. The single points between RIO of -4 and 9 are identified as a reason for that the mean trend line is not at a lower level for higher risk. These single points deviate from the rest of the overall pattern and with the exclusion of these, the correlation between speed and risk level would be more distinct.

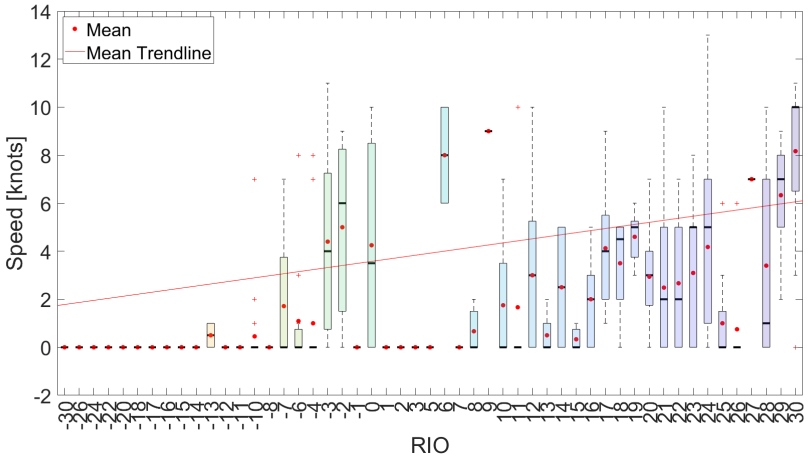

Figure 5.21: Box plot of RIO and Speed, Svalbard

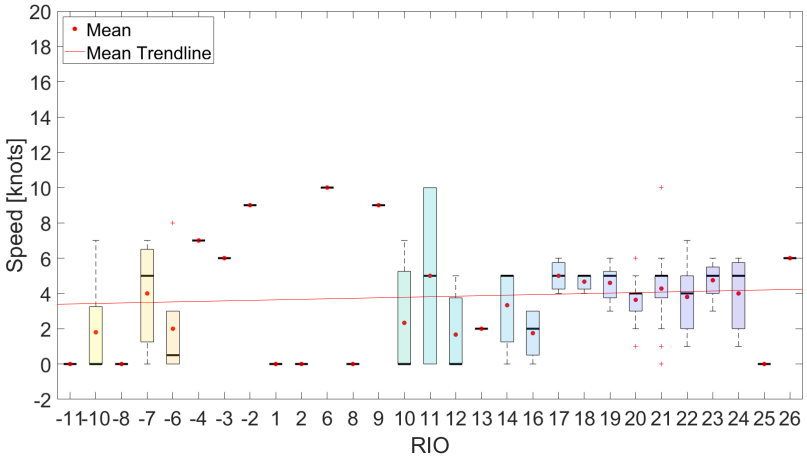

Figure 5.22: Box plot of RIO and Speed Transit in Ice, Svalbard

5.7.4 Georg Land

The purpose of the IB Pobedy voyages is cruise expeditions, therefore Figure 5.23 includes all ship activities. For these data sets, the speed and RIO are in general quite high. The mean trend line is lower than the mean points in general, due to one significant deviation at RIO 25. Considering the mean points for each box, the correlation between the speed and RIO value is significant. It must be emphasized that the ship speeds reported from IB Pobedy is of significant size.

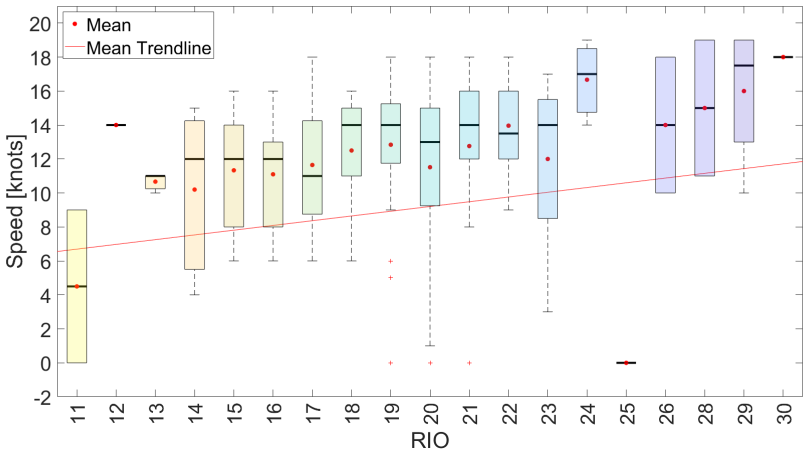

Figure 5.23: Box plot of RIO and Speed, Georg Land

5.8 Comparison

Normally the speed is set based on the ice conditions surrounding the vessel. If the vessel has research as its purpose, the speed might be decided on a different basis, such as observations or test sampling. If the ice conditions do not govern the speed, it might be challenging to find a correlation with the RIO, which is depended on the ice conditions. For this thesis, a large share of the vessels is conducting research. From Figure 5.16, it was found that for a large share of the data points the vessel is reported *on station*, which indicates behavior not dependent on ice conditions. For the activity *traveling in ice* one would assume normal operation, but as seen in Figure 5.22 there

is numerous recordings of zero speed for this activity. This can indicate that for this ship activity, the vessel is not only dependent on the ice conditions. Despite this, a correlation between speed and RIO can be established. The distinction of this correlation varies for each of the areas. The exception is for IB Pobedy, which has cruise expeditions as its purpose. For these voyages, the speed is more likely to be dependent on the ice conditions and this is reflected in Figure 5.23 as it has the clearest correlation of all areas. Two studies of vessels in transit are considered to investigate and validate that the correlation found from the data at IceWatch, 2019 is not only applicable for this data but in general.

For vessels in elevated risk there exist speed limitations according to POLARIS, as given in Table 2.5. For high levels of risk, operations are subjected to special consideration. From Figure 5.18, Figure 5.20 and Figure 5.21 it is found logging's of relative high speeds both in the areas of elevated risk and high level of risk. Not all the vessel follows the restriction according to POLARIS, but if they had then lower speed would be reported. The consequence would probably be a decreasing RIO distribution for the lower RIO, and then also a more distinct speed dependence for the RIO.

Panci et al., 2020 aims to investigate if the ships in the Kara Sea region remain within their operational limitations, according to POLARIS. The speeds have been analyzed for the periods January through April for 2017-2019. Figure 5.24 plot speed against RIO to investigate any changes in the speed as the RIO increased. From Figure 5.24, it is identified a general increase in the RIO as the speed increases. It was summarized that despite the RIO not being directly linked to the speed, a dependency is found. The RIO contains information about the ice conditions around a vessel, which dictates the speed. This is clearly reflected in Figure 5.24.

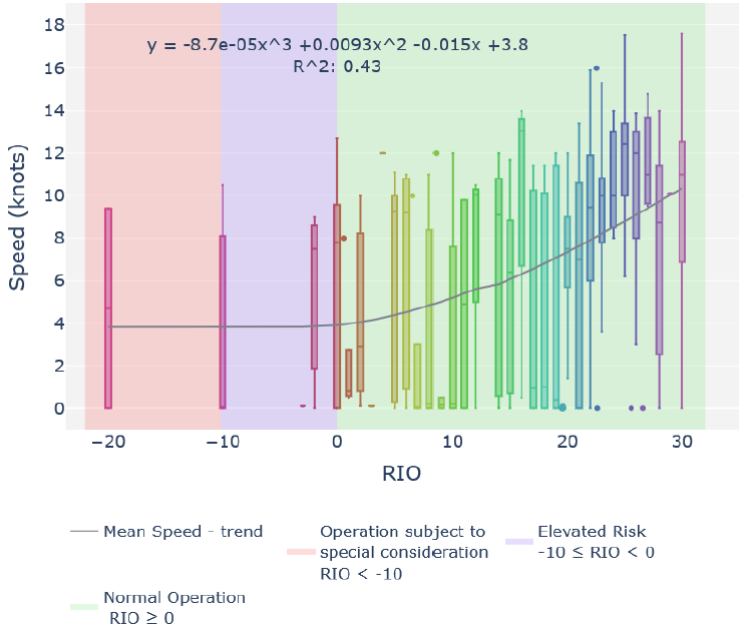

Figure 5.24: Speed of the vessel plotted against the RIO along with a best fit curve for the mean speeds for corresponding RIO values (Panci et al., 2020)

The purpose of the article ENFOTEC Technical Services Inc et al., 1996 is to assess and validate the hypothesis that there exists a correlation between Ice Decision Numerals and safe speed for Type B, D and E vessels. The article considers ASPPR, not POLARIS. From Section 2.1, it is known that the basis of POLARIS is the practices from the Canadian experience and the RIO system is therefore directly comparable to the Ice Decision Numerals. Figure 5.25 illustrates the preliminary

guideline for establishing safe speeds in different ice conditions for Type ships. It was created from the transit records of the Tanker Navigation Safety System (TNSS) and successfully reflects the transit speeds. For increase in the Decision numeral, the risk level decreases. From Figure 5.25, the correlation between the speed and risk is clear and that as the risk decreases, the speed can increase.

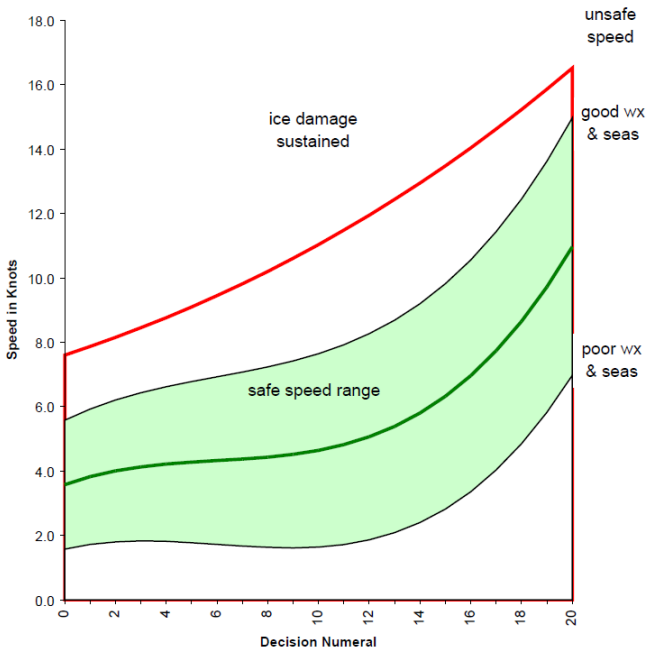

Figure 5.25: Safe speed in ice and weather conditions (ENFOTEC Technical Services Inc et al., 1996)

From the two studies, Panci et al., 2020 and ENFOTEC Technical Services Inc et al., 1996, it is clear that the tendencies of data from IceWatch, 2019 are valid. It can be concluded that a correlation between the speed and the RIO exists.

Chapter 6

Predictive Simulation

To investigate whether it is possible to establish a link between the operational risk index and the global ice load, predictive simulation software can be utilized. It is necessary to understand what input data and parameters are necessary for such a model. This chapter considers cases of different risk levels from the data sets evaluated in Chapter 5. Finally, it is established how these cases can be implemented in a predictive simulation model.

6.1 Critical Cases

Which cases to evaluated further must be chosen. A case is defined as a logged data point from the recording available at IceWatch, 2019. In order for a case to be considered, the following criteria must be fulfilled. The egg code must be from a voyage of RV Oden because this is the available structural model in SAMS. For each of the egg codes, the speed of the ship must be recorded. It is defined that the critical cases must include a range from the minimum to the maximum RIO from the available egg codes. Thus, the best and worst cases from a risk point of view are considered. These criteria are necessary to preserve the correct relation between all the aspects of the analyses. (*Personal communication, Kim* 2020)

There exist some limitations as to what SAMS can simulate. The thickness must be above 20 cm, as thicknesses less than this have not been tested in SAMS. Brash (or rubble) ice can not be modeled as an initial ice condition as it would result in too many ice bodies. It is necessary to know the floe size and therefore those ice floes defined as pancakes, new sheet ice or brash ice as according to Table 3.4 can not be considered in SAMS (*Personal communication, Berg* 2020).

In order to set up for predictive simulation, it is necessary to decide the ice fields. To consider the relation between the operational risk index and the global ice loads ice fields with different levels of risk should be considered. Based on the limitations mentioned above, six egg codes with different level of risk was chosen for closer consideration. These egg codes describe a variety of different ice conditions. The RV Oden voyage in Svalbard in 2018 is chosen as the considered voyage from where the critical cases are retrieved. The speed is logged for most of the data points. For the selected voyage the lowest RIO is found to be 12 from Table D.3 in Appendix D, which indicates a fairly low risk. From Figure D.5 in Appendix D RIO's of 13, 14, 16 and 17 are identified, though for these cases no speed reported or a total concentration of 100 % was reported. For the cases with full coverage of ice, SAMS struggles with the creation of a field without overlapping the ice floes. Thus no ice field reflecting the egg code is managed to obtain. The lowest RIO possible to create in SAMS with an appropriate egg code has an RIO of 18.

The chosen Egg Codes are listed in Table 6.1. In Table 6.2 specific information regarding each egg code is given. In Table 6.1 the variations of the selected ice conditions are stated, both in regards to concentration, stage of development, and floe size. From Table 6.2 more detailed information regarding each chosen egg code is highlighted. The data point from the data set is given. The domain sizes vary due to the floe size. For larger floe sizes, a larger domain has been set. Smaller domain size is chosen if possible due to the increase in domain size also increases the running time of the simulation. A smaller field is chosen if possible to simulate due to lower running time.

Table 6.1: Egg Codes

Egg Code 1	Egg Code 2	Egg Code 3
0.1	0.7	0.8
0.1	0.7	0.6 0.2
60	70	75 70
500	600	700 600

Egg Code 4	Egg Code 5	Egg Code 6
0.8	0.9	0.9
0.2 0.6	0.2 0.7	0.3 0.6
85 80	85 75	85 70
500 600	500 700	500 600

Table 6.2: Egg Code Information (IceWatch, 2019)

Egg Code #	RIO	Data Point	Speed [knots]	Thickness [cm]	Domain size [m] (x_{min}, x_{max})	(y_{min}, y_{max})
Egg Code 1	29	89	5	40	(0,2000)	(-750, 750)
Egg Code 2	23	81	5	110	(0,2000)	(-750, 750)
Egg Code 3	22	59	4	200, 100	(0,4000)	(-1500, 1500)
Egg Code 4	20	55	3	250, 150	(0,2000)	(-750, 750)
Egg Code 5	19	23	5	220, 160	(0,4000)	(-1500, 1500)
Egg Code 6	18	43	5	220, 130	(0,2000)	(-750, 750)

6.2 Ice Field Generation

The stand-alone application FieldCreation creates digital ice fields that can be imported to SAMS. It is of interest to create ice fields with ice conditions according to given egg codes. An input ice field is considered for the geometry of the ice floes. The field type is defined as egg, and the egg code data is given. Then the ice field dimensions, a random seed, and the filename of the output are set. The egg code data includes the partial concentration, the ice thickness, the minimum, and the maximum floe size for each of the partial ice types, which are given in the Egg Code of the ice field. According to Berg, M. van den, 2019 a random seed is defined in order to place the floes at random locations within the field domain. In that way, the ice field geometry can be different even though the rest of the input data is equal. An iteration process will continue moving the ice floes until there is no overlapping of floes. The creation time and the number of iterations of an ice field vary depending on the floe size, domain size, and ice concentration. In general, higher concentration and larger floes

imply more iterations necessary in order to obtain no overlapping. If the floes are large, then a larger ice field domain might be necessary to obtain no overlapping. In some cases, it might not be possible to obtain this. By observing the visual ice field iterations, it is noticed that if floes are overlapping, they will be clipped out. If only some parts of the edges are overlapping, then the generated ice field could still be considered. If significant parts of the ice floes are overlapping and a more substantial part is clipped away, then this will impact the ice concentration and the floe size. Following this, the created ice field might not be representative of the input information, and it should be considered with care whether the ice field can be used in further analysis.

6.3 Input Parameters SAMS

Before a simulation can be run in SAMS, multiple input parameters must be set. In this section, each of the chosen input is listed. Some of the input parameters will vary for the different scenarios, and these will be marked.

In Table 6.3 the simulation settings are specified. The choice of the frequency is described in detail in Section 6.7. The maximum simulation time reflects the time the structure needs to fulfill its route. Consequently, it depends on the speed and route of the vessel. Fracturing is enabled as ice fracture plays an important role in the ice-structure interaction.

Table 6.3: SAMS Simulation setting

Simulation settings		
Parameter	**Unit**	**Value**
Frequency	Hz	100.00
Max simulation time	s	*
Enable fracturing		True

* Individual for each simulation. Depend on the length of the route and the speed.

The parameters in Table 6.4 are set as the default values in SAMS. In accordance with *Personal communication, Berg* 2020 they are considered accurate for the simulations in the current work. For a given rubble deletion area threshold, the ice rubble with an area less than the given one will be deleted. For ice rubble further away than the minimum distance between the structure center of gravity (CG) and the ice rubble body CG, will be deleted. The purpose of this is to speed up the simulation as the number of ice bodies decreases.

Table 6.4: SAMS Advanced User Input

Advanced User Input		
Parameter	**Unit**	**Value**
Warm starting factor		0.7
Max number of iterations		10 000
Ice structure rigid upper limit area		1.0
Max velocity error		0.0001
Max error penetration		0.01
Position correction time		0.33
Max iterations penetration		10
Min fracture body area	m^2	8.0
Min ice body area	m^2	1.0
Circumferential crack angle step	deg	45.0
Radial crack angle step	deg	90.0
Kink search step		1.0
Max ice buffer zone		3.0
Max bending area ratio		0.5
Max hydro triangles		10 000 000
Max current mesh points		1 000 000
Max initial bodies		20 000
Max floe size		20 000 000
Apply ventilation		false
Rubble deletion area threshold	m^2	0.0
Rubble deletion radius	m	60.0
Rubble structure crushing		false
Number of threads		1

In Table 6.5 the sea ice field properties are given. They are given according to Raza et al., 2019. For multi-year sea ice the actual value for the density, CSE and flexural strength might be different than the one listed in Table 6.5 (*Personal communication, Kim* 2020). As the sea ice ages, some of the properties tend to change, but in SAMS can only handle one input set.

Table 6.5: SAMS Ice field properties (Raza et al., 2019)

Ice field properties		
Parameter	**Unit**	**Value**
Ice data file		"*.ice"
Ice density	kg/m^3	910
Crushing specific energy (CSE)	MPa	2
Young's Modulus	GPa	5
Poisson ration		0.3
Fracture toughness	kPa $\sqrt{m}$	150
Flexural strength	kPa	500
Tensile strength	kPa	500
Friction ice-ice		0.15
Friction ice-structure		0.15
Friction ice-walls		0.15

* Individual for each simulation.

In Table 6.6 the structural properties for RV Oden is given. The mass is stated in Berg, M. van den, 2019 and the radius of gyration are following *Personal communication, Berg* 2020. The .obj geometry file is given in SAMS. Some different parameters regarding the structure's initial position and rotation are given. The initial position will vary with different tracks. For each time step, the towing track file will include information regarding the time, position, linear and angular velocity for the directions in the global axis system, heading axis, and heading rotation. The vessel will move with a constant forward speed, according to Table 6.2. The set speed will determine the time steps in the track file. Thus, the speed of the vessel is taken into account. The interaction mechanism is set to rigid. Thus, the structure will follow the path of points with no deviation at all (Berg, M. van den, 2019). Also, for a fixed interaction mechanism, the radius of gyration will not have an impact as the vessel will no dynamically react to any forces. Rigid interaction mechanism is chosen to have more control over the exact path of the structure. Consequently, the structure will not dynamically react to any forces, as described in Chapter 4. When setting the carriage to rigid, it will limit the dynamics of the ship, but according to *Personal communication, Berg* 2020, not to such extent that it will have a significant impact on the ice loads. It is the ice loads that are of interest, and therefore this is considered as an acceptable assumption.

Table 6.6: SAMS Structure Properties

Structure Properties		
Parameter	**Unit**	**Value**
Structure .obj file		"Oden.obj"
Structure Mass	tonnes	13 000
Structure radius of gyration	m	[7.45, 30.90, 30.30]
Structure position	m	[*, *, 0.0]
Structure rotation axis	deg	[0.0, 0.0, 1.0]
Structure rotation angle	deg	0.0
Flexible carriage		false
Linear towing		false
Towing track file		"*.txt"

* Individual for each simulation.

In Table 6.7 the ice 3D export settings are listed. It is enabled in order to produce output data, though the export current is disabled since it produces huge output files. The output time step stride controls the visual output frequency to the time step size (Berg et al., 2019).

Table 6.7: SAMS Ice 3D Export Settings

Ice 3D Export Settings		
Parameter	**Unit**	**Value**
Enable		true
Export current		false
Output time step stride		50

In Table 6.8 the environmental properties are given. The reason behind enabling confinements are discussed in detail in Section 6.8. It is assumed no wind and no current, as not extensive enough information is given in the reported data in IceWatch, 2019. The rest of the properties and coefficients are set in accordance with Lubbad, Loset, et al., 2018 and *Personal communication, Berg* 2020.

Table 6.8: SAMS Environmental Properties

Environmental Properties		
Parameter	**Unit**	**Value**
Confined domain		True
Tank wall height	m	10
Water depth	m	Infinity
Air density	kg/m^3	1.04
Water density	kg/m^3	1025.0
Max body mesh size		100.0
Wind velocity vector		[0.0, 0.0, 0.0]
Current velocity vector		[0.0, 0.0, 0.0]
Water skin friction coefficient		0.005
Water form drag coefficient		[0.1, 0.1, 0.5]
Air skin friction coefficient		0.0
Max velocity for linear drag	m/s	0.1
Fluid 3D mesh size		[100.0, 100.0, 1.0]
Number of fluid mesh layers		1

An example of the necessary input files for one simulation is given in Appendix F. The .ice file to the specified ice field must be obtained to run the simulation.

6.4 Route Choice

Several different routes can be chosen when transiting an ice field. According to the RIO, the risk level is constant, but the ice loads are likely to vary. It is of interest to choose a set of routes that have different interactions with the ice floes. Following this, it can be studied how the ice loads vary. The routes are chosen manually, considering the floe sizes. The thickness is known from Table 6.2, though it is not always easy to distinguish the ice floes with different thicknesses from each other. To some degree, this reflects the real world, as it can be difficult for a person on the bridge to distinguish between the thickness of ice floes in the ice field ahead.

As the interaction mechanism is rigid, it is important with a continuous route that considers the turning radius of the ship. According to the Swedish Maritime Administration, 2010 the turning radius of RV Oden is one ship length in 0.8m ice. For most of the chosen egg codes, the ice is thicker than this. Therefore it is assumed that the turning radius will be increased for the considered cases. For all cases, when RV Oden is turning, it will be with a radius of 300 m or more. This radius is around three times the ship length given in Swedish Maritime Administration, 2010 and should be plausible.

Confinements are considered in the simulation, and the reason is explained in detail in Section 6.8. When selecting a route, the confinements must be considered as they can have a significant impact on the ice loads. The confinements are included to represent the surrounding ice environment, but if the structure is moving close to the confinement walls, it is not easy to know how they will affect the ice loads on the structure. The routes will have some distance to the confinements to avoid such uncertainties. The routes end at a confinement wall. Therefore the results at the end of the simulation should be considered with extra care. The routes for all ice fields are illustrated in Figure 6.1.

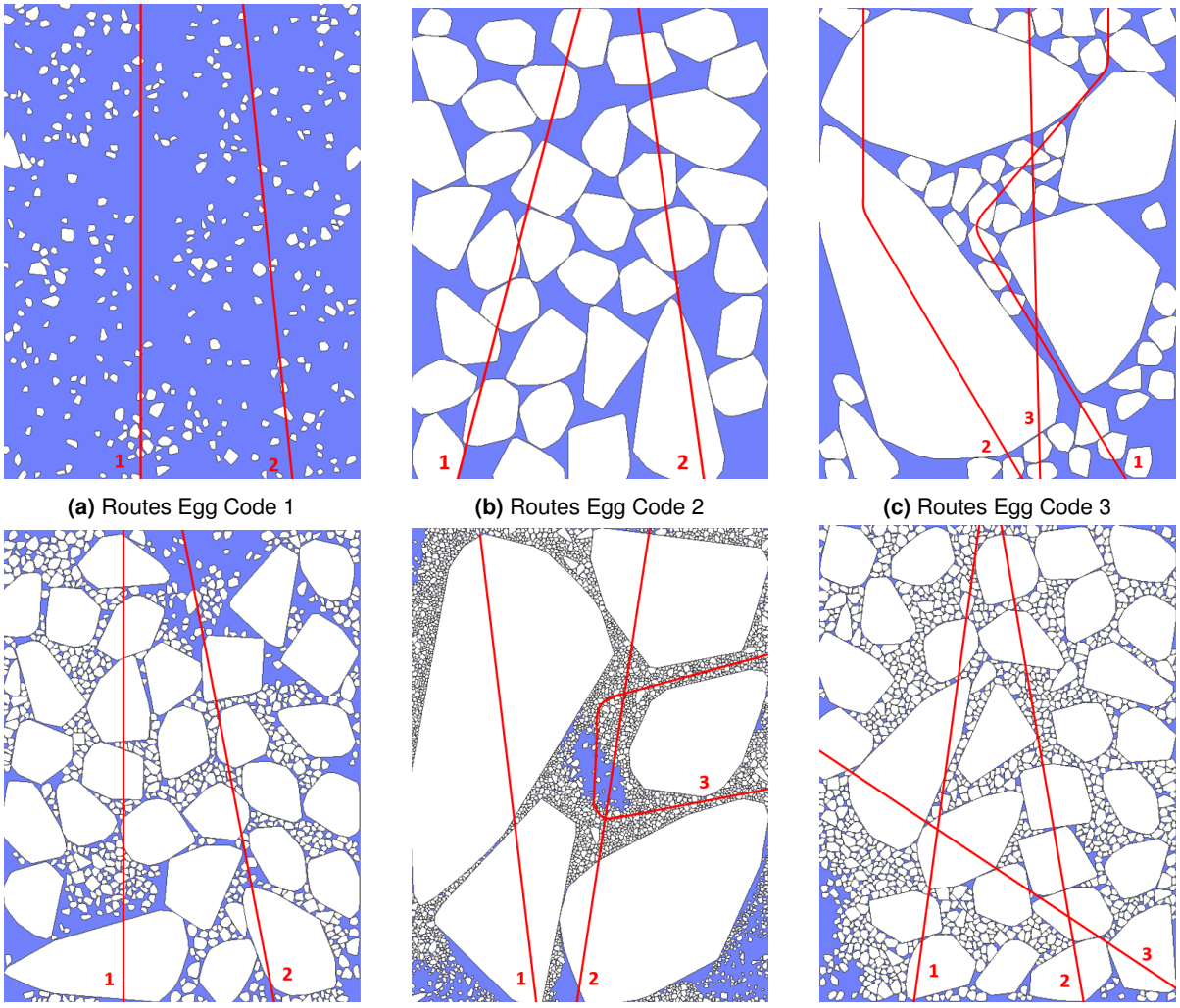

(a) Routes Egg Code 1 **(b)** Routes Egg Code 2 **(c)** Routes Egg Code 3

(d) Routes Egg Code 4 **(e)** Routes Egg Code 5 **(f)** Routes Egg Code 6

Figure 6.1: The chosen routes, indicated as a red line, for the different ice fields

6.5 Running the Analysis

To run the analysis a configuration file of .itconfig format for each route is set up including all the parameters from Section 6.3 according to *Personal communication, Berg* 2020. The configuration file for one simulation can be found in Appendix F.1. SAMS is run from the command window on the computer. One simulation for each route must be run, and the running time varies dependent on the ice field and the speed of the vessel. The running time varies from around 15 to 24 hours for all simulations. Before the simulations can be run, a few aspects must be considered. The choice of frequency is considered in Section 6.7. The impact of confinement is evaluated in Section 6.8. Each time step in the simulation defines the route. The time, position, linear velocity, angular velocity, heading axis, and heading rotation must be given. First, the routes are defined as illustrated in Figure 6.1. Then these routes must be given on the specific format in Appendix F.3 before the simulation can start. All files necessary for one simulation can be seen in Appendix F.

6.6 Different Segments of the Route

Along each of the routes, the ship will be exposed to different types of ice conditions, as these vary locally in an ice field. Thus, the ice loads will vary as the ship advances through the route. Therefore the route can be divided into different segments where the force distribution is similar. It is of importance to recognize what impacts the force variation. In general, the force will change when the ship enters an area with different floes. The interaction between the structure and the ice floe will also impact the force. Whether the floes fractures or not, in addition to the size of the splits, will all impact the force as fracture function as a load release. The load variation from different segments is illustrated in Figure 6.2 for egg code 4 Track 2.

6.7 Frequency

The frequency is a user-controlled simulation setting. It defines the number of simulation steps per second, and it may influence the accuracy of the results. It is important to choose a frequency that is not too low. According to Berg, M. van den, 2019 the simulation frequency is recommended to be 20 times the characteristic velocity in m/s. The characteristic velocity for this thesis will be the constant forward velocity. The frequency will impact the running time of the simulation, as it will increase with increasing frequencies due to the increase in the number of steps. In order to prevent too large running time, an evaluation of the impact of the frequencies was performed.

From Table 6.2, the speed in knots is known for all the cases which are analyzed. Comparing these speeds with the recommendation for frequency, a frequency of around 50 Hz should give an accurate enough result. Different frequencies were chosen, and the results from the analysis compared. Simulations with frequencies of 10 Hz, 50 Hz, 100 Hz, and 150 Hz were run, including both lower and higher frequencies compared to the recommendation. Four analyses are performed in SAMS off Egg Code 4 Track 2 with the different frequencies. It is clear that for different frequencies, the loads vary in Figure 6.2, where the time-averaged forces are compared.

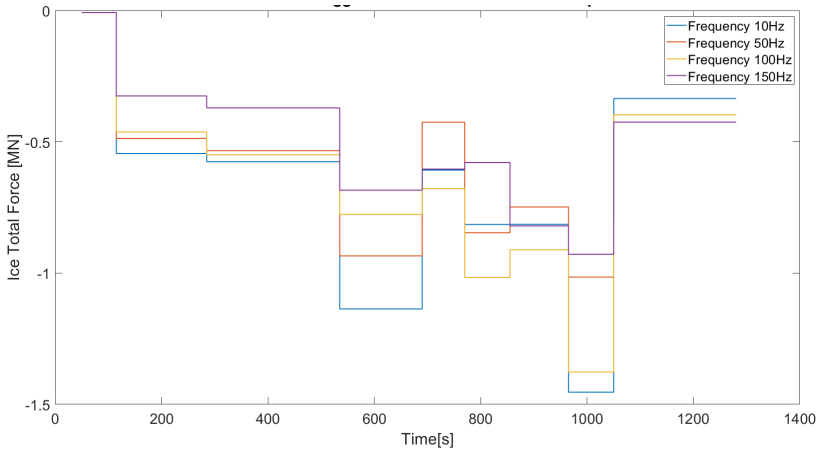

Figure 6.2: Time-Average Total Ice Force for different frequencies

From Figure 6.2 it is recognized that the magnitude of the different frequencies are inconsistent. The vessel follows the same route and has the same speed. However, there is no significant pattern for the magnitude of the loads. There is not one frequency that is more conservative than the others. The loads must be considered in detail. Figure 6.3 illustrates how RV Oden interacts with a larger ice floe for the different frequencies. The ships are in at the same time step and in the same position for all figures. An effect of the different frequencies can be seen. How the ship interacts with the ice floes

and the ice fracture differs. Such a difference in the interaction can be seen throughout the simulation. For these simulations, the same segments were considered. However, since the interaction between the ship and the ice floes are different, the segments should maybe be set individually for each frequency. This might give more accurate time-averaging loads. It is recommended that for future work, such measurements will be performed.

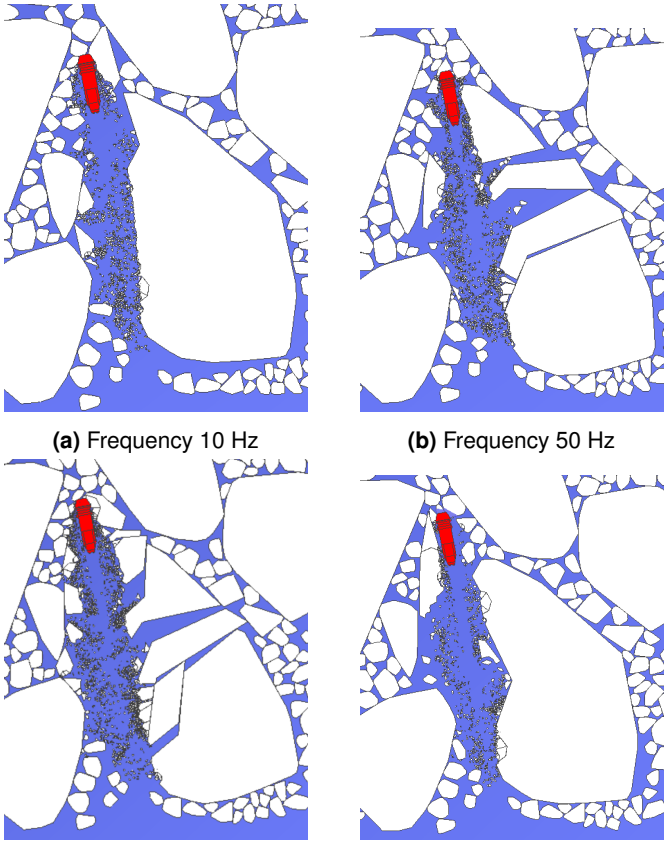

(a) Frequency 10 Hz **(b)** Frequency 50 Hz

(c) Frequency 100 Hz **(d)** Frequency 150 Hz

Figure 6.3: Interaction between Oden and ice floe for different frequencies

With a higher frequency, a more accurate result is obtained. Since there is such a difference between the time-averaged total force for the different frequencies, it is essential to choose a higher frequency in order to obtain correct results from the analysis. Though the running time of the analysis must be considered as it increases significantly with an increasing frequency. The two highest frequencies are studied closer, and it can be seen from Figure 6.2 that the frequency of a 100 Hz gives a more conservative estimate than a frequency of 150 Hz. The only deviation for this trend is from time 1050 seconds, where the higher frequency gives somewhat higher loads. A frequency of 100 Hz will be considered in the analysis in this thesis. It is concluded that the frequency will be a compromise between accuracy and running time. Based on the statement in Berg, M. van den, 2019 regarding the recommended simulation frequency and the general trend of a more conservative frequency, as illustrated in Figure 6.2.

6.8 Confinements

The ice fields considered in the analysis are a part of a large ice area, and the motion of the ice floes must be restricted. They are not free to move outside the field domain as they, in reality, would be surrounded by an ice field. Thus, confinement walls are applied in the simulation. It is also of interest

to investigate if the impact of the confinements varies for different total concentration. Therefore two ice fields with different total concentrations are considered in detail. For both ice fields, a simulation with and one without confinement will be run. The results can be seen in Figure 6.4. In Figure 6.4a the time-average force in surge for egg code 1 route 1 is illustrated. The total ice concentration for this field is 10 %. In Figure 6.4b the time-average total ice force in surge is illustrated. The total ice concentration for this field is 80 %. It can be seen that for both ice fields, the result differs when considering confinement, and the analysis will be more conservative. As seen from Figure 6.4, the force is higher during the entire simulation when confinements are considered. Though the difference is more significant for higher concentrations, indicating that confinements for ice fields with lower total concentration might not be necessary. In an ice field with low concentration, the ice floes are freer to move around, then in an ice field with higher total concentration. This will impact the amount of contact between the ice floes and, thus, also the contact forces. This aspect becomes clear from when comparing the differences from the results in Figure 6.4. From Table 6.2, it is known that for most cases that are to be analyzed, the total ice concentrations are high. Therefore confinements will be considered for all analyses.

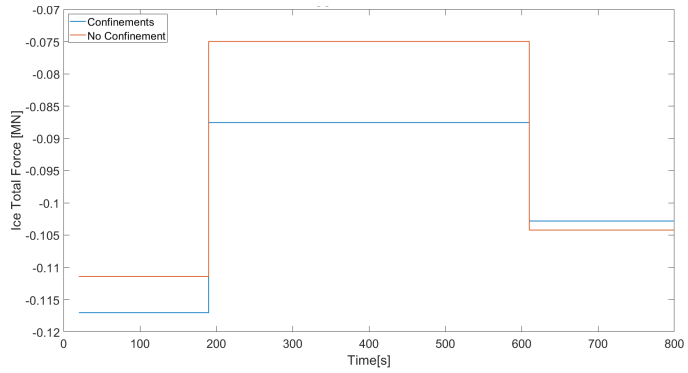

(a) Egg Code 1 Route 1 TC = 10 %

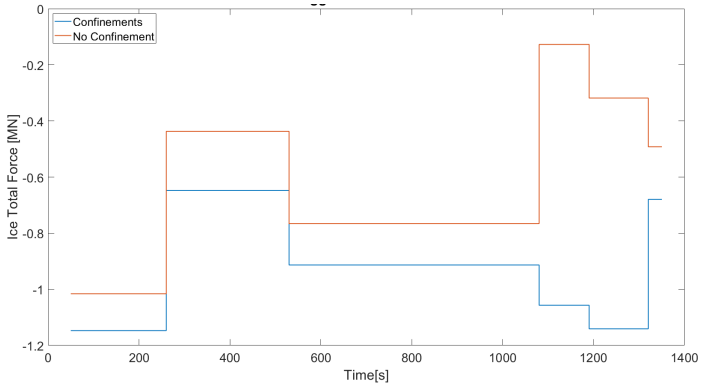

(b) Egg Code 4 Route 1 TC = 80 %

Figure 6.4: Time-Average Total Ice Force with and without confinements

The results in Figure 6.4b were simulated with the wrong ice floe thicknesses compared to the thicknesses for Egg Code 4 due to a bug in the application FieldCreation. The bug was discovered at a later time. Though the thicknesses are incorrect according to egg code 4, the results can still be considered when evaluating confinements.

Chapter 7

Results from Predictive Simulation

In this chapter, predictive simulations are performed in SAMS based on the evaluated data and established setup from Chapter 6. From the performed simulations, a link between the operational risk index and the global ice load output is established. With such a link, the correlation between the ice loads and the RIO can be investigated. When ice loads are known, then it is possible to maintain safe ship operations and protect the polar environment. The limited available data for the structural model of RV Oden does not include a large variety of RIO values, but a rather narrow spread. Nevertheless, the work is a developed method for establishing a link between the operational risk index and the global ice load. Thus in the future, a more comprehensive range of RIO can be evaluated, when more data or another structural model is in place.

Continuous ice breaking operations are simulated in SAMS. For such operations to remain safe, it is necessary to have a sufficiently strong hull to withstand the ice loads and an adequate propulsion power to overcome the ice resistance (Raza et al., 2019). According to Hu and Zhou, 2015, the definition of ice resistance is the time average of all longitudinal forces due to ice acting on the ship. The global ice loads consist of the ice breaking force and the ice rubble force from the simulation output. For a vessel advancing through an ice field, the time-average ice loads in surge direction will coincide with the ice resistance on the vessel. The component in the negative surge direction of the global ice loads will, therefore, be considered. Force contributions from the force component in the X- and Y-direction must be considered according to the vessel direction to find the surge force. The simulation output to considered closer is the time history of the ice resistance encountered by RV Oden.

7.1 Comparison of all Results

A link between the operational risk index and the global ice loads are found according to Figure 7.1. Where the distribution of ice loads are dependent on the RIO. Each RIO value also represent the different egg codes and their associated speed. Thus, for the different RIO's the forces distribution is found by consideration of the different routes within each egg code. The relevant Matlab code is given in Appendix G.

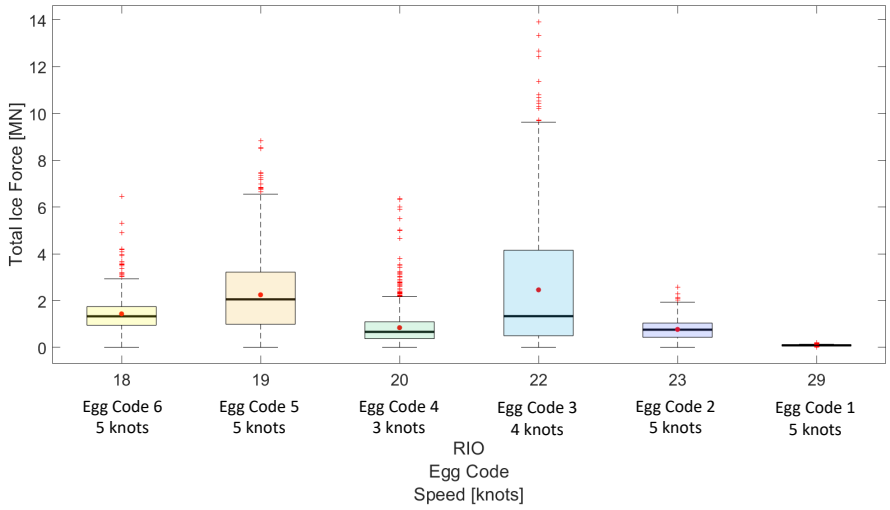

Figure 7.1: Box Plot of Time-Average Surge Force for all Egg Codes

Initially one would assume that for decreasing risk, the ice loads would increase. Though, no distinct correlation between the operational risk and the global ice loads can be found at first sight. Nevertheless, some similarities can be found when comparing the box plots to their ice field geometries from Figure 6.1. Three groupings with similar ice field geometry and force distribution are identified. First the ice fields with Egg Codes 2, 4 and 6, secondly the ice fields with Egg Codes 3 and 5, and then the last ice field of egg code 1, which deviates from the others due to a very narrow distribution.

Following closer consideration of egg codes 2, 4, and 6 is performed. From Table 6.1 and 6.2 the total concentration varies, but the partial concentration of the larger floes, see figure 6.1, are consistent at either 60 % or 70 %. The floe thickness are respectively 100 cm, 150cm and 130cm. The floe sizes and thickness indicate that the ice loads should be approximately similar, which they are according to Figure 7.1. The reason for the difference in the RIO, is that both egg code 4 and 6 have two partial ice types and higher total concentration. This will clearly impact the magnitude of the RIO. For the ice field with egg code 4 and egg code 6 the smaller ice floes have minor impact the ice loads. Figure 7.2 plot the variation of the total ice force throughout the simulation. The magnitude of the total force variate as the vessel advance through the field. The periods with lower force is identified as the areas with smaller floes. According to Table 6.2 in egg code 4 the smaller ice floe is thicker then the larger ice floes. Thus, the size of the ice floes have an impact on the magnitude of the ice force. Therefore despite the difference in RIO, the load distribution is dependent in the thickness of the larger ice floes. Resulting in similar distribution for the ice fields of egg code 4 and 6 in Figure 7.1.

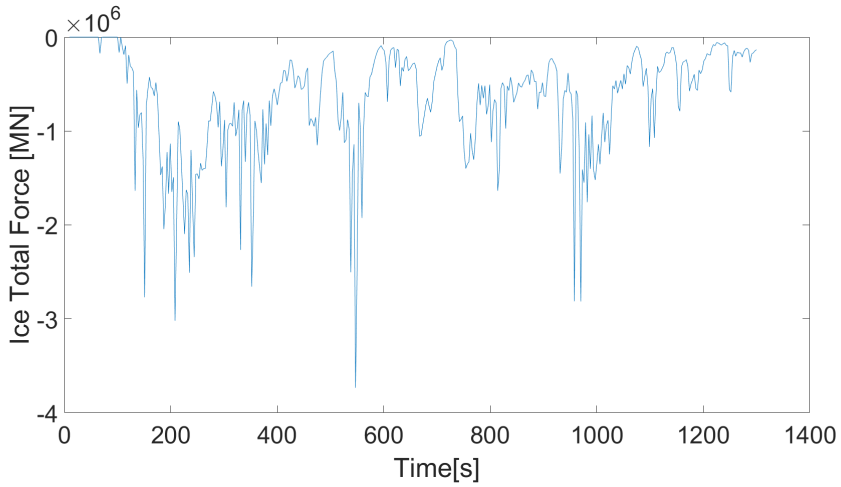

Figure 7.2: Time-Averaged Total Ice Force in Surge Direction: Egg Code 4 Route 2

Comparing the large ice floes from egg code 4 and 6, where the ice floes has the respectively thicknesses of 150cm and 130cm. Initially one would assume that the global ice loads dependent on the thickness of the ice floes. From Figure 7.1 it can be established that this is not the case. It can be seen that egg code 6 have larger global forces than egg code 4, despite having thinner ice floes. There exists other differences in the egg codes regarding thickness of the smaller floes and concentration, though these are considered minor. From Table 6.2 the speed of egg code 4 is given as 3 knots, while it is given as 5 knots for egg code 6. Thus, it is determined that the impact of speed is significant. In Section 7.2 the impact of the speed will be considered closer.

From Figure 7.1 it can be seen that the global ice loads for egg code 3 and egg code 5 clearly differs from the rest. It is established that the largest floes gives the highest loads. Thus, it is the ice loads from egg code 3 route 2 and egg code 5 route 1 that have the contributions contain the highest total ice force to these egg codes. Figure 7.3a and Figure 7.3b illustrate the variation in total ice force for surge direction throughout the simulation for the two routes. The total surge force is in general larger for egg code 3 route 2 than for egg code 5 route 1. The thickness of the large ice floes are 200cm for egg code 3 and 160 cm for egg code 5. Thus, the ice loads from egg code 3 should be larger than from egg code 5, which it is. The reason for the difference in the RIO is the the other partial ice type and the total concentration, which indicate higher risk for egg code 5. As discussed above the speed has an impact on the ice loads and it can therefore be assumed that the difference in the ice loads would be even more significant had the ship speeds been equal.

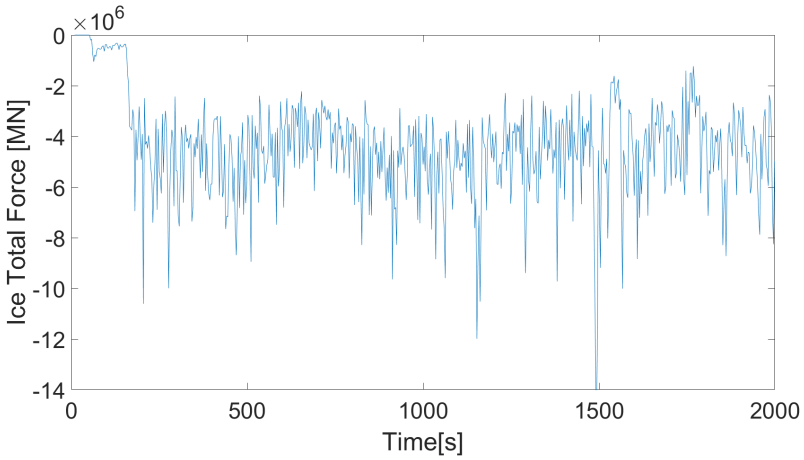

(a) Egg Code 3 Route 2

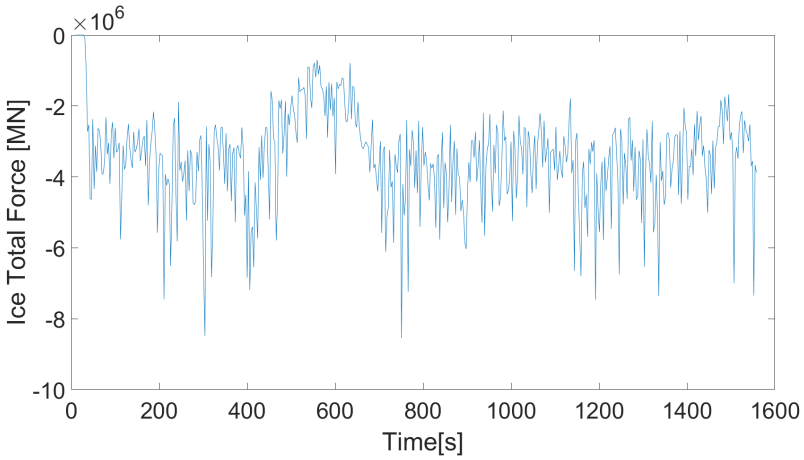

(b) Egg Code 5 Route 1

Figure 7.3: Time-Averaged Total Ice Force in Surge Direction

From the results in Figure 7.1 it is established that the size of the floes are of importance. In the following it will be investigated why the size has such an impact. The rubble force is the main contributor to the total ice force in surge. From Chapter 4 it is known that the rubble contacts are rigid and non-breakable. For the rubble force all kinetic energy is dissipated. Therefore the inertia of the floes are of importance, thus also the size. To be treated as a rigid contact the floe size must either be under the threshold or the ice - non-structure interaction occurs outside the structure region. Both these forms of contact can contribute to the rubble force. Contact with small ice floes in the vicinity of the structure will be considered as a local contribution, while contacts outside the structure region will be considered as global contribution to the rubble force.

How the rubble forces in the simulation depend on the size of the ice floes are to be investigated. In Figure 7.4 the structure interacts with a large ice floe, while in Figure 7.5 it interacts with a smaller ice floe. First it is noticed that the floes splits in different patterns with more splitting for the smaller floe. The splitting depends on the compliance forces and their criterion as explained in Chapter 4. From Equation 4.10 how the splitting force is dependent on the floe size. The larger the floe is the more force is required to move it. Even if the large floe splits, it still acquire more force to move than a smaller floe. The splitting opens up for more space which the ice floes can move in. As illustrated in Figure 7.4 where the channel restricts the motions of the rubble much more than in Figure 7.5. Thus, the movements of the rubble will be different. For Figure 7.4 more of the rubble are pushed under the hull, instead of along the sides of the hull as in Figure 7.5. A larger share of rubble floes are

also pressed below the ice floe instead of floating at the surface. Such motions require more forced movements of the rubble which will increase the rubble force. The thickness of the ice floe will impact the inertia, thus also the rubble forces. Therefore the thickness of the ice floes must be considered to have an impact on the local rubble force. In addition, the size of the rubble is dependent on the thickness of the ice floe and the speed of the structure. In Raza et al., 2019 they illustrate how the rubble size increase with the floe thickness. In Berg et al., 2019 it is demonstrated how the bending radius is dependent on the speed of the structure and how this radius will decrease with increasing speed. Thus, the rubble size will decrease with increasing speed. Thus, such impact on the floe size will consequently also impact the rubble force.

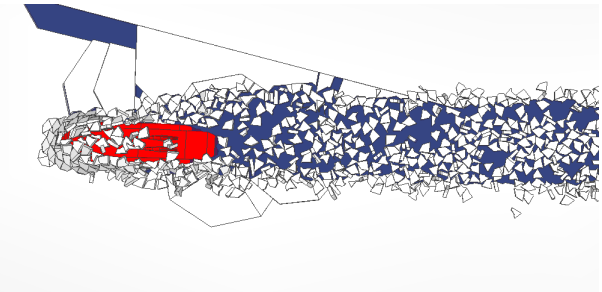

Figure 7.4: Large ice floe with ice rubble interacting with structure in SAMS, underwater view

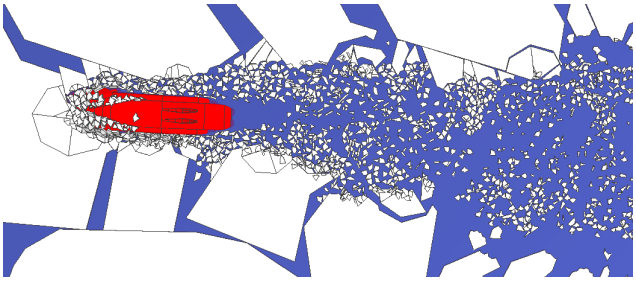

Figure 7.5: Small ice floe with ice rubble interacting with structure in SAMS, underwater view

When the structure is moving and interact with an ice floe, then the motion of this floe can impact other ice floes further away from the vessel. Motions of ice floes in the whole domain are possible through contact of floes and the force chain. These forces are considered as the global rubble forces. When the structure advances through the largest ice floes, it seems to impact more of the floes in the domain at the same time, compared to the impact from advancing through a smaller floe. This will increase the global rubble force. The concentration in the ice field is of importance since with higher concentration, there is more contact between ice floes within the ice field. Thus, the movements of the structure will induce more motions throughout the field.

Whether it is the local or global rubble force which have the most significant contribution to the rubble force is difficult to distinguish. Though both are considered significant. By considering the differences in Figure 7.1 it can be considered that the ice floe size clearly have an impact in the simulations on the total ice force in surge.

These results emphasis the significant of the route choice. Thus, the human impact is of great importance, but this is a factor that POLARIS does not consider when calculating the RIO for an ice domain. The routes which contributes to the most extreme loads within an ice regime would probably not be chosen by a competent navigator. The routes exposed to the highest loads due to floe size are route 2 for egg code 3 and route 1 for egg code 5. If these routes are excluded, then the total ice

force in surge direction would be according to Figure 7.6. Comparing this result with the one from Figure 7.1, a smaller difference in the distribution is seen. The result in Figure 7.6 indicate a small correlation and is closer to the initial consideration that the ice loads would decrease with increasing RIO than Figure 7.1.

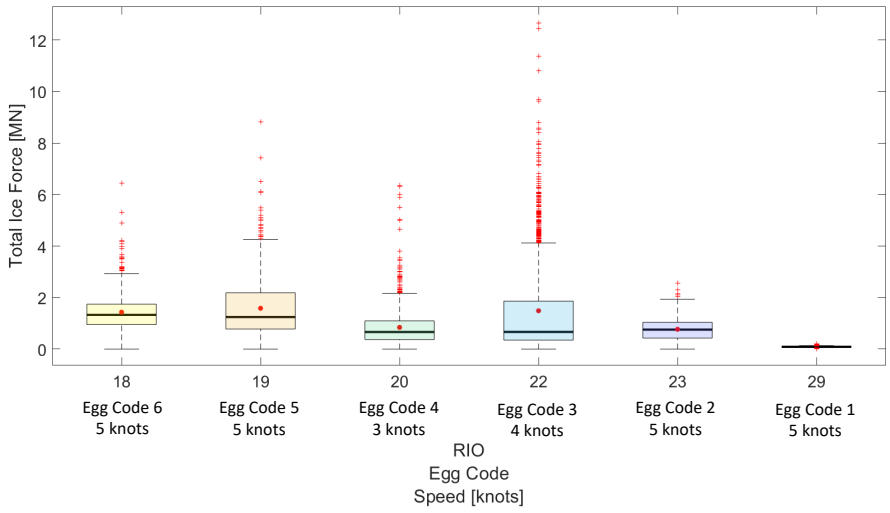

Figure 7.6: Box Plot of Time-Average Surge Force for all Egg Codes excluding most extreme routes

7.1.1 Outliers

The outliers, marked with red crosses in Figure 7.1 and Figure 7.6, indicate the points that differ significantly from the other observations. The outliers can be identified as load peaks from the simulation. To identify the situations that are causing the load peaks can be of importance as it can either indicate a situation with higher exposure of risk or an error in the simulation.

The most extreme outlier is identified in Egg Code 3 Route 2 as a peak at the time 1493 s and with a value of 14 MN, as seen in Figure 7.3a. The simulation has been considered at this time instance and in Figure 7.8 the situation can be seen in detail from a top view and an underwater view. The main deviation at this time instant compared to the the rest of the simulation, is the motion of the large ice floe indicated with a red circle in Figure 7.8. At this time instant the ice floe is not in directly contact with the structure, but due to smaller ice floes in between the structure and the large floe it is partly submerged. When the structure and the floe of interest are in contact then the floe cracks and the force drops. The simulation is working correctly, and the peak is a result of how the contact forces are defined. The peak can be recognized in the rubble force result from SAMS. Thus, as a result of being treated as a rubble force it is treated as rigid contact, until contact with the structure is made and the floe breaks, where it is treated as a compliant force. However, even though it is correctly simulated according to how the forces in SAMS are defined, it is not necessarily a correct reflection of how it would interact with the structure in the real world.

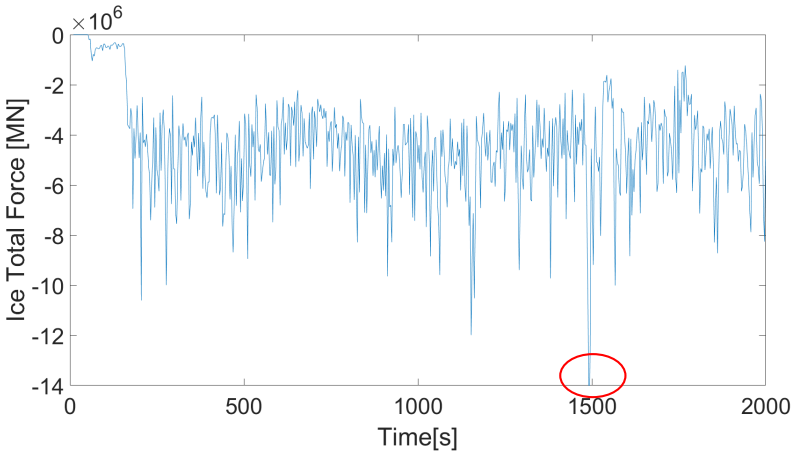

Figure 7.7: Egg Code 3 Route 2: Ice Total Force

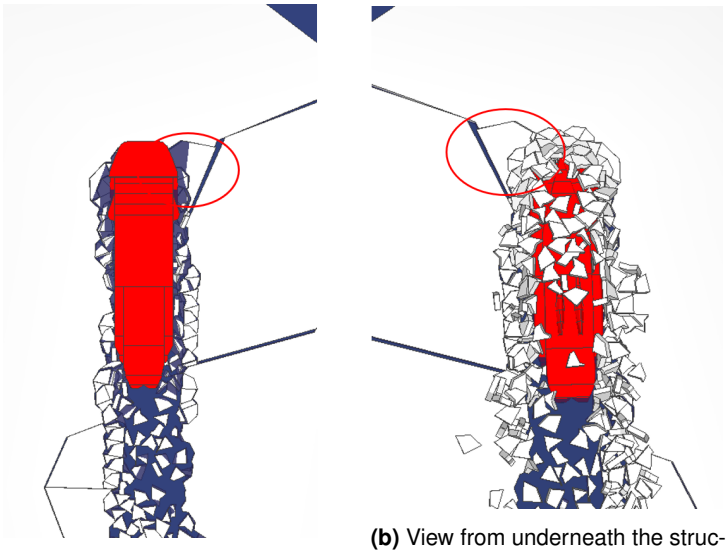

(a) Top View of the structure

(b) View from underneath the structure

Figure 7.8: Egg Code 3 Route 2, Time 1493 s in SAMS Simulation

Multiple other load peaks are considered in the same way as above. The same reasoning can be found in other cases.

7.2 Individual Study

It is of interest to consider closer the global ice loads and see how they variate. One route will be considered with varying speed. The purpose is to see how the global ice loads can vary within the same risk level. In addition, some different ice properties will be tested so influence of the ice properties can be investigated. From Section 7.1 it was clear that Egg Code 3 had a large variation of ice loads dependent on the route choice. Route 2 was the one which deviates the most from the rest of the routes and will be considered closer.

The chosen route had a logged speed of 4 knots. Additional simulations with speeds of 2, 6, 8 and 10 knots are performed. In reality, most of these ship speeds are unrealistic. Too low speed will lead

to loss of maneuverability and too high speeds are not possible to obtain with the propulsion power of Oden. The purpose is to study the force variation and it is therefore considered valid to neglect the propulsion characteristics of Oden. The three lowest speeds will be simulated with different ice properties to investigate the impact of the ice properties. For the normal ice properties the values in Table 6.5 are given. While for the weaker ice the following properties are changed: CSE is 1 MPa and the flexural strength is 250 kPa.

The box plot of the time-averaged surge force for the eighth simulations are given in Figure 7.9. From these plots the direct impact of the speed on the global ice loads can be seen, as the simulations are identical in each box plot, except for the speed, CSE and flexural strength. It can be seen that with increasing speed the global ice loads are significantly increasing. This is as expected according to Raza et al., 2019, since increasing speed will increase the ice resistance. In Figure 7.9 a clear trend is identified, as the value of the distribution and the mean value increases with increasing speed.

It is of interest to study the impact of the different ice properties. For the weaker ice properties in the right box plot of Figure 7.9, the increase in total ice force is somewhat smaller than for the normal ice properties. According to Berg et al., 2019 CSE is considered for determining contact compliance, while the flexural strength is used in the ice fracture model to determine if it is splitting or bending which will occur. The flexural strength will impact the bending force criteria, with lower flexural strength the force criterion will also decrease according to Equation 4.12. A lower criterion will according to Equation 4.9 induce failure at a lower force. Thus, the mean ice resistance will decrease. The CSE is the amount of energy necessary to crush a unit volume of ice. Thus, with decreasing CSE the contact force will decrease as according to Equation 4.5 and Equation 4.7. This will affect the force criterion from Equation 4.8 and Equation 4.9, and it will take more force to obtain the criterion of fracture. Thus, the mean ice resistance will increase. Reducing both CSE and flexural strength will affect ice fracture and mean ice resistance in different ways. When comparing the right and left plot in Figure 7.9 it can be seen that the total ice force are lower for the right plot. Thus, it seems as the flexural strength has the most impact on the ice loads.

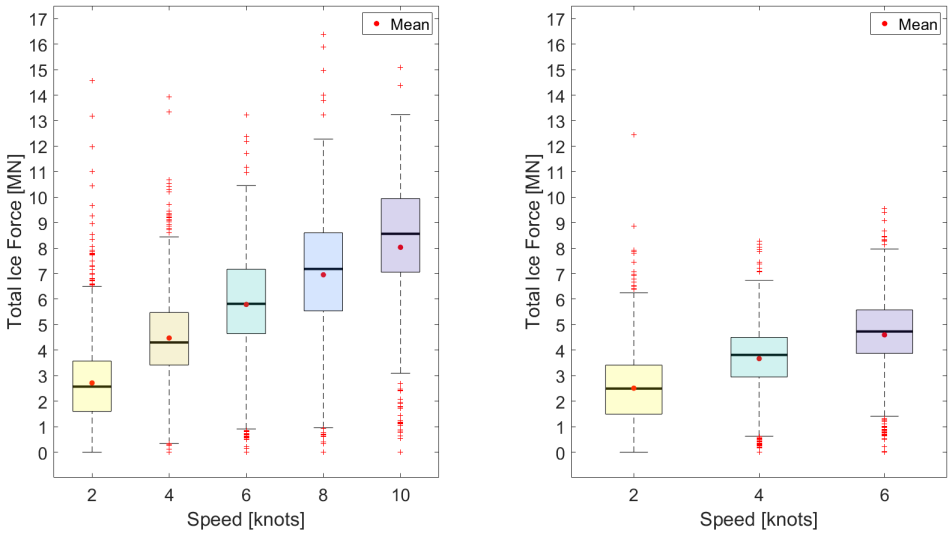

Figure 7.9: Boxplot of Time-Average Surge Force for Individual Study. Left: Normal Ice Properties. Right: Weaker Ice Properties

Considering the most extreme outliers they are in the same area despite the choice of speed. A trend is that for increasing speed the number of upper outliers decrease while the number of lower outliers

increase. This indicates that the vessel is exposed to peak loads of same magnitude despite the choice of speed. When comparing the outliers for the different ice properties, it is found that for the weaker ice the outliers are less extreme.

For all simulations only the speed and ice properties are different. From Figure 7.9 it is illustrated that this will induce different forces. In Figure 7.10 the total ice force distribution during the simulation is illustrated for a selection of different speeds for the same ice properties. The simulation time is different, but as scaled in Figure 7.10 the location are directly transferable with when comparing the plots. From Figure 7.10 it is noticed that the forces vary around higher values, but have different patterns. In addition, the loads peaks are not located at the same locations. The change in force is anticipated as the ice resistance should increase with increasing speed. Though the change in pattern and the load peaks must be considered closer.

The different load patterns indicate change in how the structure and ice interact in the simulation, as illustrated in Figure 7.11. Different ice fracture and movements of floes in the rest of the field. The frequency is equal and therefore at each time step the structure will be at different locations. In SAMS the form of contact is random and as a consequence the occurrence of a different event in the start of the simulation is likely. One different event in the beginning will affect the rest of the following events so that the final result can be completely different. The most noticeable difference is the splitting pattern. The splitting pattern depends on the contact forces and it is established that these are likely to differ for different speeds. According to *Personal communication, Kim* 2020 in ice mechanics slower speed would induce less splitting. Though when considering Figure 7.11a, 7.11b and 7.11c it seems as there is less splitting with higher the speed, which contradicts the theory of ice mechanics. Though according to *Personal communication, Berg* 2020 there is no direct link between the speed and splitting pattern in SAMS. In Figure 7.11d and 7.11e there is an increase in the splitting compared with a ship speed of 6 knots. Therefore it can be established that the splitting pattern is random in SAMS. From this the importance of considering a larger selection of simulation cases are highlighted. If only the simulation cases with 2, 4 and 6 knots where considered, then these would indicate that the splitting pattern was not random and contradicting to ice mechanics.

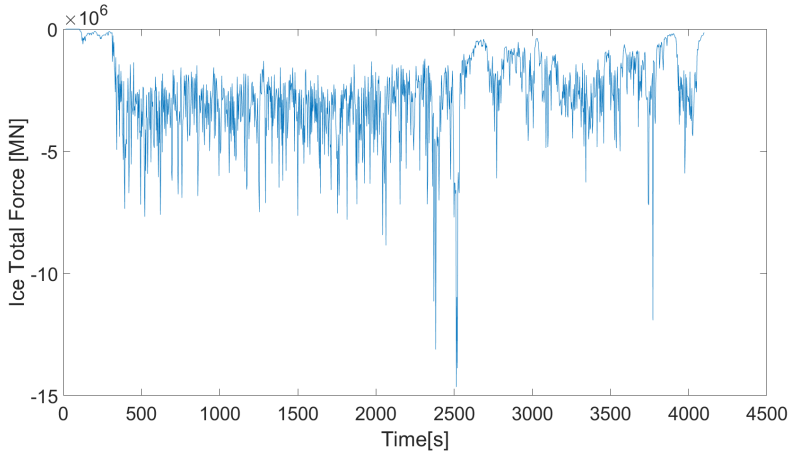

(a) Normal Ice - Speed 2 knots

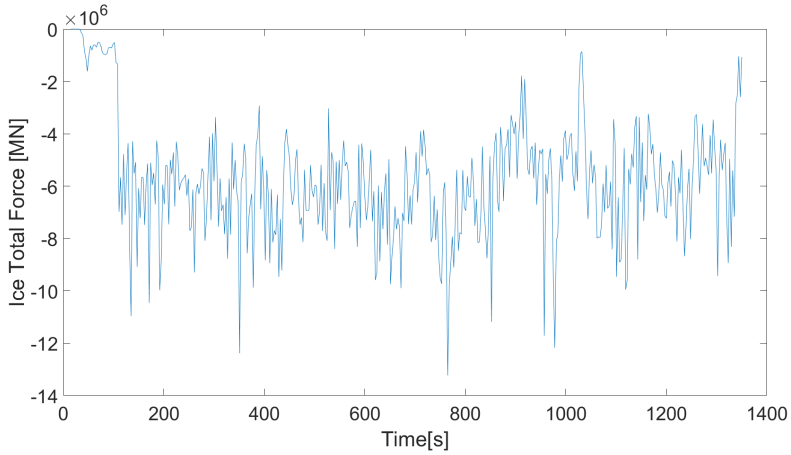

(b) Normal Ice - Speed 6 knots

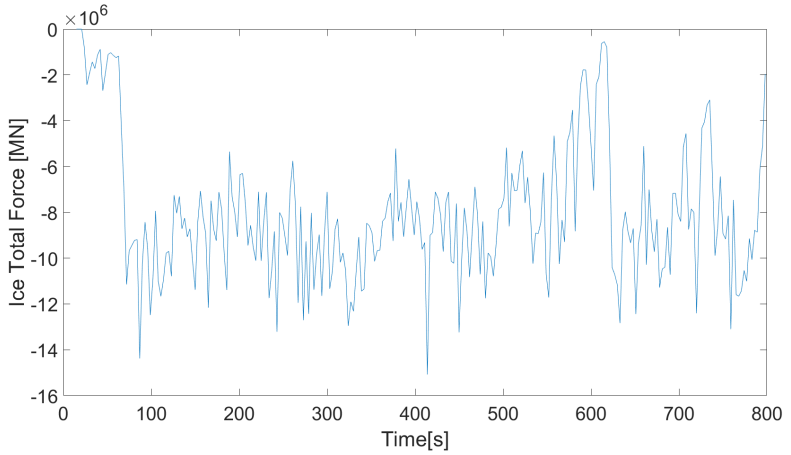

(c) Normal Ice - Speed 10 knots

Figure 7.10: Time-Averaged Total Ice Force in Surge Direction For Egg Code 3 Route 2 for different ship speeds

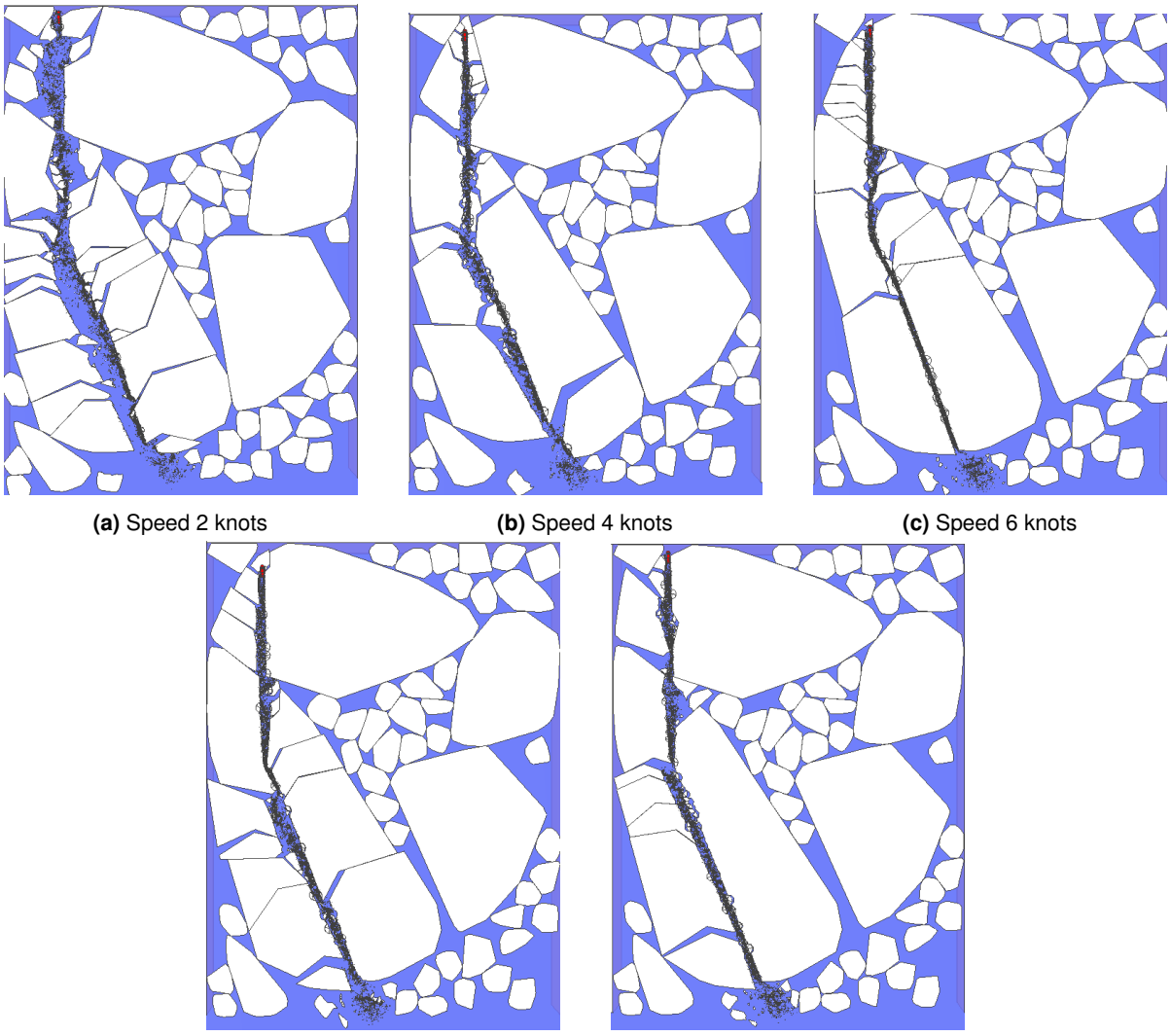

(a) Speed 2 knots **(b)** Speed 4 knots **(c)** Speed 6 knots

(d) Speed 8 knots **(e)** Speed 10 knots

Figure 7.11: Structure-Ice interaction in same ice field for different ship speeds

7.3 Concluding Remarks

The simulation results indicate that the total ice force is dependent on multiple factors such as the ice concentration, thickness, floe size, speed and the route choice. While the operational risk index RIO is found from the ice concentration and the thickness or age of the ice floes. The RIO gives an indication of the what level the operational risk is at, but as seen in the result the RIO is not directly correlated to the global ice loads. It must be emphasized that all the results in this study are within a narrow range of RIO's. Though there might not be a distinct trend from Figure 7.1, it is difficult to know if this is representative for all values of RIO.

When comparing Figure 7.1 and Figure 7.6 the impact of the route choice is clear. Through one field the ice loads can vary significantly dependent on the route. Thus, the human aspect is of great importance. POLARIS recognizes this and the importance of the judgement of the navigator is emphasized. According to IMO, 2014 an experienced ice navigator will often use active navigation to find the safest and easiest route through an ice field. Therefore the vessel can sail through an area with the presence of unsafe ice. The routes considered in this thesis are chosen due to their

distinct differences and not what would be considered the obvious route choice for an experienced navigator. Usually one is more likely to aim for the thinnest floes, but in some ice fields it can be difficult to distinguish the different ice types and therefore also the thickness of the floes. For these situations the choice of route is more incidental. The route choices in this thesis reflect the possible choices for an inexperienced navigator. The result is that the ice loads those not reflect the risk level given by the RIO value, and this highlights the necessity of experience.

The speed will in general be chosen based on the ice conditions surrounding the vessel and it will be limited due to the available propulsion power. Only for elevated risk there exists restrictions for the speed in POLARIS. As found in Section 7.2 the speed has a significant impact on the ice loads, but the choice of speed does not have a direct impact on the risk level. In other words, as long as the RIO is above zero it is up to the navigator to chose an adequate speed for the surrounding ice conditions.

The operational risk index from POLARIS gives an indication as to which risk exists within an ice field. Nevertheless, how much ice loads the vessel is exposed to is much up to the navigator and those on board the vessel. Above the importance of the route choice and speed is emphasized. The downside of this is that it open up for human mistakes. If the RIO indicate low risk, then less attention might be given and a route and speed might be chosen even though it exposes the vessel to unexpected high ice loads. Then unnecessary dangerous situations may arise.

7.4 Executive Methodology

Figure 7.12 illustrates the executive methodology for the assessment of operational risk. From retrieving observational data until establishing the link between the observational risk index and the global ice loads.

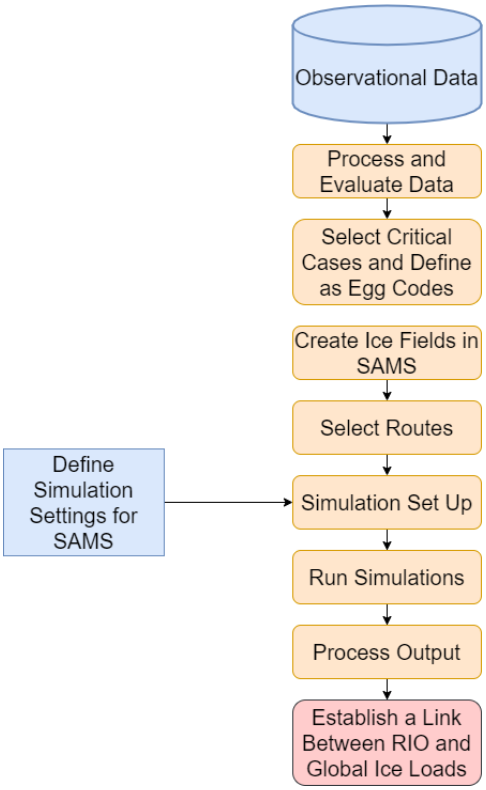

Figure 7.12: Methodology for Assessment of Operational Risk

Chapter 8

Discussion

This chapter presents a general discussion and evaluation of the performance of the open-source data, the risk analysis, and the simulation work. Also, it discusses the limitations and challenges of the work.

Ship operations in the Arctic are prone to several unique risks due to the harsh, remote, and vulnerable polar areas. IMO developed an International Code for Ships Operating in Polar Waters to maintain safe operations in these conditions. However, it exists a need for a detailed description of the limiting ice conditions that can be used in practice. Thus POLARIS was developed. The risk level vessels are exposed to, according to POLARIS, have been investigated. From the open-source at IceWatch, 2019 reported ice conditions are given. The RIO can be calculated from the available data, and risk analysis can be performed. The risk level of reported ice conditions can be utilized to evaluate and question the reason for the different risk levels. For vessels exposed to high levels of risk, it can be considered whether this is due to unforeseen severe ice conditions, poor voyage planning, or wrong information regarding ice conditions given in, for example ice charts, when planning the operation. To gain knowledge of consistency between ice charts and actual ice conditions, can improve the safety of future operations as the focus can be set on improving these aspects. Also, it is established that though not directly linked, the ship speed has an impact on the RIO.

A link between the operational risk index and the global ice loads are established using the predictive simulation software SAMS. With this link, the correlation between the ice loads and the RIO can be investigated. To evaluate this correlation will be of significance when evaluating the relevance of POLARIS. If there is no correlation, then POLARIS does not reflect the correct risk picture. The ice loads are of importance when maintaining safe ship operations and protecting the polar environment. However, it might be that for ice regimes with low risk, the navigator does not pay extra attention, or a poor route choice is made. The consequence can be critical as the global ice loads may be high. It is found that within one ice regime, the global ice loads can vary significantly. Thus active navigation of an experienced navigator is necessary to avoid the most critical ice loads.

Limitations

There exist multiple ways to evaluate the operational limitations, but only POLARIS is considered in this work. To evaluate the risk in different ways could be useful as each method has some limitations. If the risk evaluation gives similar results for multiple methods, it increases the certainty of the result.

The risk analysis and the predictive simulation are based on data from the open-source at IceWatch, 2019. Only one open-source is available. Thus, it is not easy to verify the reports on the ice conditions. If there exist errors in the data, and these are not discovered, then the analysis and simulations are performed on the wrong basis. It is, therefore, necessary when only one open-source

is available that an extensive number of data sets are considered to maintain the accuracy of the result.

For the predictive simulations, one structure, RV Oden, was available in SAMS. Only the cases from this structure with reported speed are considered in the simulation. As a consequence, only a narrow spread of RIO's with a low-risk level is then available for simulation. To run simulations for additional vessels with a wider variety of risk levels is of interest. Simulations with more data and multiple vessels will give a more extensive basis to find a correlation between the operational risk index and the global ice loads. RV Lance is an example of a vessel that could be included in the simulations, as it has RIO varying between -30 and 30.

For the predictive simulations, only six ice fields were considered. To investigate more ice fields in SAMS is of interest as it is found that the ice loads depend on the ice field geometry. In Chapter 7, it was indicated that similar ice field geometries tended to result in similar ice load distributions. With six ice fields, it is difficult to know if this is random or an actual dependency. It would be valuable to have a greater understanding of the impact on the ice loads from the ice field geometry.

The theoretical basis for the software SAMS is reviewed in Chapter 4. Compared to reality it has some simplifications which will induce some limitations of the result. For example the splitting pattern is random in SAMS, though according to ice mechanics it is dependent in the ship speed which can impact the contact forces and thus the global ice loads. The software is validated in multiple studies and therefore the results from the simulations are considered to be valid.

Observational Data

In ASSIST, extensive information can be reported regarding ice and environmental conditions. When studying the data sets in detail, it is found that much information can be filled out. Indicating that possibilities for more complex descriptions are present. For many ice regimes, only one partial ice type is reported, even though it is rare with only one ice type within an ice regime. If the ice regimes were described in more detailed, it would give a more comprehensive understanding of the ice conditions.

The data reports are a simplified version of the real ice field. It is the most commonly observed ice type that is reported. Not all ice floes are of the same thickness, and if the mean of the typical ice types is reported, then there might exist thicker ice floes than does reported. Some ice types can be reported, but are not considered in POLARIS. An example of this is brash ice. It is of great importance that the data is reported in detail and commented on in order to create a greater understanding of the real ice conditions.

It must also be considered that the observer has a misconception of the ice conditions. The weather or snow layer can impact the conception of the surrounding conditions. The thickness can be difficult to estimate correctly. The more educated and experienced the observer is, the more accurate the results should be.

Predictive Simulation

The simulation results are prone to human factors. What data is considered is of importance as it has an impact on the output. Therefore, it is essential to consider the input when performing the simulation and the analysis to obtain the most objective result. When only a part of the data is considered, it is of importance to chose representative data. An example is the performed simulation, where only six ice fields were chosen to consider closer. If these ice fields were not representative

of the overall trends from the location of the ice fields, then the result from the simulation would not reflect the situations in reality. The more ice fields are considered, the more certain is it that the obtained result is applicable. In SAMS, the ice field can vary in thickness, but all ice bodies must have the same ice properties. In a field, there will be variations in ice properties for first-year ice and multiyear ice. To take into account that not all bodies are homogeneous can make a difference.

A rigid interaction mechanism is considered in the simulations, thus non-contact loads are not taken into account. For instance, the hydrodynamic effect will have a contribution to the ice loads. It would be of interest to consider this effect. An estimate of the ice resistance can be made by consideration of Raza et al., 2019. The difference between the maximum net thrust and the net thrust at the given ship speed and ice thickness will indicate the ice resistance.

In SAMS, thruster configurations can be specified, but a constant speed is set from the tracking files and the propulsion power is not considered. The thruster configuration can impact the ice field around the vessel as it creates movement of the water. This can impact the ice loads and it would be interesting to find out how and to what extent. In reality, the speed will not be constant but vary due to the net thrust when the ice interacting with the structure changes. The propulsion effect should be considered closer in further work.

In Chapter 7, it was clear that the results were prone to the human factors in regards to the choice of route and speed. Resulting in possible large variations of ice loads for an ice field with the same RIO. It is essential for experienced navigators to make carefully considered operational decisions. POLARIS places much responsibility on the navigators, but also imposes that suitable training should be received (IMO, 2016). With increasing activity in the polar areas, it is critical that all navigational personnel have comprehensive experience when POLARIS is as it is. The route choice made for these simulations is made with the purpose of finding a considerable variation in exposure of forces and are not necessarily the route choices an experienced navigator would make.

When choosing a route it is of interest to aim for the route with the least resistance through the ice mass. If the ice resistance surpasses the propulsion power, then a vessel can get stuck in the ice. Also, between two floes, large compressive forces may exist. If the edges of two ice floes are in contact, it is difficult to know what forces exist. A vessel sailing along the edges can experience critical compressive forces on the hull and, in the worst case, get stuck between two floes. These forces can arise from current or wind, but the performed simulations does not take these factors into account. If they did, then the output result might be more severe than obtained in the current work.

Chapter 9

Conclusion and Further work

9.1 Conclusion

The research objective in this thesis was to consider observational sea ice data in predictive simulations to evaluate the operational risk. A comprehensive review of research on the development and use of POLARIS, the framework for ASSIST, and the theoretical basis for SAMS were carried out. These fields were combined with validation of preprocessed data, evaluation of operational risk according to POLARIS, development of predictive simulation framework for vessel transit in ice, and evaluation of global ice loads.

Preprocessing of observational sea ice data were considered as an essential part of the required work and were therefore conducted to an extent. By considering the extent of the data sets and areas with a significant concentration of data, reliable data was obtained despite only one open-source being available. The risk dependency on speed was established.

Predictive simulations were established based on a selection of critical cases from the risk evaluation. Simulations of a variety of ice fields and route choices were performed. From the current work, a link between the operational risk and the global ice loads was established based on observational sea ice data. From this link, no distinct trend or correlation was identified. This indicates that POLARIS does not necessarily reflect the risk level according to the structural capabilities. It is found that within one ice regime, the global ice loads can vary significantly. Thus active navigation of an experienced navigator is necessary to avoid the most critical ice loads. If the human factor is considered, then an indication of a correlation is identified. This emphasis on the importance of a competent navigator. The main achievement from the current work is the established methodology process of evaluating POLARIS and if its operational risk index reflects the actual risk level due to the ice loads. The development of a methodology establishes the basis for more comprehensive predictive simulations.

9.2 Further Work

During the development process of this thesis, several topics for further improvements and investigations have emerged. The main recommendations and suggestions for further work are described below.

More comprehensive predictive simulations should be performed. From evaluation of these results one can learn about the weaknesses of POLARIS and how to develop and improve it in the future.

Sea Ice Data

The reported data in ASSIST is, in general, very inconsistent. Though the set-up is user-friendly, it would be preferable with more consistency in the data sets in regards to what data is reported and the time step between reports. Today a description of the voyage can be given, but it would be valuable to have a more detailed description of the voyage. This can give a better understanding of the data, for example, why the time step between the reports differs to such extent.

In the future, two open-sources should be available to ensure the quality of the data information. The additional source could either be photos or comments. There are great opportunities to describe the surrounding conditions in detail. Unfortunately, this opportunity is not fully exploited. The more information is available regarding the ice conditions and meteorology, the more one can learn about the ice regimes, and the better one can recreate them for further use. The weather conditions can be useful when evaluating to what extent the data can be trusted. If visibility is poor, it is a higher chance of misreporting.

Further comparisons of ice charts and reported ice conditions should be executed. From this, valuable insight can be learned. The ice charts are essential for voyage planning, and it is inevitable for the safety that they reflect the real conditions. A thorough comparison can investigate the accuracy of the ice charts and the data reported in ASSIST.

When the data from ASSIST is more consistent, a framework for evaluation of risk according to POLARIS can be standardized. If more vessels reported ice conditions and the reports were received in ASSIST as soon as they were reported, then ice conditions could be updated continuously. This, together with automatic risk evaluation, could result in continuous scenario risk maps. These maps can be considered aboard vessels, onshore for voyage planning or by observers of maritime activity.

Simulation

A greater variety of risk levels should be analyzed to investigate if there exists a correlation between the operational risk index and global ice loads. To considered multiple vessels of different purposes and ice-classes are of interest. Also, a more considerable variation of ice fields for the predictive simulations will result in a greater variety of risk levels.

The predictive simulation in SAMS is a simplified version of reality. In the future, it should be more extensive. This can be obtained by consideration of flexible interaction mechanisms to consider hydrostatic forces. The effect of wind and current can be simulated to create a more comprehensive environment. The current outline considers constant speed, though a thruster configuration should be considered to reflect the accurate propulsion power and behavior of the vessel for the transit through the ice. The result of all these factors is the restricted accuracy of the result due to the simplified input.

Bibliography

ALLIANZ (2016). “Safety and Shipping Review 2016: An Annual Review of Trends and Developments in Shipping Losses and Safety”. In: *Insurance Newslink*. Place: Farnham Publisher: Shillito Market Intelligence Ltd. URL: https://www.agcs.allianz.com/content/dam/onemarketing/agcs/agcs/reports/AGCS-Safety-Shipping-Review-2016.pdf (visited on 03/12/2020).

— (2018). “Safety and Shipping Review 2018: An Annual Review of Trends and Developments in Shipping Losses and Safety”. In: *Insurance Newslink*. Place: Farnham Publisher: Shillito Market Intelligence Ltd. URL: https://www.agcs.allianz.com/content/dam/onemarketing/agcs/agcs/reports/AGCS-Safety-Shipping-Review-2018.pdf (visited on 03/12/2020).

American Bureau of Shipping (2016). *IMO Polar Code Advisory*. URL: https://ww2.eagle.org/content/dam/eagle/advisories-and-debriefs/ABS_Polar_Code_Advisory_15239.pdf (visited on 03/15/2020).

ARICE (2020a). *IB Oden*. Arctic Research Icebreaker Cons. URL: https://www.arice.eu/vessels/ib-oden (visited on 02/15/2020).

— (2020b). *PRV Polarstern*. Arctic Research Icebreaker Cons. URL: https://www.arice.eu/vessels/prv-polarstern (visited on 02/15/2020).

— (2020c). *RV Kronprins Haakon*. Arctic Research Icebreaker Cons. URL: https://www.arice.eu/vessels/rv-kronprins-haakon (visited on 02/15/2020).

— (2020d). *RV Sikuliaq*. Arctic Research Icebreaker Cons. URL: https://www.arice.eu/vessels/rv-sikuliaq (visited on 02/15/2020).

Ashley Roach, J. (2018). “Beyond the Polar Code: IMO Measures for Assuring Safe and Environmentally Sound Arctic Navigation”. In: *Sustainable Shipping in a Changing Arctic*. Ed. by L. P. Hildebrand, L. W. Brigham, and T. M. Johansson. Cham: Springer International Publishing, pp. 51–71. URL: https://doi.org/10.1007/978-3-319-78425-0_4.

Berg, M. van den (2019). *SAMS User Manual Version 1.0*. (Visited on 03/15/2020).

Berg, M. van den, W. Lu, and A. Tsarau (2019). *SAMS Technical Manual Version 0.6*. (Visited on 03/15/2020).

Canadian Ice Service (2019). *Ice Chart Descriptions*. Canada.ca. URL: https://www.canada.ca/en/environment-climate-change/services/ice-forecasts-observations/latest-conditions/products-guides/chart-descriptions.html (visited on 04/05/2020).

— (2020). *Ice Archive - Search Criteria*. Canada.ca. URL: https://iceweb1.cis.ec.gc.ca/Archive/page1.xhtml?lang=en (visited on 04/05/2020).

Carmeli, A. (2020). *Alluvial flow diagram*. URL: https://www.mathworks.com/matlabcentral/fileexchange/66746-alluvial-flow-diagram (visited on 03/10/2020).

Daley, C. (2014). “Ice Class Rules - Description and Comparison”. Lecture Notes. Lecture Notes. Memorial University, St. John’s, Canada. URL: https://www.engr.mun.ca/~cdaley/8074/Ice%20Class%20Rules_CD.pdf (visited on 02/15/2020).

Dempsey, J. and Z. Mu (2014). “Weight function for an edge-cracked rectangular plate”. In: *Engineering Fracture Mechanics* 132. Place: Netherlands, pp. 93–103. URL: http://dx.doi.org/10.1016/j.engfracmech.2014.10.023 (visited on 05/11/2020).

ENFOTEC Technical Services Inc, GeoInfo Solutions Ltd., and J. McCallum (1996). *Safe Speed in Inc: An analysis of transit speed and ice decision numerals*. URL: http://www.geoinfosolutions.com/projects/Safeice.pdf.

Fedi, L., O. Faury, and L. Etienne (2020). “Mapping and analysis of maritime accidents in the Russian Arctic through the lens of the Polar Code and POLARIS system”. In: *Marine Policy* 118. Publisher: Elsevier Ltd. (Visited on 05/25/2020).

Government of Canada (2005). *Manual of Ice (MANICE): chapter 2*. Canada.ca. URL: https://www.canada.ca/en/environment-climate-change/services/weather-manuals-documentation/manice-manual-of-ice/chapter-2.html (visited on 02/20/2020).

— (2017). *Arctic Ice Regime Shipping System (AIRSS)*. Canada.ca. URL: https://www.tc.gc.ca/eng/marinesafety/debs-arctic-acts-regulations-airss-291.htm (visited on 02/20/2020).

— (2020). *CCGS: Louis S. St-Laurent*. Canadian Coast Guard. URL: https://inter-j01.dfo-mpo.gc.ca/fdat/vessels/vessel-details/81 (visited on 02/15/2020).

Hindley, R. (2016). *How to use POLARIS*. (Visited on 02/10/2020).

Hu, J. and L. Zhou (2015). “Experimental and numerical study on ice resistance for icebreaking vessels”. In: *International Journal of Naval Architecture and Ocean Engineering* 7.3. Publisher: Elsevier B.V, pp. 626–639. (Visited on 04/29/2020).

Hutchings, J., J. Delamere, and P. Heil (2018). *The Ice Watch Manual*. (Visited on 02/10/2020).

IACS (2016). *Requirments Concerning Polar Class*.

IceWatch (2019). *IceWatch*. Ice Watch. URL: https://icewatch.met.no (visited on 01/20/2020).

IMO (2014). *Consideration and adoption of amendments to mandatory instruments MSC 94/INF.13*. (Visited on 01/20/2020).

— (2016). *Guidance on methodologies for assessing operational capabilities and limitiations in ice MSC.1/Circ. 1519*. (Visited on 01/20/2020).

— (2017). *International code for ships operating in poar waters (polar code)*. (Visited on 03/19/2020).

— (2020). *International Code for Ships Operating in Polar Waters (Polar Code)*. International Maritime Organization. URL: http://www.imo.org/en/MediaCentre/HotTopics/polar/Pages/default.aspx (visited on 02/10/2020).

Lubbad, R., S. Løset, et al. (2018). “Simulator for arctic marine structures (SAMS)”. In: *Proceedings of the International Conference on Offshore Mechanics and Arctic Engineering - OMAE*. Vol. 8. American Society of Mechanical Engineers (ASME).

Lubbad, R., S. Loset, et al. (2018). “An overview of the Oden Arctic Technology Research Cruise 2015 (OATRC2015) and numerical simulations performed with SAMS driven by data collected during the cruise”. In: *Cold Regions Science And Technology* 156. Publisher: ELSEVIER SCIENCE BV, pp. 1–22.

Norwegian Polar Institute (2017). *RV Lance*. Norwegian Polar Institute. URL: https://web.archive.org/web/20180818074046/http://www.npolar.no/en/about-us/stations-vessels/lance (visited on 02/15/2020).

Panci, N., E. Kim, and S. Xu (2020). *Do vessles remain within their operational limitations in ice? Analyzing the risks of vessels operatin in the Kara sea region using POLARIS*. (Visited on 03/17/2020).

Personal communication, Berg (2020). In collab. with M. van den Berg.

Personal communication, Kim (2020). In collab. with E. Kim.

Raza, N. et al. (2019). “Analysis of Oden Icebreaker Performance in Level Ice using Simulator for Arctic Marine Structures (SAMS)”. In:

Ship Technology (2020). *50 Years of Victory*. Ship Technology. URL: https://www.ship-technology.com/projects/fiftyyearsofvictoryi/ (visited on 02/15/2020).

Stoddard, M. et al. (2016). "Making sense of Arctic maritime traffic using the Polar Operational Limits Assessment Risk Indexing System (POLARIS)". In: *IOP Conference Series: Earth and Environmental Science*. Vol. 34. ISSN: 17551307 Issue: 1. Institute of Physics Publishing.

Swedish Maritime Administration (2010). *Research Vessel/Icebreaker Oden*. Swedish Maritime Administration. URL: https://web.archive.org/web/20110515211253/http://www.sjofartsverket.se/en/About-us/Activities/Icebreaking/Our-Icebreakers/Research-VesselIcebreaker-Oden/Icebreaker-Oden/ (visited on 04/27/2020).

Transports Canada (2019). *Guidelines for assessing ice operational risk*. (Visited on 02/20/2020).

Wikipedia (2019). *KV Svalbard*. Wikipedia. URL: https://no.wikipedia.org/wiki/KV_%C2%ABSvalbard%C2%BB (visited on 02/15/2020).

— (2020). *USCGC Healy (WAGB-20)*. Wikipedia. URL: https://en.wikipedia.org/wiki/USCGC_Healy_(WAGB-20) (visited on 02/15/2020).

Williams, B. and S. Zimmermann (2017). *Joint Ocean Ice Study (JOIS) 2017 Cruise Report*. Fisheries and Oceans Canada: Institute of Ocean Sciences Sidney, B.C. URL: https://dfo-mpo.gc.ca/science/documents/atsea-enmer/missions/2018/jois/2017-11-LSSL-Cruise-Report-v2018-04-30b.pdf (visited on 03/16/2020).

WMO (2014). *WMO Sea Ice Nomenclature (WMO No. 259)*. URL: https://www.jcomm.info/index.php?option=com_oe&task=viewDocumentRecord&docID=14598 (visited on 02/16/2020).

Worby, A., I. Allison, and V. Dirita (1999). *A Technique for Making Ship-Based Observations of Antarctic Sea Ice Thickness and Characteristics*. Research report (Antarctic CRC) ; no.14. Australia: Antarctic CRC and Australian Antarctic Division. (Visited on 02/11/2020).

Appendix A

ASSIST

ASSIST Header Codes

Data fields of .csv output

GENERAL	
Date	YYYY-MM-DD HH:MM:SS UTC
PO	Primary Observer
AO	Additional Observer
LAT	Latitude Decimal Degrees
LON	Longitude Decimal Degrees

SHIP	
ShP	Ship Power
ShS	Ship Speed
ShH	Ship Heading
ShA	Ship Activity

PHOTOS	
Photo	Number of photographs

COMMENTS	
Comments	Comments

ICE	
TC	Total Concentration
OW	Open Water
OT	Other Ice Type(Thin)
TH	Other Ice Type(Thick)

FAUNA	
FN	Fauna Name
FC	Fauna Count

NOTES	
note0	1st Note
note1	2nd Note
note2	3rd Note

PRIMARY ICE	
PPC	Primary Partial Concentration
PT	Primary Ice Type
PZ	Primary Thickness
PF	Primary Floe Size
PSY	Primary Snow Type
PSH	Primary Snow Thickness
PTop	Primary Topography Feature Type
PTopC	Primary Topography Concentration
PRH	Primary Topograhpy Feature Height
POld	Primary Topography Feature Old?
PCs	Primary Topography Feature Consolidated?
PSC	Primary Topography Feature Snow Covered?
PMPC	Primary Melt Pond Concentration
PMPD	Primary Melt Pond Depth
PMPP	Primary Melt Pond Pattern
PMPT	Primary Melt Pond Surface Type
PMPF	Primary Melt Pond Freeboard
PMBT	Primary Melt Pond Bottom
PMDI	Primary Melt Dried Ice
PMRI	Primary Melt Rotten Ice
PA	Primary Algae
PSD	Primary Sediment
PAD	Primary Algae Density
PAL	Primary Algae Location

SECONDARY ICE	
SPC	Secondary Partial Concentration
ST	Secondary Ice Type
SZ	Secondary Thickness
SF	Secondary Floe Size
SSY	Secondary Snow Type
SSH	Secondary Snow Thickness
STop	Secondary Topography Feature Type
STopC	Secondary Topography Concentration
SRH	Secondary Topograhpy Feature Height
SOld	Secondary Topography Feature Old?
SCs	Secondary Topography Feature Consolidated?
SSC	Secondary Topography Feature Snow Covered?
SMPC	Secondary Melt Pond Concentration
SMPD	Secondary Melt Pond Depth
SMPP	Secondary Melt Pond Pattern
SMPT	Secondary Melt Pond Surface Type
SMPF	Secondary Melt Pond Freeboard
SMBT	Secondary Melt Pond Bottom
SMDI	Secondary Melt Dried Ice
SMRI	Secondary Melt Rotten Ice
SA	Secondary Algae
SSD	Secondary Sediment
SAD	Secondary Algae Density
SAL	Secondary Algae Location

TERTIARY ICE	
TPC	Tertiary Partial Concentration
TT	Tertiary Ice Type
TZ	Tertiary Thickness
TF	Tertiary Floe Size
TSY	Tertiary Snow Type
TSH	Tertiary Snow Thickness
TTop	Tertiary Topography Feature Type
TTopC	Tertiary Topography Concentration
TRH	Tertiary Topograhpy Feature Height
TOld	Tertiary Topography Feature Old?
TCs	Tertiary Topography Feature Consolidated?
TSC	Tertiary Topography Feature Snow Covered?
TMPC	Tertiary Melt Pond Concentration
TMPD	Tertiary Melt Pond Depth
TMPP	Tertiary Melt Pond Pattern
TMPT	Tertiary Melt Pond Surface Type
TMTF	Tertiary Melt Pond Freeboard
TMBT	Tertiary Melt Pond Bottom
TMDI	Tertiary Melt Dried Ice
TMRI	Tertiary Melt Rotten Ice
TA	Tertiary Algae
TSD	Tertiary Sediment
TAD	Tertiary Algae Density
TAL	Tertiary Algae Location

METEOROLOGY	
WX	Weather
V	Visibility
HY	High Cloud Type
HV	High Cloud Cover
HH	High Cloud Height
MY	Medium Cloud Type
MV	Medium Cloud Cover
MH	Medium Cloud Height
LY	Low Cloud Type
LV	Low Cloud Cover
LH	Low Cloud Height
TCC	Total Cloud Concentration
WS	Wind Speed
WD	Wind Direction
AT	Air Temperature
WT	Water Temperature
RelH	Relative Humidity
AP	Air Pressure

Figure A.1: ASSIST Header Codes

Figure A.2: ASSIST Data Fields and Codes

ASSIST Data Fields/Codes

Data fields and lookup tables for Ice Watch observations.

GENERAL

PRIMARY OBSERVER (PO)
ADDITIONAL OBSERVER/S (AO)
Full name
Add your name to the menu on first observation.
OBSERVATION DATE/TIME (Date)
YYYY-MM-DD HH:MM:SS UTC
Converts computer time to UTC automatically.
LATITUDE (LAT)
LONGITUDE (LON)
DDD.DDD or DDD MM SS or DD MM.MMM
Converts to decimal degrees automatically.

SHIP HEADING (ShH) degrees
Nearest degree

SHIP POWER (ShP)
Not Specified
0
1/4
1/2
3/4
Full

SHIP SPEED (ShS) knots
Nearest knot

SHIP ACTIVITY (ShA)
Not Specified
10 :: Traveling in leads
20 :: Traveling in ice
30 :: Back and ramming
40 :: On station
50 :: Traveling along ice edge

FAUNA NAME (FN)
Common or scientific name
Any number of fauna types can be added
FAUNA COUNT (FC)
Number of reported species

NOTES (note0, note1, & note2)
Observer's notes, free format
Use these three fields for additional obervables you create

PHOTOS

PHOTO NAME (Photo)
Uploaded photo

PHOTO PERSPECTIVE (PhP)
Not Specified
Port
Forward
Other

COMMENTS

COMMENTS (COMM)
Observer's comments

ICE

TOTAL ICE CONCENTRATION (TC) Tenths
PARTIAL ICE CONCENTRATION (*C)
0 :: 1/10
1 :: 1/10
2 :: 2/10
3 :: 3/10
4 :: 4/10
5 :: 5/10
6 :: 6/10
7 :: 7/10
8 :: 8/10
9 :: 9/10
10 :: 10/10

OPEN WATER (OW)
0 :: No openings
1 :: Small cracks
2 :: Very narrow breaks, <50m
3 :: Narrow breaks, 50-200m
4 :: Wide breaks, 200-500m
5 :: Very wide breaks >500m
6 :: Leads
7 :: Polynya
8 :: Water broken only by scattered floes
9 :: Open sea
10 :: Strips and patches

ICE TYPE (*T)
OTHER ICE TYPE THIN (OT)
OTHER ICE TYPE THICK (TH)
10 :: Frazil
11 :: Shuga
12 :: Grease
13 :: Slush
20 :: Nilas
30 :: Pancakes
40 :: Young Grey Ice, 10-15cm
50 :: Young Grey Ice, 15-30cm
60 :: First Year, < 70cm
70 :: First Year, 70-120cm
80 :: First Year, > 120cm
75 :: Second Year
85 :: Multiyear
90 :: Brash
95 :: Fast Ice

ICE THICKNESS (*Z) cm
Total ice thickness in cm

FLOE SIZE (*F)
100 :: Pancakes
200 :: New sheet ice
300 :: Brash/Broken ice
400 :: Cake ice, < 20m
500 :: Small floes, 20-100m
600 :: Medium floes, 100-500m
700 :: Large floes, 500-2000m
800 :: Vast floes, >2000m
900 :: Bergy floes

SNOW TYPE (*SY)
00 :: No snow observation
01 :: No snow, ice or brash
02 :: Cold new snow, <1 day old
03 :: Cold old snow
04 :: Cold wind-packed snow
05 :: New melting snow(wet new)
06 :: Old melting snow
07 :: Glaze
08 :: Melt slush
09 :: Melt puddles
10 :: Saturated snow
11 :: Sastrugi

SNOW DEPTH (*SN) cm
Depth of surface snow

TOPOGRAPHY TYPE (*Top)
100 :: Level ice
200 :: Rafted Pancakes
300 :: Cemented Pancakes
400 :: Rafting
500 :: Ridges

TOPOGRAPHY CONC (*TopC) Tenths
0 :: 0/10
1 :: 1/10
2 :: 2/10
3 :: 3/10
4 :: 4/10
5 :: 5/10
6 :: 6/10
7 :: 7/10
8 :: 8/10
9 :: 9/10
10 :: 10/10

RIDGE HEIGHT (*RH) m
To nearest half meter

TOPO FEATURE OLD? **(*Old)**
TOPO FEATURE CONSOLIDATED? **(*Cs)**
TOPO FEATURE SNOW-COVERED? **(*SC)**
Yes :: True
No :: False

MELT POND CONC (*MPC) Tenths
0 :: 0/10
1 :: 1/10
2 :: 2/10
3 :: 3/10
4 :: 4/10
5 :: 5/10
6 :: 6/10
7 :: 7/10
8 :: 8/10
9 :: 9/10
10 :: 10/10

MELT POND PATTERN (*MPP)
1 :: Linked
2 :: Discrete

MELT POND SURFACE TYPE (*MPT)
1 :: Frozen
2 :: Open
3 :: Bottom up

MELT POND FREEBOARD (*MPF) cm
Height of MP freeboard above MP surface

MELT POND DEPTH (*MPD) cm
1 :: 0-10cm
2 :: 10-30cm
3 :: 30-50cm
4 :: >50cm
-9 :: Unknown

MELT POND BOTTOM TYPE (*MBT)
1 :: Solid
2 :: Some have thaw holes
3 :: All have thaw holes

DRIED ICE? (*MDI)
ROTTEN ICE? (*MRI)
Yes :: True
No :: False

ALGAE CONC. (*A) %
SEDIMENT CONC. (*SD)
0 :: 0%
1 :: <30%
2 :: <60%
3 :: >60%

ALGAE LOCATION (*AL)
1 :: Top
2 :: Middle
3 :: Bottom

ALGAE DENSITY (*AD)
0 :: Not Visible
1 :: Trace
2 :: Light
3 :: Medium
4 :: Strong
See Colour Chart

METEOROLOGY

VISIBILITY (V) m-km
90 :: <50m
91 :: 50-200m
92 :: 200-500m
93 :: 500-1000m
94 :: 1-2km
95 :: 2-4km
96 :: 4-10km
97 :: >10km

TOTAL CLOUD COVER(TCC) Oktas
HIGH CLOUD COVER (HV)
MEDIUM CLOUD COVER (MV)
LOW CLOUD COVER (LV)
0 :: 0
1 :: 1/8 or less, but not 0
2 :: 2/8
3 :: 3/8
4 :: 4/8
5 :: 5/8
6 :: 6/8
7 :: 7/8 or more, but not 8/8
8 :: 8/8

HIGH CLOUD TYPE (HY)
Ci :: Cirrus
Cs :: Cirrostratus
Cc :: Cirrocumulus

MED. CLOUD TYPE (MY)
As :: Altostratus
Ac :: AltoCumulus

LOW CLOUD TYPE (LY)
St :: Stratus
Sc :: Stratocumulus
Ns :: Nimbostratus
Cu :: Cumulus
Cn :: Cumulonimbus

HIGH CLOUD HEIGHT (HH) km
3 - 8km

MEDIUM CLOUD HEIGHT (MH) km
2 - 4km

LOW CLOUD HEIGHT (LH) km
Surface - 2km

WIND SPEED (WS) Knot
Nearest knot

WIND DIRECTION (WD) Degree
Nearest degree

AIR TEMPERATURE (AT) °C
Nearest degree, C

WATER TEMPERATURE (WT) °C
Nearest degree, C

RELATIVE HUMIDITY (RelH)
Nearest %

AIR PRESSURE (AP) mBar
Nearest mBar

WEATHER (WX)

00-03 Sky Change During Past Hour
000:: Clouds not observable/observed
001 :: Clouds dissolving/becoming less developed
002 :: State of sky as a whole unchanged
003 :: Clouds forming or developing

10-13 Mist and Shallow Fog
010 :: Mist (Visibility 1/2 nm or more)
011 :: Shallow fog in patches
012 :: Shallow fog, more or less continuous

14-16 Precipitation not at ship
014 :: Precipitation in sight, not reaching surface
015 :: Precipitation beyond 3nm, reaching surface
016 :: Precipitation within 3nm, reaching surface

20-29 Past Hour but NOT at Ob
020 :: Drizzle not freezing or snow grains
021 :: Rain not freezing or snow grains
022 :: Snow not freezing or snow grains
023 :: Rain and snow or ice pellets
024 :: Drizzle or rain, freezing
025 :: Showers of rain
026 :: Showers of snow, or of rain and snow
027 :: Showers of hail, or of rain and hail
028 :: Fog in past hour, not at present
029:: Thunderstorm, with or without precip

36-39 Unique Snow Conditions
036 :: Drifting snow below eye level, slight/moderate
037 :: Drifting snow below eye level, heavy
038 :: Blowing snow, above eye level, slight/moderate
039 :: Blowing snow, above eye level, heavy

40-49 Fog at the Time of Ob
040:: Fog: distance, not at ship in past hour**Vis may b
041 :: Fog in patches
042 :: Fog thinning in last hour, sky discernable
043 :: Fog thinning in last hour, sky not discernable
044 :: Fog unchanged in last hour, sky discernable
045 :: Fog unchanged in last hour, sky not discernable
046 :: Fog beginning/thickening in last hour, sky discerr
047 :: Fog beginning/thickening in last hour, sky not dis
048 :: Fog depositing rime, sky discernable
049 :: Fog depositing rime, sky not discernable

50-59 Drizzle
050 :: Slight drizzle, intermittent
051 :: Slight drizzle, continuous
052 :: Moderate drizzle, intermittent
053 :: Moderate drizzle, continuous
054 :: Dense drizzle, intermittent
055 :: Dense drizzle, continuous
056 :: Freezing drizzle, slight
057 :: Freezing drizzle, moderate or dense
058 :: Drizzle and rain, slight
059 :: Drizzle and rain, moderate or dense

60-69 Rain NOT Falling as Showers
060 :: Slight rain, intermittent
061 :: Slight rain, continuous
062 :: Moderate rain, intermittent
063 :: Moderate rain, continuous
064 :: Heavy rain, intermittent
065 :: Heavy rain, continuous
066 :: Freezing rain, slight
067 :: Freezing rain, moderate or heavy
068 :: Rain or drizzle and snow, slight
069 :: Rain or drizzle and snow, moderate/heavy

70-79 Solid Precip. Not as Showers
070 :: Slight fall of snow flakes, intermittent
071 :: Slight fall of snow flakes, continuous
072 :: Moderate fall of snow flakes, intermittent
073 :: Moderate fall of snow flakes, continuous
074 :: Heavy fall of snow flakes, intermittent
075 :: Heavy fall of snow flakes, continuous
076 :: Ice prisms, with/without fog
077 :: Snow grains, with/without fog
078 :: Isolated star like crystals
079 :: Ice pellets

80-84 Rain Showers
080 :: Slight rain showers
081 :: Moderate or heavy rain showers
082 :: Violent rain showers
083 :: Slight showers of rain and snow
084 :: Moderate/heavy showers of rain and snow

85-90 Solid Precipitation in Showers
085 :: Slight snow showers
086 :: Moderate or heavy snow showers
087 :: Slight showers of soft or small hail
088 :: Moderate/heavy showers of soft/small hail
089 :: Slight showers of hail
090 :: Moderate or heavy showers of hail

Appendix B

Data Evaluation and Associated Matlab Codes

Vessel and File Name

Vessel and year	file name
Amundsen 2018	observations1
Expedition 2016	observations2
Healy 2011	observations3
Healy 2015	observations4
Healy 2018	observations5
Kronprins Haakon 1 2018	observations6
Kronprins Haakon 2 2018	observations7
Lance 2012	observations8
Lance 2013	observations9
Lance 1 2014	observations10
Lance 2 2014	observations11
Lance 1 2015	observations12
Lance 2 2015	observations13
Lance 3 2015	observations14
Lance 2016	observations15
Lance 2017	observations16
Oden 2012	observations17
Oden 2013	observations18
Oden 2018	observations19
Pobedy 2015	observations20
Pobedy 2016	observations21
Pobedy 2017	observations22
Pobedy 1 2018	observations23
Pobedy 2 2018	observations24
Pobedy 3 2018	observations25
Pobedy 1 2019	observations26
Pobedy 2 2019	observations27
Pobedy 3 2019	observations28
Polarstern 2012	observations29
Polarstern 2014	observations30
Polarstern 2015	observations31
Polarstern 2017	observations32
Polarstern 2018	observations33
Sikuliaq 2015	observations34
Sikuliaq 2019	observations35
StLaurent 2006	observations36
StLaurent 2007	observations37
StLaurent 2008	observations38

```
StLaurent 2009          observations39
StLaurent 2010          observations40
StLaurent 2011          observations41
StLaurent 2012          observations42
StLaurent 2013          observations43
StLaurent 2014          observations44
StLaurent 2015          observations45
StLaurent 2016          observations46
StLaurent 2017          observations47
StLaurent 2018          observations48
Svalbard 2015           observations49
```

Data Alaska

```
%% Ship Data from Area: North of Alaska

% Vessel in area
% USCGC Healy, Polar Class: PC2
% RV Sikuliaq, Polar Class: PC5
% Louis St. Laurent, Polar Class: PC3

year = [2018 2015 2019 2006 2007 2008 2009 2010 2012 2013 2014 2015 ...
         2016 2017 2018]; % Year of data
findx = [5 34 35 36 37 38 39 40 42 43 44 45 46 47 48]; % Data file name
% Vessel data: [Healy(1) Sikuliaq(2) St. Laurent(12)]

% Location of data files
for i=1:length(year)
    fname{i}=['C:\Users\47988\OneDrive - NTNU\Master Thesis\Matlab\IceWatch Data\observations'...
            num2str(findx(i)) '.mat'];
    data(i).table=load(fname{i});
    s{i}=['observations' num2str(findx(i))];
end

RIV_Matrix = [3 3 3 3 2 2 2 2 2 1 1;  %  Risk Index Value Table, POLARIS
    3 3 3 3 2 2 2 2 2 1 1 0;
    3 3 3 3 2 2 2 2 2 1 0 -1;
    3 3 3 3 2 2 2 2 1 0 -1 -2;
    3 3 3 3 2 2 1 1 0 -1 -2 -2;
    3 2 2 2 2 1 1 0 -1 -2 -3 -3;
    3 2 2 2 1 1 0 -1 -2 -3 -3 -3;
    3 2 2 2 2 1 0 -1 -2 -3 -4 -4;
    3 2 2 2 1 0 -1 -2 -3 -4 -5 -5;
    3 2 2 1 0 -1 -2 -3 -4 -5 -6 -6;
    3 2 1 0 -1 -2 -3 -4 -5 -6 -7 -8;
    3 1 0 -1 -2 -3 -4 -5 -6 -7 -8 -8];

for k=1:numel(s)

    % Varying RIV dependent on Polar Class, boundaries must be set manually

    if findx(k) == 5                        % Healy
      RIV = RIV_Matrix(2,:);
    elseif findx(k) == 34 || findx(k) == 35 % Sikuliaq
      RIV = RIV_Matrix(5,:);
    elseif findx(k) == 36 || findx(k) == 37 || findx(k) == 38 ||...
```

```
          findx(k) == 39 || findx(k) == 40 || findx(k) == 42 ||...
          findx(k) == 43 || findx(k) == 44 || findx(k) == 45 ||...
          findx(k) == 46 || findx(k) == 47 || findx(k) == 48
    RIV = RIV_Matrix(3,:);              % St.Laurent
  else
    disp('Error')
  end

TC  = data(k).table.(s{k}).TC;     % TC = Total concentration
PPC = data(k).table.(s{k}).PPC;    % PPC = Primary Partial Concentration
PT  = data(k).table.(s{k}).PT;     % PT = Primary Ice Type
SPC = data(k).table.(s{k}).SPC;    % SPC = Secondary Partial Concentration
ST  = data(k).table.(s{k}).ST;     % ST = Secondary Ice Type
TPC = data(k).table.(s{k}).TPC;    % TPC = Tertiary Partial Concentration
TT  = data(k).table.(s{k}).TT;     % TT = Tertiary Ice Type

noDataPoints(k) = length(TC);          % Number of datapoints
max_noDataPoints = max(noDataPoints); % Find the longest dataset

noDataPoints_TC(k) = sum(~isnan(TC));
noDataPoints_primary(k) = sum(~isnan(PPC));
noDataPoints_secondary(k) = sum(~isnan(SPC));
noDataPoints_tertiary(k) = sum(~isnan(TPC));

% Defining the RIV value according to the Primary Ice Type
for i=[10 11 12 13 20 30] % Frazil, Shuga, Grease, Slush, Nilas, Pancakes
    PT(PT==i)=RIV(2);
end

PT(PT==40)=RIV(3);                  % *T = 40, Young Grey Ice, 10-15cm
PT(PT==50)=RIV(4);                  % *T = 50, Young Grey Ice, 15-30cm
PT(PT==60)=RIV(6);                  % *T = 60, First Year, <70cm
PT(PT==70)=RIV(8);                  % *T = 70, First Year, 70-120cm
PT(PT==80)=RIV(9);                  % *T = 80, First Year, >120cm
PT(PT==75)=RIV(10);                 % *T = 75, Second Year
PT(PT==85)=RIV(12);                 % *T = 85, Multiyear
PT(PT==95)=RIV(12);                 % *T = 95, Fast Ice

% Defining the RIV value according to the Secondary Ice Type
for i=[10 11 12 13 20 30]
    ST(ST==i)=RIV(2);
end

ST(ST==40)=RIV(3);
ST(ST==50)=RIV(4);
ST(ST==60)=RIV(6);
ST(ST==70)=RIV(8);
ST(ST==80)=RIV(9);
ST(ST==75)=RIV(10);
ST(ST==85)=RIV(12);
ST(ST==95)=RIV(12);

% Defining the RIV value according to the Tertiary Ice Type
for i=[10 11 12 13 20 30]
    TT(TT==i)=RIV(2);
end
TT(TT==40)=RIV(3);
TT(TT==50)=RIV(4);
TT(TT==60)=RIV(6);
TT(TT==70)=RIV(8);
TT(TT==80)=RIV(9);
TT(TT==75)=RIV(10);
```

```
  TT(TT==85)=RIV(12);
  TT(TT==95)=RIV(12);

  PT(isnan(PT))=0;
  ST(isnan(ST))=0;
  TT(isnan(TT))=0;
  TC(isnan(TC))=0;
  PPC(isnan(PPC))=0;
  TPC(isnan(TPC))=0;
  SPC(isnan(SPC))=0;

  PT_RIV{1,k} = PT;      % Saving the RIV values
  ST_RIV{1,k} = ST;
  TT_RIV{1,k} = TT;

  % Risk Index Outcome, RIO
  % Sum of concentrations equal to 10 and brash ice not considered
   for j = 1:length(TC)
       if (10-TC(j))+PPC(j)+SPC(j)+TPC(j) == 10 ...
                && PT(j) ~= 90 && ST(j) ~= 90 && TT(j) ~= 90
           RIO{1,k}(j,1)=(10-TC(j))*RIV(1)+PPC(j)*PT(j)+SPC(j)*ST(j)+...
               TPC(j)*TT(j);
       else
           RIO{1,k}(j,1) = NaN;
       end
   end

  clear TS TC PPC PT SPC ST TPC TT
end

for k=1:numel(s)

  TC{1,k}=data(k).table.(s{k}).TC;          % TC = Total Concentration
  OW{1,k}=data(k).table.(s{k}).OW;          % OW = Open Water

  PT{1,k}=data(k).table.(s{k}).PT;          % PT = Primary Ice Type
  ST{1,k}=data(k).table.(s{k}).ST;          % ST = Secondary Ice Type
  TT{1,k}=data(k).table.(s{k}).TT;          % TT = Tertiar Ice Type

  PPC{1,k}=data(k).table.(s{k}).PPC;        % PT = Primary Partial Conc.
  SPC{1,k}=data(k).table.(s{k}).SPC;        % ST = Secondary Partial Conc.
  TPC{1,k}=data(k).table.(s{k}).TPC;        % TT = Tertiar Partial Conc.

  PF{1,k}=data(k).table.(s{k}).PF;          % PF = Primary Ice Floe Size
  SF{1,k}=data(k).table.(s{k}).SF;          % SF = Secondary Ice Floe Size
  TF{1,k}=data(k).table.(s{k}).TF;          % TF = Tertiar Ice Ice Floe Size

  PZ{1,k}=data(k).table.(s{k}).PZ;          % PF = Primary Thickness
  SZ{1,k}=data(k).table.(s{k}).SZ;          % SF = Secondary Thickness
  TZ{1,k}=data(k).table.(s{k}).TZ;          % TF = Tertiar Thickness

end

% Pre-allocating the size of the matrices. Due to different sizes of
% datasets, set everything to NaN, so the size of the matrix and data sets
% will be correct, despite different lengths.

 TC_tot = nan(max_noDataPoints,numel(s));
 OW_tot = nan(max_noDataPoints,numel(s));

 PT_tot = nan(max_noDataPoints,numel(s));
 ST_tot = nan(max_noDataPoints,numel(s));
```

```
 TT_tot = nan(max_noDataPoints,numel(s));

 PPC_tot = nan(max_noDataPoints,numel(s));
 SPC_tot = nan(max_noDataPoints,numel(s));
 TPC_tot = nan(max_noDataPoints,numel(s));

 PF_tot = nan(max_noDataPoints,numel(s));
 SF_tot = nan(max_noDataPoints,numel(s));
 TF_tot = nan(max_noDataPoints,numel(s));

 PZ_tot = nan(max_noDataPoints,numel(s));
 SZ_tot = nan(max_noDataPoints,numel(s));
 TZ_tot = nan(max_noDataPoints,numel(s));

for i = 1:numel(s)
  for j = 1:numel(PT{1,i})

    TC_tot(j,i) = TC{1,i}(j,1);
    OW_tot(j,i) = OW{1,i}(j,1);

    PT_tot(j,i) = PT{1,i}(j,1);
    ST_tot(j,i) = ST{1,i}(j,1);
    TT_tot(j,i) = TT{1,i}(j,1);

    PPC_tot(j,i) = PPC{1,i}(j,1);
    SPC_tot(j,i) = SPC{1,i}(j,1);
    TPC_tot(j,i) = TPC{1,i}(j,1);

    PF_tot(j,i) = PF{1,i}(j,1);
    SF_tot(j,i) = SF{1,i}(j,1);
    TF_tot(j,i) = TF{1,i}(j,1);

    PZ_tot(j,i) = PZ{1,i}(j,1);
    SZ_tot(j,i) = SZ{1,i}(j,1);
    TZ_tot(j,i) = TZ{1,i}(j,1);
  end
end

%% Egg Code
% Saving the the egg code format.

for i = 1:numel(s)
    for j = 1:max_noDataPoints
  EggCode{j,i} = [0 TC_tot(j,i) 0; PPC_tot(j,i) SPC_tot(j,i) TPC_tot(j,i);
                  PT_tot(j,i) ST_tot(j,i) TT_tot(j,i);...
                  PF_tot(j,i) SF_tot(j,i) TF_tot(j,i)];
    end
end

% ---- RIO and Ship Speed -----

RIO_tot = nan(max_noDataPoints,numel(s));

for i=1:numel(s)
    for j = 1:numel(RIO{1,i})
    RIO_tot(j,i) = RIO{1,i}(j,1);
    end
end

for k=1:numel(s)
  ShS{1,k}=data(k).table.(s{k}).ShS;            % ShS = Ship Speed
end
```

```
ShS_tot = nan(max_noDataPoints,numel(s));

for i=1:numel(s)
    for j = 1:numel(ShS{1,i})
    ShS_tot(j,i) = ShS{1,i}(j,1);
        if  ShS_tot(j,i) > 40 || ShS_tot(j,i) < 0
           ShS_tot(j,i) = NaN;
        end
    end
end

% --------- Corelation Speed vs RIO -------

% Must only consider the speeds that are supposed to be evaluated
% Must change manually after evaluation

ShS_area = nan(max_noDataPoints,5);
ShS_area(:,1) = ShS_tot(:,1);
ShS_area(:,2) = ShS_tot(:,3);
ShS_area(:,3) = ShS_tot(:,12);
ShS_area(:,4) = ShS_tot(:,14);
ShS_area(:,5) = ShS_tot(:,15);

[length_ShS_area data_sets_ShS_area] = size(ShS_area);

RIO_area = nan(max_noDataPoints,data_sets_ShS_area);
RIO_area(:,1) = RIO_tot(:,1);
RIO_area(:,2) = RIO_tot(:,3);
RIO_area(:,3) = RIO_tot(:,12);
RIO_area(:,4) = RIO_tot(:,14);
RIO_area(:,5) = RIO_tot(:,15);


% ----------- RIO for the different Polar Classes ------------

RIO_PC1 = nan(max_noDataPoints,1);
RIO_PC2 = nan(max_noDataPoints,1);
RIO_PC3 = nan(max_noDataPoints,1);
RIO_PC4 = nan(max_noDataPoints,1);
RIO_PC5 = nan(max_noDataPoints,1);
RIO_PC7 = nan(max_noDataPoints,1);
RIO_PC10 = nan(max_noDataPoints,1);

% Retriving the RIO data for each data set and storing for the different
% Polar Classes

for i=1
    RIO_PC2(:,i) = RIO_tot(:,i);
end

for i=2:3
    RIO_PC5(:,i-1) = RIO_tot(:,i);
end

for i=4:15
    RIO_PC3(:,i-3) = RIO_tot(:,i);
end

% ----------- Ship Activity for the for the different Polar Classes ------

for k=1:numel(s)
```

```
  ShA{1,k}=data(k).table.(s{k}).ShA;          % ShA = Ship Activity
end

ShA_tot = nan(max_noDataPoints,numel(s));

for i=1:numel(s)
    for j = 1:numel(ShA{1,i})
    ShA_tot(j,i) = ShA{1,i}(j,1);

     if isnan(ShA{1,i}(j,1))
       ShA_tot(j,i) = 0;
     end
    end
end

ShA_area = nan(max_noDataPoints,5);
ShA_area(:,1) = ShA_tot(:,1);
ShA_area(:,2) = ShA_tot(:,3);
ShA_area(:,3) = ShA_tot(:,12);
ShA_area(:,4) = ShA_tot(:,14);
ShA_area(:,5) = ShA_tot(:,15);

% ----------- Categorize RIO for boxplot of RIO and ShS ------------

RIO_area_all = RIO_area(:);

for j = 1:length(RIO_area_all)

    if RIO_area_all(j) >= 20
        RIO_area_all(j) = 5;
    elseif RIO_area_all(j) >= 10 && RIO_area_all(j) <= 19
        RIO_area_all(j) = 4;
    elseif RIO_area_all(j) >= 0 && RIO_area_all(j) <= 9
        RIO_area_all(j) = 3;
    elseif RIO_area_all(j) >= -10 && RIO_area_all(j) <= -1
        RIO_area_all(j) = 2;
    elseif RIO_area_all(j) <= -11
        RIO_area_all(j)  = 1;
    elseif isnan(RIO_area_all(j))
        RIO_area_all(j) = NaN;
    else
      disp('Out of scope')
    end

end
```

Data Plots

```
clc; clear all; close all

%% -------- PLOTS (GENERIC) ---------

% This script only includes generic codes.
% Data regarding each area must be retireved from another file
% The data_all do not function for the whole script
```

```
% data_alaska()
% data_fram_strait()
% data_svalbard()
% data_georg_land()

% data_all()

%% ------ RIO vs. time ---------
% RIO evolment during voyages

for kk=1:numel(s)

date{kk} = load(fname{kk});
date{1,kk} = date{1,kk}.(s{1,kk});
Date{1,kk} = table2array(date{1,kk}(:,1));
dn{1,kk} = datenum(Date{1,kk}, 'yyyy-mm-dd HH:MM:SS UTC');

ShS{:,kk}=data(kk).table.(s{kk}).ShS;          % ShS = Ship speed

figure(kk)
plot(dn{1,kk}, RIO{1,kk}); hold on
ylim([-31; 31])
xlim auto;
datetick('x', 'yyyy-mm-dd','keepticks')      % 'yyyy-mm-dd HH:MM:SS UTC'
xlabel('Date')
ylabel('RIO')
ax = gca;
ax.XTickLabelRotation = -15;

% Color background
patch([0 max(xlim) max(xlim) 0], [0 0 max(ylim) max(ylim)], [0.1 0.9 0.2])
patch([0 max(xlim) max(xlim) 0], [-10 -10 0 0], [1 0.5 0.2])
patch([0 max(xlim) max(xlim) 0], [min(ylim) min(ylim) -10 -10], [1 0 0])
alpha(0.3)
plot(dn{1,kk}, RIO{1,kk}, 'k', 'LineWidth',1.5);
datetick('x', 'yyyy-mm-dd','keepticks')      % 'yyyy-mm-dd HH:MM:SS UTC'
set(gca,'FontSize',22)
hold off

end


%% ------------ RIO distribution regarding Polar Class ----------------
% All possible polar classes from data is listed below
% Remember to change legend for each data set

min_RIO = min(min(RIO_tot));

Edges_RIO = min_RIO:1:30;
pdf_RIO_PC1 = histcounts(RIO_PC1(~isnan(RIO_PC1)),[Edges_RIO inf],...
    'Normalization','probability');
pdf_RIO_PC2 = histcounts(RIO_PC2(~isnan(RIO_PC2)),[Edges_RIO inf],...
    'Normalization','probability');
pdf_RIO_PC3 = histcounts(RIO_PC3(~isnan(RIO_PC3)),[Edges_RIO inf],...
    'Normalization','probability');
pdf_RIO_PC4 = histcounts(RIO_PC4(~isnan(RIO_PC4)),[Edges_RIO inf],...
'Normalization','probability');
pdf_RIO_PC5 = histcounts(RIO_PC5(~isnan(RIO_PC5)),[Edges_RIO inf],...
    'Normalization','probability');
pdf_RIO_PC7 = histcounts(RIO_PC7(~isnan(RIO_PC7)),[Edges_RIO inf],...
    'Normalization','probability');
```

```
pdf_RIO_vector_all = [pdf_RIO_PC1; pdf_RIO_PC2; pdf_RIO_PC3; pdf_RIO_PC4;...
                        pdf_RIO_PC5; pdf_RIO_PC7];
pdf_RIO_vector = pdf_RIO_vector_all(all(~isnan(pdf_RIO_vector_all),2),:);

size_pdf_RIO_vector = size(pdf_RIO_vector);
Legend = cell(size_pdf_RIO_vector(1),1);
idx = [1 2 3 4 5 7];
k = 0;

figure()
bar(Edges_RIO,pdf_RIO_vector')
title(sprintf('RIO for different ships'))
xlabel(sprintf('RIO'));
ylabel(sprintf('Probability'));
% xlim([min_RIO-1 29.5])                    % To limit the axis
% ylim([0 0.205])
grid on
hold on
% Manually change the leged according to area
% legend('USCGC Healy', 'CCGS St. Laurent', 'RV Sikuliaq')  % Alaska
% legend('RV Oden','RV Polarstern','RV Kronprins Haakon','KV Svalbard',...
    %     'RV Lance','location','northwest') % Svalbard
legend('IB 50 let Pobedy','location','northwest')        % Georg land
set(gca,'FontSize',22)


%% ------------ pdf: RIO, ShS, T, PC, F, Z, RIV, ShA  ----------------
% Various plot of probability density distibutions of RIO, ship speed,
% ice type, polar class, floe size, floe thickness, RIV and Ship Activity

max_ShS = max(max(ShS_tot));

Edges_ShS = 0:1:max_ShS;
pdf_ShS = histcounts(ShS_tot(~isnan(ShS_tot)),[Edges_ShS inf],...
    'Normalization','probability');

Edges_RIO = min_RIO:1:30;
pdf_RIO = histcounts(RIO_tot(~isnan(RIO_tot)),[Edges_RIO inf],...
'Normalization','probability');

Edges_T = 10:5:95;
pdf_PT = histcounts(PT_tot(~isnan(PT_tot)),[Edges_T inf],...
    'Normalization','probability');
pdf_ST = histcounts(ST_tot(~isnan(ST_tot)),[Edges_T inf],...
    'Normalization','probability');
pdf_TT = histcounts(TT_tot(~isnan(TT_tot)),[Edges_T inf],...
    'Normalization','probability');

Edges_PC = 0:1:10;
pdf_PPC = histcounts(PPC_tot(~isnan(PPC_tot)),[Edges_PC inf],...
    'Normalization','probability');
pdf_SPC = histcounts(SPC_tot(~isnan(SPC_tot)),[Edges_PC inf],...
    'Normalization','probability');
pdf_TPC = histcounts(TPC_tot(~isnan(TPC_tot)),[Edges_PC inf],...
    'Normalization','probability');

Edges_F = 100:100:900;
pdf_PF = histcounts(PF_tot(~isnan(PF_tot)),[Edges_F inf],...
    'Normalization','probability');
pdf_SF = histcounts(SF_tot(~isnan(SF_tot)),[Edges_F inf],...
    'Normalization','probability');
pdf_TF = histcounts(TF_tot(~isnan(TF_tot)),[Edges_F inf],...
```

```
    'Normalization','probability');

max_PZ = max(PZ_tot);
max_PZ = max(max_PZ);

Edges_Z = 0:50:max_PZ;
pdf_PZ = histcounts(PZ_tot(~isnan(PZ_tot)),[Edges_Z inf],...
    'Normalization','probability');
pdf_SZ = histcounts(SZ_tot(~isnan(SZ_tot)),[Edges_Z inf],...
    'Normalization','probability');
pdf_TZ = histcounts(TZ_tot(~isnan(TZ_tot)),[Edges_Z inf],...
    'Normalization','probability');

PT_RIV_tot = nan(max_noDataPoints,numel(s));
ST_RIV_tot = nan(max_noDataPoints,numel(s));
TT_RIV_tot = nan(max_noDataPoints,numel(s));

for i = 1:numel(s)
  for j = 1:numel(PT{1,i})
    PT_RIV_tot(j,i) = PT_RIV{1,i}(j,1);
    ST_RIV_tot(j,i) = ST_RIV{1,i}(j,1);
    TT_RIV_tot(j,i) = TT_RIV{1,i}(j,1);
  end
end

Edges_RIV = -8:1:3;
pdf_PT_RIV = histcounts(PT_RIV_tot(~isnan(PT_RIV_tot)),[Edges_RIV inf],...
    'Normalization','probability');
pdf_ST_RIV = histcounts(ST_RIV_tot(~isnan(ST_RIV_tot)),[Edges_RIV inf],...
    'Normalization','probability');
pdf_TT_RIV = histcounts(TT_RIV_tot(~isnan(TT_RIV_tot)),[Edges_RIV inf],...
    'Normalization','probability');

max_ShA = max(ShA_tot);
max_ShA = max(max_ShA);

Edges_ShA = 0:1:max_ShA;
pdf_ShA = histcounts(ShA_tot(~isnan(ShA_tot)),[Edges_ShA inf],...
    'Normalization','probability');

figure()
histogram(RIO_tot(~isnan(RIO_tot)),Edges_RIO,'Normalization','probability')
xlabel(sprintf('RIO'));
ylabel(sprintf('Probability'));
xlim([-30 30]);
xticks([-30:5:30]);
grid on
hold on
set(gca,'FontSize',42)

figure()
subplot(1,2,1)
histogram(RIO_tot(~isnan(RIO_tot)),Edges_RIO,'Normalization','probability')
title(sprintf('RIO'));
xlabel(sprintf('RIO'));
ylabel(sprintf('Probability'));
legend('RIO')
grid on
hold on
set(gca,'FontSize',22)

subplot(1,2,2)
```

```
bar(Edges_PC,[pdf_PPC; pdf_SPC; pdf_TPC]')
title(sprintf('Ice Concentration'));
xlabel(sprintf('Ice Concentration [x/10]'));
ylabel(sprintf('Probability'));
legend('PPC','SPC','TPC')
grid on
hold on
set(gca,'FontSize',22)

figure()
histogram(ShS_tot(~isnan(ShS_tot)),Edges_ShS,'Normalization','probability')
xlabel(sprintf('Ship Speed [knots]'));
ylabel(sprintf('Probability'));
grid on
set(gca,'FontSize',22)

figure()
bar(Edges_T,[pdf_PT; pdf_ST; pdf_TT]')
title(sprintf('Ice Types'));
xlabel(sprintf('Ice Types'));
ylabel(sprintf('Probability'));
legend('PT','ST','TT')
grid on
hold on
set(gca,'FontSize',22)

figure()
subplot(1,2,1)
bar(Edges_F,[pdf_PF; pdf_SF; pdf_TF]')
title(sprintf('Ice Floe Size'));
xlabel(sprintf('Ice Floe Size'));
ylabel(sprintf('Probability'));
legend('PF','SF','TF')
grid on
hold on
set(gca,'FontSize',22)

subplot(1,2,2)
bar(Edges_Z,[pdf_PZ; pdf_SZ; pdf_TZ]')
title(sprintf('Ice Thickness'));
xlabel(sprintf('Ice Thickness'));
ylabel(sprintf('Probability'));
legend('PZ','SZ','TZ')
grid on
hold on
set(gca,'FontSize',22)

figure()
bar(Edges_RIV,[pdf_PT_RIV; pdf_ST_RIV; pdf_TT_RIV]')
title(sprintf('RIV values'));
xlabel(sprintf('RIV'));
ylabel(sprintf('Probability'));
legend('Primary RIV','Secondary RIV','Tertiary RIV')
grid on
hold on
set(gca,'FontSize',22)

figure()
histogram(ShA_tot(~isnan(ShA_tot)),Edges_ShA,'Normalization','probability')
title(sprintf('Ship Activity'));
xlabel(sprintf('Ship Activity'));
ylabel(sprintf('Probability'));
```

```
xticks([0:10:50])
legend('ShA')
grid on
set(gca,'FontSize',22)


%% ------ Illustratet routes in Area on map ------
% Mapping all relevant roules

for k=1:numel(s)
  LAT{k,1}=data(k).table.(s{1,k}).LAT;           % LAT = Latitude
  LON{k,1}=data(k).table.(s{1,k}).LON;           % LON = Longitude
end

figure()
load coastlines
axesm('eqaazim','MapLatLimit',[60 90])      % Define area of plot
axis on
framem on
gridm on
mlabel on
plabel on;
setm(gca,'MLabelParallel',0)
plotm(coastlat,coastlon)            % define coastlines

geoshow('landareas.shp','FaceColor',[0.6 0.8 1])

for k=1:numel(s)
geoshow(LAT{k,1},LON{k,1},'Color','r');     % show lat and lon coordinates
end
% zoom()


%% --------- Corelation Speed vs RIO -------
% Divide speed into three categories: Slow, medieum and High

 Speed_Slow = nan(max_noDataPoints,data_sets_ShS_area);
 Speed_Med = nan(max_noDataPoints,data_sets_ShS_area);
 Speed_High = nan(max_noDataPoints,data_sets_ShS_area);

for i = 1:data_sets_ShS_area
    for j = 1:length_ShS_area
        if ShS_area(j,i) <= 4
            Speed_Slow(j,i) = ShS_area(j,i);
        elseif ShS_area(j,i) >= 5 && ShS_area(j,i) <= 10
            Speed_Med(j,i) = ShS_area(j,i);
        elseif ShS_area(j,i) >= 11
            Speed_High(j,i) = ShS_area(j,i);
        end
    end
end

% Couple RIO to speed groups
RIO_categorized_slow_num = 0;
RIO_categorized_med_num = 0;
RIO_categorized_high_num = 0;
RIO_categorized_slow = nan(max_noDataPoints,data_sets_ShS_area);
RIO_categorized_med = nan(max_noDataPoints,data_sets_ShS_area);
RIO_categorized_high = nan(max_noDataPoints,data_sets_ShS_area);

for i = 1:data_sets_ShS_area
    for j = 1:max_noDataPoints
```

```
        if ~isnan(Speed_Slow(j,i))
            RIO_categorized_slow_num = RIO_categorized_slow_num + 1;
            RIO_categorized_slow(j,i) = RIO_area(j,i);
        elseif ~isnan(Speed_Med(j,i))
            RIO_categorized_med_num = RIO_categorized_med_num + 1;
            RIO_categorized_med(j,i) = RIO_area(j,i);
        elseif ~isnan(Speed_High(j,i))
            RIO_categorized_high_num = RIO_categorized_high_num + 1;
            RIO_categorized_high(j,i) = RIO_area(j,i);
        end
    end
end

% pdf: RIO for speed categories

Edges_RIO = min_RIO:1:30;
pdf_RIO_cat_slow = histcounts(RIO_categorized_slow(~isnan...
    (RIO_categorized_slow)),[Edges_RIO inf],'Normalization','probability');
pdf_RIO_cat_med = histcounts(RIO_categorized_med(~isnan...
    (RIO_categorized_med)),[Edges_RIO inf],'Normalization','probability');
pdf_RIO_cat_high = histcounts(RIO_categorized_high(~isnan...
    (RIO_categorized_high)),[Edges_RIO inf],'Normalization','probability');

figure()
bar(Edges_RIO,[pdf_RIO_cat_slow; pdf_RIO_cat_med; pdf_RIO_cat_high]')
title(sprintf('pdf RIO for Categorized Speed'));
xlabel(sprintf('RIO'));
ylabel(sprintf('Probability'));
legend('Slow Speed','Medium Speed','High Speed')
% xlim([-3 29.5])               % Too zoom in
grid on
hold on
set(gca,'FontSize',22)
```

Appendix C

Route Information

In Table C.1, Table C.2, Table C.3 and Table C.4 various route information is listed. Some of the headings are explained in the following.

Days: Number of days for the length of the voyage.

Data: Number of days when data is logged for the length of the voyage, given as the ratio of total days. Data do not need to be logged every day of the voyage.

Ice: Number of days when the vessel is moving through the ice, given as the ratio of total days. Necessary that the total concentration is not equal to zero for any of the data points during one day.

TC, TC0, OS = Total Concentration, Total Concentration = 0, Open Sea: The number of data points for the total concentration of ice, total concentration equal to zero meaning ice-free and open sea indicating no sea ice present.

P, S, T = Primary, Secondary, Tertiary: The number of data points for the primary, secondary and tertiary partial ice

(TC-TCO) per ice day: The number of data points which is logged each data when the ships are in a non ice-free environment

Table C.1: Route Information, North of Alaska (IceWatch, 2019)

Ship Year	**Date** *From* *To*	**Days** **Data, Ice**	**TC, TC0, OS** **P, S, T**	**(TC-TCO)** **per ice day**
USCGC Healy 2018	2018-09-19 2018-09-26	8 0.88, 0.63	57, 20, 22 37, 32, 13	7
RV Sikuliaq 2015	2015-10-05 2015-11-04	31 0.97, 0.97	407, 49, 62 359, 251, 84	12
RV Sikuliaq 2019	2019-11-12 2019-11-24	13 1.00, 0.92	299, 87, 91 210, 133, 18	18
CCGS St. Laurent 2006	2006-08-07 2006-09-12	37 0.89, 0.89	320, 0, 4 318, 173, 53	10
CCGS St. Laurent 2007	2007-07-29 2007-08-27	30 1.00, 1.00	362, 33, 1 325, 245, 50	11
CCGS St. Laurent 2008	2008-07-27 2008-08-20	25 0.72, 0.72	88, 0, 0 85, 77, 60	5
CCGS St. Laurent 2009	2009-09-20 2009-10-13	24 0.96, 0.96	195, 0, 0 188, 166, 97	8
CCGS St. Laurent 2010	2010-09-21 2010-10-13	23 0.83, 0.83	77, 0, 0 73, 68, 54	4
CCGS St. Laurent 2012	2012-08-08 2012-08-29	22 0.59, 0.59	40, 0, 0 38, 22, 3	3
CCGS St. Laurent 2013	2013-08-04 2013-08-31	28 1.00, 0.96	327, 11, 11 299, 226, 134	12
CCGS St. Laurent 2014	2014-09-22 2014-10-15	24 1.00, 0.96	191, 12, 9 162, 96, 23	8
CCGS St. Laurent 2015	2015-09-22 2015-10-15	24 1.00, 0.96	502, 65, 47 432, 264, 83	19
CCGS St. Laurent 2016	2016-09-22 2016-10-06	15 0.80, 0.80	65, 6, 10 62, 37, 13	5
CCGS St. Laurent 2017	2017-09-07 2017-09-20	14 0.93, 0.93	79, 15, 13 66, 31, 3	5
CCGS St. Laurent 2018	2018-09-15 2018-10-02	18 0.78, 0.72	161, 6, 9 155, 130, 68	12

Table C.2: Route Information, Fram Strait (IceWatch, 2019)

Ship Year	**Date** *From* *To*	**Days** **Data, Ice**	**TC, TC0, OS** **P, S, T**	**(TC-TCO)** **per ice day**
RV Kronprins Haakon 2018	2018-08-28 2018-09-09	13 1.00, 1.00	98, 19, 10 79, 35, 0	7
RV Lance 2012	2012-08-18 2012-09-10	24 0.88, 0.83	115, 16, 0 105, 34, 8	5
RV Lance 2013	a) 2013-08-13 b) 2013-09-01 2013-09-11	14 1.00, 1.00	36, 3, 1 34, 22, 4	2
RV Lance 2014	2014-08-25 2014-09-11	18 1.00, 1.00	112 , 3, 9 108, 64, 18	6
RV Lance 2015	2015-08-25 2015-09-09	16 1.00, 1.00	90, 0, 0 89, 50, 4	6
RV Lance 2016	2016-08-26 2016-09-11	17 0.94, 0.94	104, 4, 8 98, 63, 11	6
RV Lance 2017	2017-05-19 2017-05-23	5 1.00, 1.00	61, 9, 7 55, 32, 6	10
RV Oden 2012	2012-09-12 2012-09-23	12 0.75, 0.67	64, 1, 3 62, 51, 47	8
RV Oden 2013	2013-08-21 2013-08-31	11 0.73, 0.73	74, 0, 1 74, 72, 71	9
RV Polarstern 2014	2014-07-08 2014-07-31	24 0.96, 0.96	285, 10, 10 272, 39, 0	12

Table C.3: Route Information, North of Svalbard (IceWatch, 2019)

Ship Year	**Date** *From* *To*	**Days** **Data, Ice**	**TC, TC0, OS** **P, S, T**	**(TC-TCO)** **per ice day**
RV Lance 2014	2014-02-21 2014-02-28	8 1.00, 1.00	34, 1, 2 33, 14, 2	4
RV Lance 2015	2015-01-12 2015-03-26	73 1.00, 1.00	152, 3, 5 148, 121, 58	2
RV Lance 2015	2015-04-11 2015-06-22	73 0.96, 0.96	113, 3, 5 109, 92, 40	2
KV Svalbard 2015	2015-01-12 2015-01-17	6 1.00, 0.83	24,3, 3 22, 11, 2	4
RV Polarstern2015	2015-05-27 2015-06-24	29 0.97, 0.97	192, 0, 1 187, 75, 8	7
RV Polarstern2017	2017-05-27 2017-07-11	46 0.35, 0.33	24, 3, 1 21, 10, 2	1
RV Oden 2018	2018-08-02 2018-09-18	48 0.31, 0.31	97, 1, 1 94, 42, 3	6
RV KronprinsHaakon 2018	2018-08-15 2018-08-21	7 1.00, 0.71	34, 6, 2 20, 15, 0	6

Table C.4: Route Information, Georg Land (IceWatch, 2019)

Ship Year	**Date** *From* *To*	**Days** **Data, Ice**	**TC, TC0, OS** **P, S, T**	**(TC-TCO)** **per ice day**
IB 50 let Pobedy 2015	2015-08-03 2015-08-17	15 0.53, 0.53	41, 0, 0 39, 37, 14	5
IB 50 let Pobedy 2016	2016-07-17 2016-08-08	23 0.39, 0.39	32, 0, 0 32, 30, 5	4
IB 50 let Pobedy 2017	2017-06-17 2017-07-03	17 0.65, 0.65	41, 1, 1 40, 25, 11	4
IB 50 let Pobedy 2018	2018-07-12 2018-07-15	4 0.75, 0.75	17, 0, 0 16, 10, 5	6
IB 50 let Pobedy 2018	2018-07-24 2018-07-26	3 0.67, 0.67	15, 0, 0 15, 13, 2	8
IB 50 let Pobedy 2018	2018-08-03 2018-08-06	4 0.75, 0.75	17, 0, 0 17, 17, 16	6
IB 50 let Pobedy 2019	2019-07-11 2019-07-15	5 1.00, 1.00	23, 0, 0 23, 18, 0	5
IB 50 let Pobedy 2019	2019-07-21 2019-07-26	6 0.83, 0.83	20, 1, 1 20, 15, 2	4
IB 50 let Pobedy 2019	2019-08-02 2019-08-05	4 0.75, 0.75	10, 0, 0 10, 10, 1	3

Appendix D

Individual Study of RIO for Individual Areas

D.1 Alaska

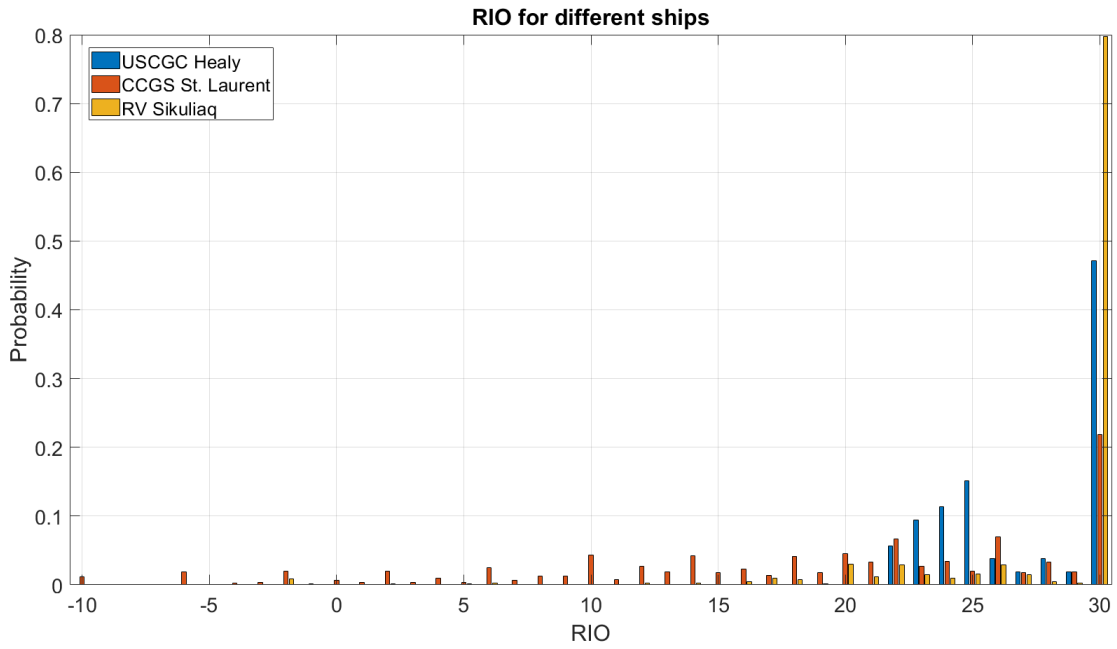

Figure D.1: pdf of RIO for different ships, North of Alaska

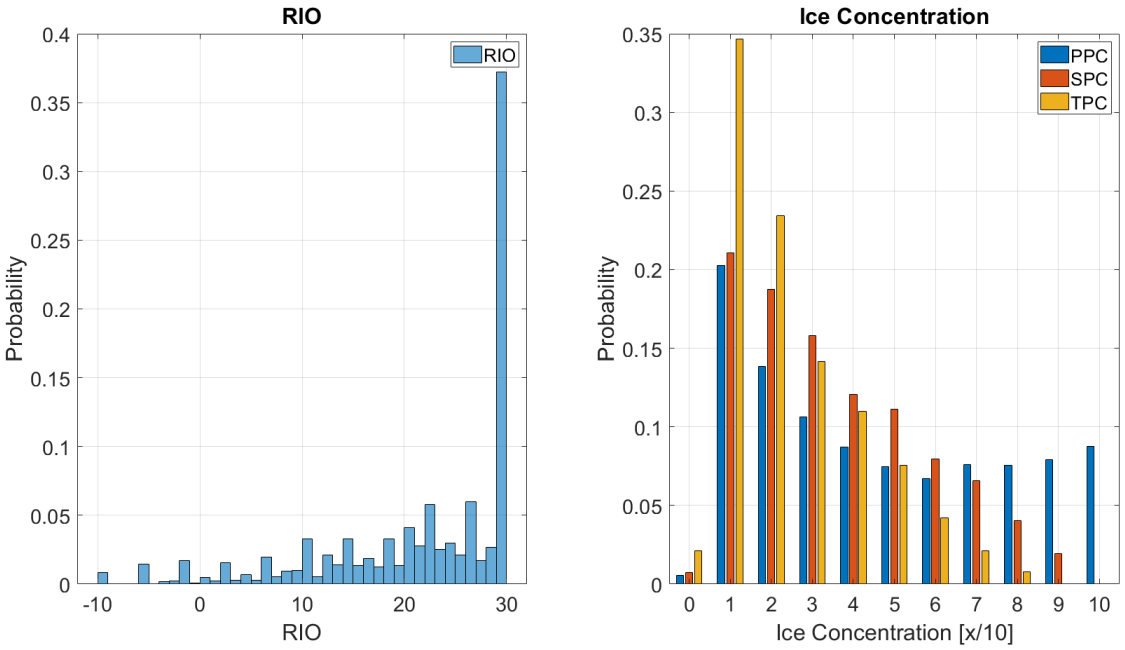

Figure D.2: pdf of RIO and concentrations, North of Alaska

Table D.1: RIO North of Alaska, max & min values

Vessel Year	Max RIO	Min RIO
USCGC Healy 2018	30	22
RV Sikuliaq 2015	30	-2
RV Sikuliaq 2019	30	20
CCGS St. Laurent 2006	28	-10
CCGS St. Laurent 2007	30	-10
CCGS St. Laurent 2008	29	10
CCGS St. Laurent 2009	30	-6
CCGS St. Laurent 2010	30	-2
CCGS St. Laurent 2012	28	8
CCGS St. Laurent 2013	30	-10
CCGS St. Laurent 2014	30	-10
CCGS St. Laurent 2015	30	-10
CCGS St. Laurent 2016	30	4
CCGS St. Laurent 2017	30	-10
CCGS St. Laurent 2018	30	-2

D.2 Fram Strait

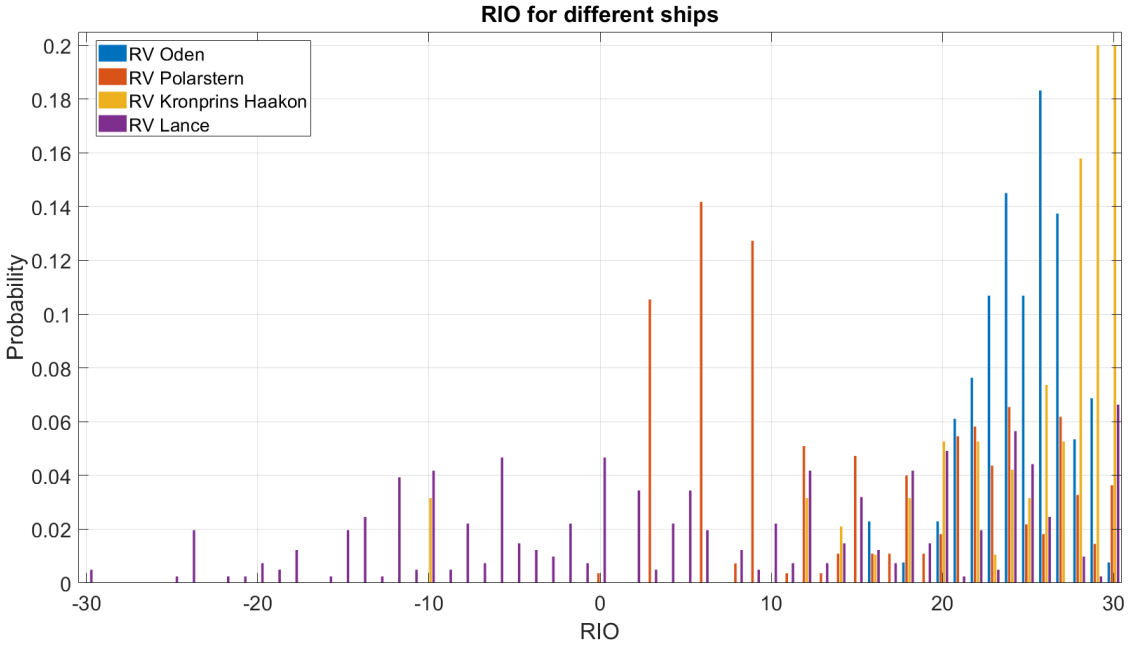

Figure D.3: pdf of RIO for different PC's, Fram Strait

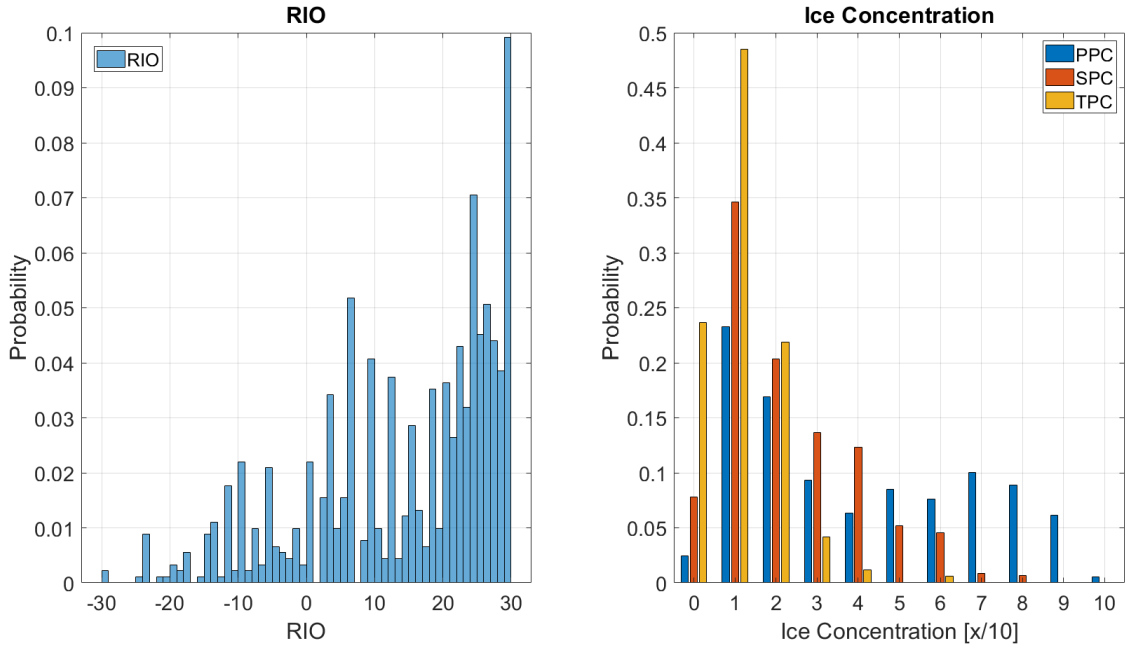

Figure D.4: pdf of RIO and concentrations, Fram Strait

Table D.2: RIO Fram Strait, max & min values

Vessel Year	Max RIO	Min RIO
RV Kronprins Haakon 2018	30	-10
RV Lance 2012	30	-30
RV Lance 2013	30	-15
RV Lance 2014	30	-24
RV Lance 2015	24	-30
RV Lance 2016	30	-24
RV Lance 2017	30	-24
RV Oden 2012	30	16
RV Oden 2013	29	20
RV Polarstern 2014	30	0

D.3 Svalbard

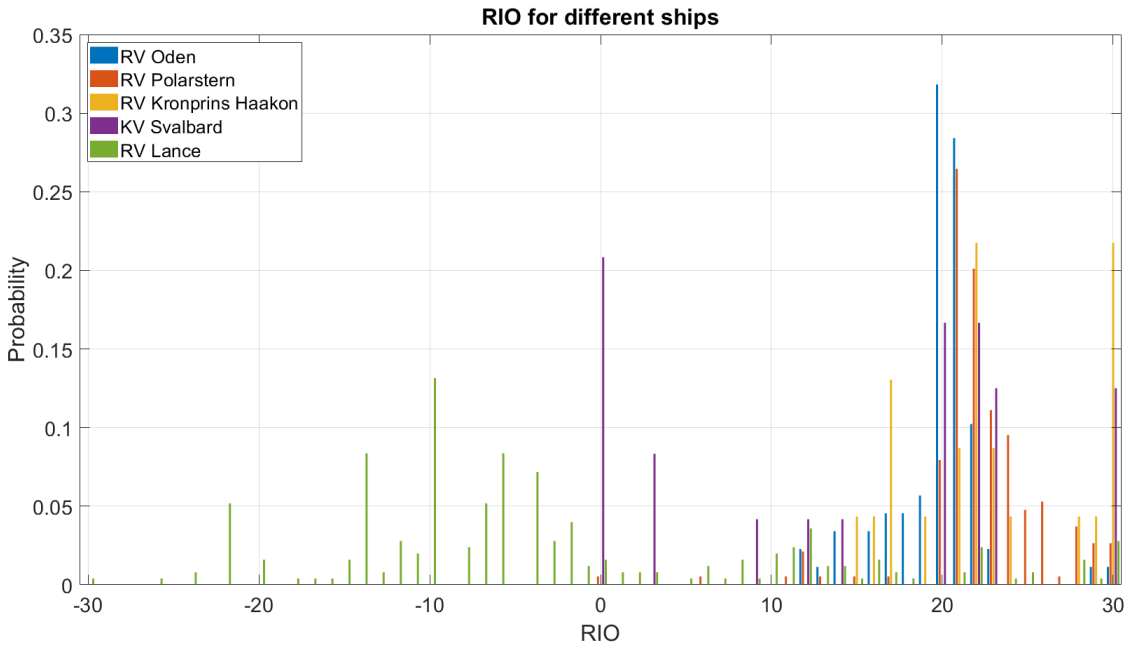

Figure D.5: pdf of RIO for different PC's, North of Svalbard

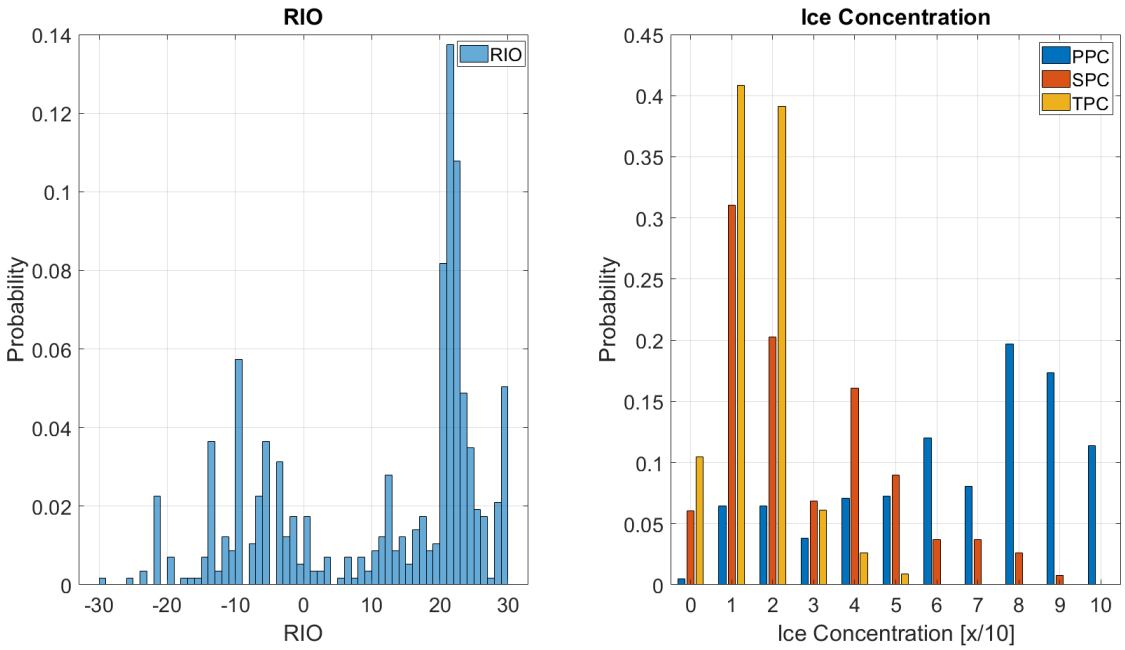

Figure D.6: pdf of RIO and concentrations, North of Svalbard

Table D.3: RIO North of Svalbard, max & min values

Vessel Year	Max RIO	Min RIO
RV Lance 2014	30	-10
RV Lance 2015	30	-30
RV Lance 2015	30	-16
KV Svalbard 2015	30	0
RV Polarstern 2015	30	0
RV Polarstern 2017	30	12
RV Oden 2018	30	12
RV Kronprins Haakon 2018	30	15

D.4 Georg Land

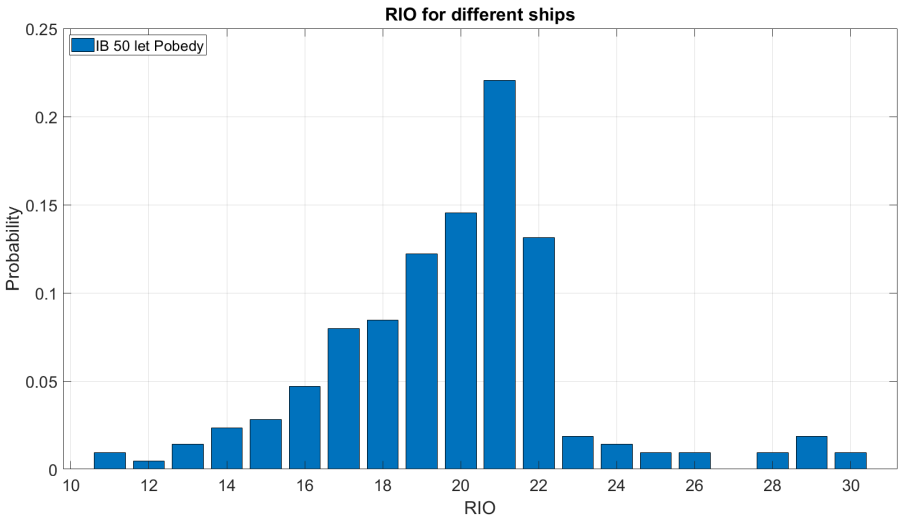

Figure D.7: pdf of RIO and Concentrations, Georg Land

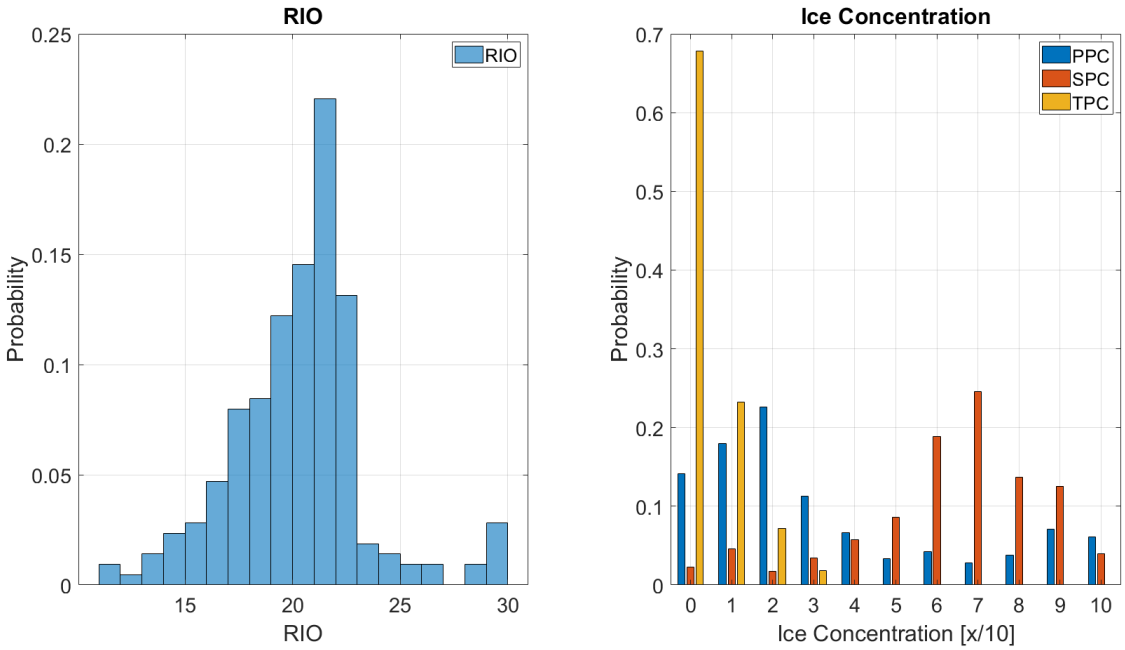

Figure D.8: pdf of RIO and Concentrations, Georg Land

Table D.4: RIO Georg Land, max & min values

Vessel Year	Max RIO	Min RIO
IB 50 let Pobedy 2015	29	18
IB 50 let Pobedy 2017	30	13
IB 50 let Pobedy 2018	21	14
IB 50 let Pobedy 2018	23	11
IB 50 let Pobedy 2018	22	15
IB 50 let Pobedy 2019	25	11
IB 50 let Pobedy 2019	30	12
IB 50 let Pobedy 2019	23	14

Appendix E

Ice Charts Comparison

For voyages such as those for RV Lance, it would be interesting to consider what the reason for sailing into severe ice conditions is. When planning a voyage, it is common to consider ice charts, therefore in the following comparison of an ice chart and reported conditions from one of the voyages would be performed. When compare ice charts with the recorded ice conditions available from IceWatch, 2019, then there should exist similarities in the ice conditions as the two sources are recording the ice conditions in the same area. If similarities are not found, the reasons for this should be considered closer. Vessels can use reported ice charts to set their route, but if these charts do not reflect the real ice conditions, then it can potentially create dangerous situations with a high level of risk. Due to that, the vessel may go into waters with too severe ice conditions compared to their structural capabilities. If the ice charts report more severe ice conditions than the reality, then the vessel might choose a less optimal route for the voyage.

According to the Canadian Ice Service, 2019, daily ice charts can be considered for tactical planning and operational purposes. The charts are based on multiple sources, such as satellite and visual observations from ships and air crafts. Based on the integration of information from these sources estimates the ice conditions at the correct time. The ice charts report the ice conditions from an area by dividing the area on the map into different ice regimes defined by egg codes. The format off the Egg Code is explained in Section 2.4. Also, the ice charts often utilize the WMO color code for the stage of development. This way, an impression of the different ice regimes and their severity can quickly be made. To compare the recordings from IceWatch, 2019 with ice charts, the recordings must be written in the format of the Egg Codes and not the format following the definitions in Section 3.1.

From Table E.1 three different recordings from the same day, 22 of September 2015, are listed. They are listed on the format off the Egg Codes, but have symbols from ASSIST following Section 3.1. The corresponding Table E.2 follows the correct egg code format and has been defined in order to compare the recordings with an ice chart. The findings in Table E.2 are from comparing Table E.1 with the definitions and symbols in Section 3.1 and Section 2.4.

Table E.1: Recordings 22 September 2015 Alaska (IceWatch, 2019)

	Time (LAT , LON)					
	23:00 (72.45 , -134.38)		**18:53 (72.29 , -133.76)**		**15:01 (71.93 , -132.43)**	
TC	1		4		10	
***C**	1		1	3	1	9
***T**	85		85	85	90	20
***F**	400		500	400	300	200

When considering the three random recordings from the same day, it can be seen that there are some variations between them.

It can be seen that the concentration varies greatly and that for two of the data points, multi-year ice is recorded. While for the last brash ice and nilas are recorded. Even though the concentration here varies greatly, it must be considered that for the last recording, nilas has a concentration of 90 %, which will impact the risk level though not as much as older and thicker ice will. It is noticed that the observations are made quite close in time and with a position not too far from each other.

Table E.2: Egg Codes 22 September 2015 Alaska (IceWatch, 2019)

	Time (LAT , LON)		
	23:00 (72.45 , -134.38)	**18:53 (72.29 , -133.76)**	**15:01 (71.93 , -132.43)**
TC	1	4	10
***C**	1	1 3	1 9
***S**	9 ·	9 · 9 ·	4 · ** 2
***F**	2	3 2	1 1 ***

** Brash Ice not listed in Table 2.6. Have from Table 3.8 a definition of brash ice which is considered.

*** New Sheet Ice not listed in Table 2.7. It is assumed that new sheet ice is equivalent to small ice cake.

Figure E.1 is the daily ice chart of the Alaskan Coast on the 22 September 2015 from Canadian Ice Service, 2020.

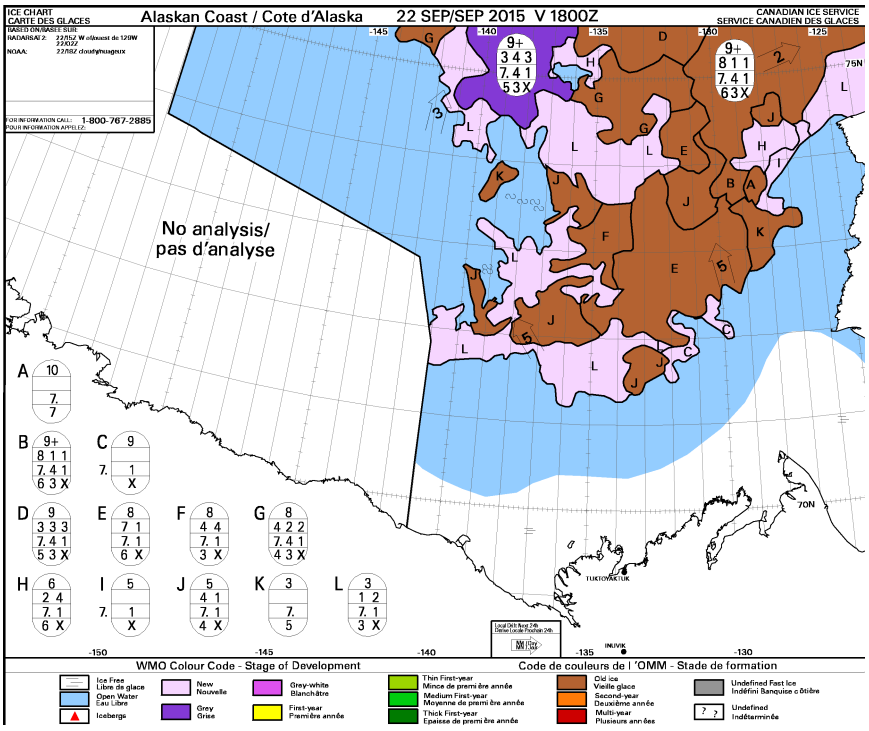

Figure E.1: Ice Chart Alaskan Coast 22 September 2015 (Canadian Ice Service, 2020)

The latitudinal and longitudinal coordinates can be recognized in Figure E.1. It is identified that the coordinates of the recordings from ASSIST are in the following ice regimes defined by Figure E.1.

The relevant Egg Codes are stated in Figure E.1.

- (72.45, -134.38) in ice regime L.
- (72.29, -133.76) in ice regime E.
- (71.93, -132.43) in ice regime J.

For (72.45, -134.38) in ice regime L the ice chart report of the total concentration of 3 and with two different ice types. Where the primary ice type have concentration 1, stage of development 7·, old ice, and form of ice 3, small floe. The secondary ice type has a concentration of 2, stage of development 1, new ice, and no form of ice recorded. The recordings from ASSIST report of the total concentration of 1 with only one ice type. Where the primary ice type has concentration 1, stage of development 9·, multi-year ice, and form of ice 2, ice cake. From this, it can be seen that the ice chart has a higher concentration than the recordings, but that the primary ice type in the ice chart has the same concentration as the recordings from ASSIST. The secondary ice type has significantly lower thickness than the primary one, and the ice type will probably not be critical in regards to the risk. Therefore the primary ice type from the ice chart can be considered when comparing to the recordings from ASSIST. From this, it can be seen that the stage of development is less severe for the ice charts, but that the floe size is larger. Even though there is a difference here, the recorded ice condition and the one from the Ice Charts are quite similar.

Comparing the Egg Code of recording (72.29, -133.76) and the ice regime E, it can be seen that the total concentration is higher for the Ice Charts than in the recordings from the ships. Where the Ice Chart has a total concentration of 8, the recorded total concentration is four. The partial concentrations, stage of development, and form of ice differ as well. Where the primary ice type have concentration of seven, stage of development 7·, old ice, and form of ice 7, vast floe. The secondary ice type has a concentration of one, stage of development one, new ice, and has not recorded the form of ice. Compared to the recordings from IceWatch, the primary ice type has a concentration of 1, stage of development 9·, multi-year ice, and form of ice 3, small floe. The secondary ice type has a concentration of 3, stage of development 9·, multi-year ice, and form of ice 2, ice cake. In comparison, both records of heavy ice conditions due to either multi-year ice or old ice, but the concentration reported from the Ice Chart is higher than the recordings from the ships. Even though for the recordings, both the primary and secondary ice types are of multi-year ice with different floe sizes, their total concentration is still significantly smaller than the primary one in the Ice Chart. Therefore it is concluded that the ice conditions represented in the Ice Charts are more severe than the ones recorded.

Comparing the Egg Code of recording (71.93, -132.43) and the ice regime J, it can be seen that the total concentrations differ significantly. Where the Ice Chart reports of the total concentration of five, it is recorded a total concentration of ten. The partial concentrations, stage of development, and form of ice differ as well. Where the primary ice type have concentration of four, stage of development 7·, old ice, and form of ice 4, medium floe. The secondary ice type has a concentration of one, stage of development one, new ice, and has not recorded the form of ice. Compared to the recordings from IceWatch, the primary ice type has a concentration of 1, stage of development 4·, thick first-year ice, and form of ice 1, small ice cake, or brash ice. The secondary ice type has a concentration of 9, stage of development 2, nilas, and form of ice 1, small ice cake, or brash ice. In comparison, the ice conditions, according to the ice chart, are more severe than those recorded from the vessel. Even though the total concentration is less for the ice chart, the primary ice floes are both older and larger. Thus, they will be of higher risk than the high concentration of nilas which is recorded from the ship.

From the comparison performed above, it can be concluded that the ice charts estimate ice conditions that are equal or more severe than the ones the ships actually are experiencing and recording. Above only one ice chart and three points from one day are compared. Therefore it is not easy to know if this is representative in general. The three recordings were chosen randomly, and they are not necessarily representative of the entire surrounding ice regime. When choosing recordings to compare with the ice chart, more care should be taken in order to choose representative ice conditions. More extensive comparisons should be performed in order to check multiple ice charts against more evaluated recordings. Nevertheless, the comparison above can be considered as a procedure to analyses the similarities between the ice chart and recordings from a ship.

Appendix F

Simulation in SAMS

F.1 Configuration File


```
{
  "simulationSettings": {
    "advancedUserInputFile": "AdvancedUserInput.itconfig",
    "frequency": 100.0,
    "maxSimulationTime": 1500.0,
    "enableFracturing": true
  },
  "iceFieldProperties": {
    "iceDataFile": "EggCode1.ice",
    "iceDensity": 910.0,
    "crushingSpecificEnergy": 2000000.0,
    "youngsModulus": 5000000000.0,
    "poissonsRatio": 0.3,
    "fractureToughness": 150000.0,
    "flexuralStrength": 500000.0,
    "tensileStrength": 500000.0,
    "friction_Ice_Ice": 0.15,
    "friction_Ice_Structure": 0.15,
    "friction_Ice_Walls": 0.15
  },
  "structureProperties": {
    "structuresFile": "structures_EggCode1Track1.txt"
  },
  "structureHydrodynamicProperties": {},
  "ice3DResultExportSettings": {
    "enable": true,
    "exportCurrent": false,
    "outputTimeStepStride": 50
  },
  "environmentalProperties": {
    "confinedDomain": true,
    "tankWallHeight": 10.0,
    "waterDepth": 1.7976931348623157e308,
    "airDensity": 1.04,
    "waterDensity": 1025.0,
    "maxBodyMeshSize": 100.0,
    "windVelocityVector": [0.0, 0.0, 0.0],
    "currentVelocityVector": [0.0, 0.0, 0.0],
    "waterSkinFrictionCoefficient": 0.005,
    "waterFormDragCoefficient": [0.1, 0.1, 0.5],
    "airSkinFrictionCoefficient": 0.0,
```

```
    "maxVelocityForLinearDrag": 0.1,
    "fluid3DMeshSize": [100.0, 100.0, 1.0],
    "numberOfFluidMeshLayers": 1
  }
}
```

F.2 Structure File

```
{
    "structures": [
        {
            "structureProperties": {
                "structureObjFile": "Oden.obj",
                "structureMass": 13000000.0,
                "structureRadiusOfGyration": [7.45,30.90,30.30],
                "structurePosition": [0.0, 0.0, 0.0],
                "structureRotationAxis": [0.0, 0.0, 1.0],
                "structureRotationAngle": 0.0
            },
            "InteractionMechanismProperties": {
                "InteractionMechanismType": "rigid",
                "linearTowing": false
            },
            "trackInteractionMechanismProperties":{
                "towingTrackFile": "EggCode1Track1_Input.txt"
            }
            }
    ]
}
```

F.3 Track File

For each time step a new location with associated information is given through the simulation time. Due to extensive file, only the two first and the last time step is found below.

```
{
    "timeSteps": [
        {
            "time": 0,
            "position": [-120,-200,0],
            "linearVelocity": [2.57222222,0,0],
            "angularVelocity": [0,0,0],
            "headingAxis": [0,0,1],
            "headingRotation": 0
        },
        {
            "time": 8.325151627,
            "position": [-98.58586,-200,0],
            "linearVelocity": [2.57222222,0,0],
            "angularVelocity": [0,0,0],
            "headingAxis": [0,0,1],
            "headingRotation": 0
        },
.
.
.
.
.
```

```
        {
            "time": 815.8648595,
            "position": [1978.58586,-200,0],
            "linearVelocity": [2.57222222,0,0],
            "angularVelocity": [0,0,0],
            "headingAxis": [0,0,1],
            "headingRotation": 7.604526212e-14
        }
    ]
}
```

Appendix G

Global Load Comparison

Find Time-Average Ice Force in Surge Direction

```
clear all; clc , close all

% Define frequency, result file and time step interval. This may differ
% from result to result.

frequency = 100;
timeStep = 1/frequency;

DataResult = readmatrix('EggCode6Track3_Result.txt', 'headerlines', 6);
timeSteps = 10:3:660;

time = DataResult(:,1);
x_position = DataResult(:,2);
y_position = DataResult(:,3);
vesselTrack = [x_position,y_position];
dxy = diff(vesselTrack);
vesselHeading_deg = [0;atan2(dxy(:,2),dxy(:,1))]*180/pi;
vesselHeading_rad = [0;atan2(dxy(:,2),dxy(:,1))];

% Dependent on old or new version of SAMS the relevant output will be found
% at different places in the result file.

% Old SAMS version
% IceBreakingForceX = DataResult(:,20);
% IceBreakingForceY = DataResult(:,21);
%
% IceRubbleForceX = DataResult(:,23);
% IceRubbleForceY = DataResult(:,24);

% New SAMS version
IceBreakingForceX = DataResult(:,30);
IceBreakingForceY = DataResult(:,31);

IceRubbleForceX = DataResult(:,33);
IceRubbleForceY = DataResult(:,34);

IceTotalForceX = IceBreakingForceX + IceRubbleForceX;
IceTotalForceY = IceBreakingForceY + IceRubbleForceY;

% Find the total ice force in surge direction
IceTotalForce = IceTotalForceX.*cos(vesselHeading_rad) +...
                  IceTotalForceY.*sin(vesselHeading_rad);
```

```
IceTotalForce_time = IceTotalForce((timeSteps(1)-3)*frequency:timeSteps(end)*frequency);

n = 3*frequency;        % Average by three seconds
IceTotalForceAverage = arrayfun(@(i) mean(IceTotalForce_time(i:i+n-1)),1 ...
                        :n:length(IceTotalForce_time)-n+1)';

AvgIceTotalForce = [timeSteps; IceTotalForceAverage'];

dlmwrite('EggCode6Track3_AvgIceTotalForce.txt',AvgIceTotalForce)

figure()
plot(timeSteps, IceTotalForceAverage)
xlabel('Time[s]')
ylabel('Ice Total Force [MN]')
set(gca,'FontSize',22)
```

Global Load Comparison

```
close all; clear all; clc

%% SAMS Result Files
% The results from SAMS are decomposed to surge direction and time-averaged

EggCode1Track1 = abs(readmatrix('EggCode1Track1_AvgIceTotalForce.txt'));
EggCode1Track2 = abs(readmatrix('EggCode1Track2_AvgIceTotalForce.txt'));

EggCode2Track1 = abs(readmatrix('EggCode2Track1_AvgIceTotalForce.txt'));
EggCode2Track2 = abs(readmatrix('EggCode2Track2_AvgIceTotalForce.txt'));

EggCode3Track1 = abs(readmatrix('EggCode3Track1_AvgIceTotalForce.txt'));
EggCode3Track2 = abs(readmatrix('EggCode3Track2_AvgIceTotalForce.txt'));
EggCode3Track3 = abs(readmatrix('EggCode3Track3_AvgIceTotalForce.txt'));

EggCode4Track1 = abs(readmatrix('EggCode4Track1_AvgIceTotalForce.txt'));
EggCode4Track2 = abs(readmatrix('EggCode4Track2_AvgIceTotalForce.txt'));

EggCode5Track1 = abs(readmatrix('EggCode5Track1_AvgIceTotalForce.txt'));
EggCode5Track2 = abs(readmatrix('EggCode5Track2_AvgIceTotalForce.txt'));
EggCode5Track3 = abs(readmatrix('EggCode5Track3_AvgIceTotalForce.txt'));

EggCode6Track1 = abs(readmatrix('EggCode6Track1_AvgIceTotalForce.txt'));
EggCode6Track2 = abs(readmatrix('EggCode6Track2_AvgIceTotalForce.txt'));
EggCode6Track3 = abs(readmatrix('EggCode6Track3_AvgIceTotalForce.txt'));


%% Boxplot

% Make a boxplot of the load and RIO, where each RIO also represent an egg
% code and a speed. Find the mean of each box

EggCode1_AvgForce = [EggCode1Track1(2,:) EggCode1Track2(2,:)];
EggCode2_AvgForce = [EggCode2Track1(2,:) EggCode2Track2(2,:)];
EggCode3_AvgForce = [EggCode3Track1(2,:) EggCode3Track2(2,:) EggCode3Track3(2,:)];
EggCode4_AvgForce = [EggCode4Track1(2,:) EggCode4Track2(2,:)];
EggCode5_AvgForce = [EggCode5Track1(2,:) EggCode5Track2(2,:) EggCode5Track3(2,:)];
EggCode6_AvgForce = [EggCode6Track1(2,:) EggCode6Track2(2,:) EggCode6Track3(2,:)];
```

```
EggCode1_RIO = 29*ones(1,length(EggCode1_AvgForce));
EggCode2_RIO = 23*ones(1,length(EggCode2_AvgForce));
EggCode3_RIO = 22*ones(1,length(EggCode3_AvgForce));
EggCode4_RIO = 20*ones(1,length(EggCode4_AvgForce));
EggCode5_RIO = 19*ones(1,length(EggCode5_AvgForce));
EggCode6_RIO = 18*ones(1,length(EggCode6_AvgForce));

AvgForce = [EggCode1_AvgForce EggCode2_AvgForce EggCode3_AvgForce ...
            EggCode4_AvgForce EggCode5_AvgForce EggCode6_AvgForce];
RIO = [EggCode1_RIO EggCode2_RIO EggCode3_RIO EggCode4_RIO ...
        EggCode5_RIO EggCode6_RIO];

AvgForce_RIO_vector = [AvgForce(:)  RIO(:)];

AvgForce_RIO_fir = (AvgForce_RIO_vector(all(~isnan(AvgForce_RIO_vector),2),:));
AvgForce_fir = AvgForce_RIO_fir(:,1);
RIO_fir = AvgForce_RIO_fir(:,2);
AvgForce_RIO_fir = array2table(AvgForce_RIO_fir,'VariableNames',{'AvgForce' 'RIO'});

% create the a function of a polynomial of 1 degree for the mean
f = fit(AvgForce_fir,RIO_fir,'poly1');
mean_var = varfun(@mean,AvgForce_RIO_fir,'GroupingVariable','RIO');
mean_value = table2array([mean_var(:,1) mean_var(:,3)]);
fit_mean = fit(mean_value(:,1),mean_value(:,2)/10^6,'poly1');

% Plot
color_all(1,1) = 0.01;
for i = 1:6
color_all(1,i+1) = color_all(1,i) + 0.3;
end

figure()
H = boxplot(AvgForce(:)/10^6,RIO(:),'ColorGroup',[]); % Does not count NaN
hold on
plot(mean_value(:,2)/10^6,'ro', 'MarkerFaceColor','r')

get(H,'tag');
set(H(6,:),'color','k','linewidth',3.0);
color = color_all;
h = findobj(gca,'Tag','Box');

for i = 1:length(h)
    patch(get(h(i),'XData'),get(h(i),'YData'),color(i),'FaceAlpha',0.2);
end

xlabel({'','','RIO','Egg Code','Speed [knots]'})
ylabel('Total Ice Force [MN]')
set(gca,'FontSize',22)
hold off
```

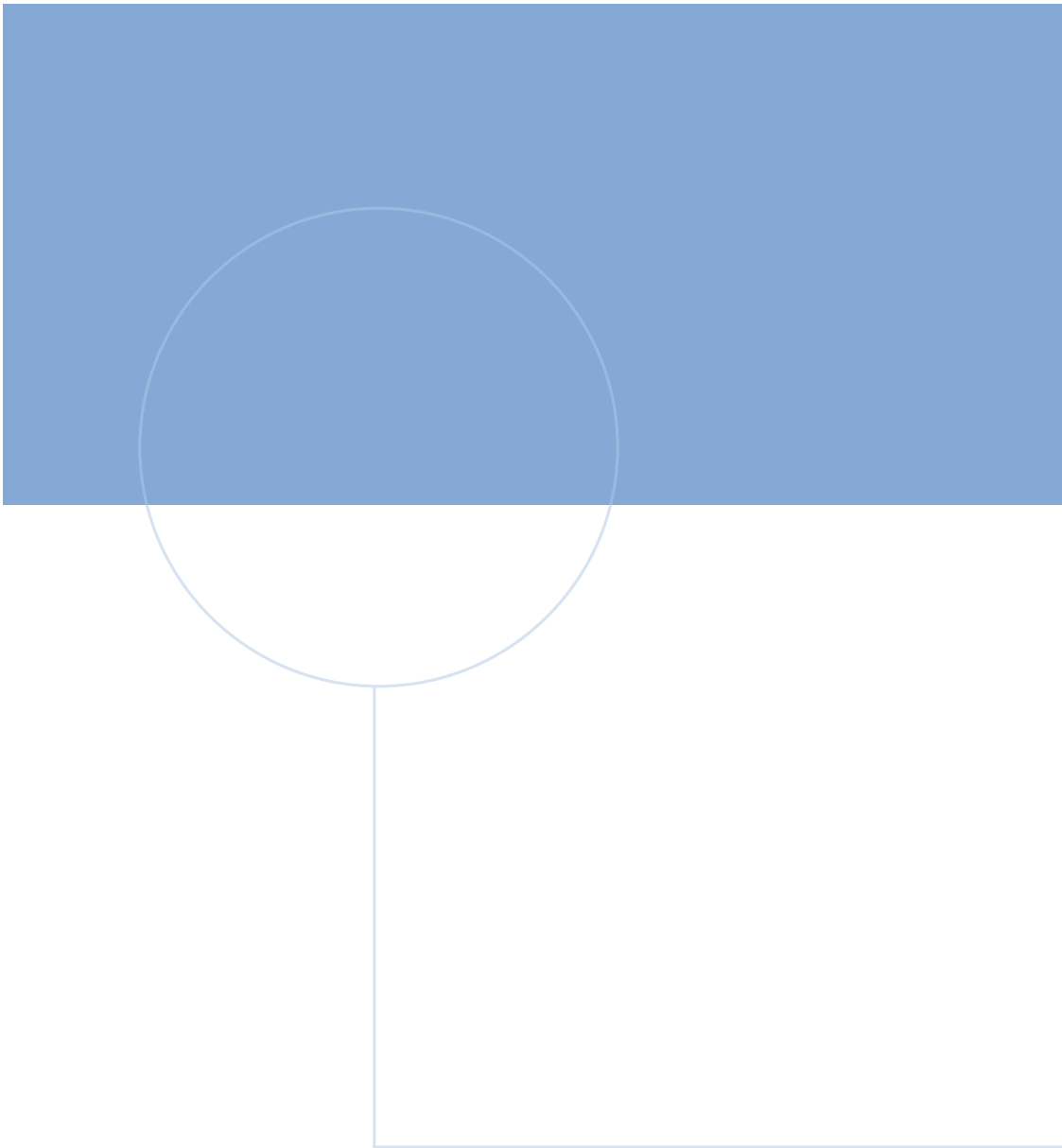

NTNU

Norwegian University of
Science and Technology